

**Klotho: A Paracrine Mediator of Skeletal Muscle Regeneration**

by

**Amrita Sahu**

BTech Biomedical Engineering, Manipal University, India, 2011

MS Biomedical Engineering, Carnegie Mellon University, 2013

Submitted to the Graduate Faculty of the  
Department of Environmental and Occupational Health  
Graduate School of Public Health in partial fulfillment  
of the requirements for the degree of  
Doctor of Philosophy

University of Pittsburgh

2019

UNIVERSITY OF PITTSBURGH

GRADUATE SCHOOL OF PUBLIC HEALTH

This dissertation was presented

by

**Amrita Sahu**

It was defended on

December 2, 2019

and approved by

Aaron Barchowsky, PhD, Professor, Department of Environmental and Occupational Health,  
Graduate School of Public Health, University of Pittsburgh

Radosveta Koldamova, MD, PhD, Professor, Department of Environmental and Occupational  
Health, Graduate School of Public Health, University of Pittsburgh

Claudette St. Croix, PhD, Associate Professor, Department of Cell Biology, School of Medicine,  
University of Pittsburgh

**Dissertation Advisor:** Fabrisia Ambrosio, PhD, MPT, Associate Professor, Department of  
Physical Medicine and Rehabilitation, School of Medicine, University of Pittsburgh

Copyright © by Amrita Sahu

2019

**Klotho: A Paracrine Mediator of Skeletal Muscle Regeneration**

Amrita Sahu, PhD

University of Pittsburgh, 2019

**Abstract**

Thanks to advances in medical technology, people are living longer than ever before. While this increase in lifespan is exciting, it is not necessarily accompanied with a longer health-span. Increasing age is typically accompanied by a progression of tissue dysfunction. Therefore, strategies to identify key factors that promote healthy aging are needed. Age-related declines in skeletal muscle result in impaired regeneration and functional immobility. Such declines are associated with an increased morbidity in an elderly population, thereby making the need for interventions to counteract the effect of age on skeletal muscle vitality an important public health concern.

Fortunately, elegant studies using heterochronic parabiosis have suggested systemic factors, such as proteins and extracellular vesicles (EVs), present in a youthful circulation may “rejuvenate” healing capacity of aging tissues. Studies in this thesis revealed the role of one such circulating longevity factor, Klotho, in mediating the regenerative response of skeletal muscle. Specifically, findings demonstrated that Klotho is upregulated within the muscle and circulation of young mice after an injury, but that the response attenuated with aging. This decreased Klotho expression resulted in disrupted muscle progenitor mitochondrial ultrastructure and myogenic lineage progression, ultimately contributing to a blunted skeletal muscle regenerative capacity. However, supplementation with Klotho restored mitochondria of aged cells and enhanced functional regeneration of aged muscle *in vivo*. These findings suggest a paracrine role of Klotho

in the skeletal muscle regenerative cascade. Yet, while Klotho plays a major role in cellular maintenance at the organismal level, the protein itself is highly unstable and prone to degradation. Therefore, we sought to identify whether there may be mechanisms for protecting Klotho expression within the circulation, for example through storage within circulating EVs. Indeed, population-level profiling of EVs revealed Klotho mRNA expression in an age-dependent manner. This loss of Klotho mRNA over time is important, as the transfer of Klotho mRNA from young EVs to target aged cells enhanced target cell myogenic capacity and mitochondrial function. In a gain-of-function paradigm, we showed that aged muscle transplanted with young EVs displayed an increased functional regeneration, though the benefit was blunted when EVs were isolated from mice heterozygously deficient of Klotho. Collectively, these studies suggest a novel therapeutic role for Klotho, which we propose may ultimately be used to mitigate the impaired muscle healing capacity of the growing geriatric population.

**Table of Contents**

**Acknowledgements ..... xiii**

**1.0 Introduction..... 1**

**1.1 Aging in Skeletal Muscle..... 1**

**1.2 Hallmarks of Aging in Skeletal Muscle ..... 3**

        1.2.1 Cellular senescence..... 3

        1.2.2 Mitochondrial dysfunction in aging skeletal muscle..... 4

        1.2.3 Epigenetic alterations ..... 5

        1.2.4 Altered inter-cellular communication..... 6

**1.3  $\alpha$ -Klotho Attenuates Skeletal Muscle Hallmarks of Aging (Summary of our Findings)..... 8**

**2.0 Age-Related Declines in  $\alpha$ -Klotho Drive Progenitor Cell Mitochondrial Dysfunction and Impaired Muscle Regeneration ..... 10**

**2.1 Abstract ..... 10**

**2.2 Introduction ..... 11**

**2.3 Results..... 13**

        2.3.1 Aged muscle displays a blunted  $\alpha$ -Klotho response to injury ..... 13

        2.3.2 Genetic inhibition of  $\alpha$ -Klotho impairs muscle regeneration..... 15

        2.3.3  $\alpha$ -Klotho is expressed by MuSCs and their progeny ..... 16

        2.3.4 Loss of  $\alpha$ -Klotho in MPCs drives mitochondrial dysfunction..... 19

        2.3.5 Loss of  $\alpha$ -Klotho impairs mitochondrial bioenergetics..... 22

        2.3.6 Muscle regeneration is enhanced by  $\alpha$ -Klotho supplementation..... 23

<b>2.4 Discussion .....</b>	<b>25</b>
<b>2.5 Materials and Methods .....</b>	<b>28</b>
<b>2.5.1 Animals .....</b>	<b>28</b>
<b>2.5.2 Histological analysis of muscle regeneration .....</b>	<b>28</b>
<b>2.5.3 Primary muscle cell isolation .....</b>	<b>29</b>
<b>2.5.4 Primary muscle cell imaging .....</b>	<b>29</b>
<b>2.5.5 ELISA.....</b>	<b>29</b>
<b>2.5.6 Hanging-Wire Test.....</b>	<b>30</b>
<b>2.5.7 Inhibition of and supplementation with <math>\alpha</math>-Klotho .....</b>	<b>30</b>
<b>2.5.8 Epigenetic regulation of <math>\alpha</math>-Klotho.....</b>	<b>30</b>
<b>2.5.9 Analysis of MPC bioenergetics and mitochondrial DNA damage.....</b>	<b>30</b>
<b>2.5.10 SS-31 administration.....</b>	<b>31</b>
<b>2.5.11 In-vivo lentiviral knockdown of <math>\alpha</math>-Klotho .....</b>	<b>31</b>
<b>2.5.12 Supplementation of <math>\alpha</math>-Klotho in vivo .....</b>	<b>32</b>
<b>2.5.13 Data Availability .....</b>	<b>32</b>
<b>2.6 Acknowledgements .....</b>	<b>32</b>
<b>2.7 Author Information-Affiliations .....</b>	<b>33</b>
<b>2.8 Contributions .....</b>	<b>35</b>
<b>2.9 Figures .....</b>	<b>36</b>
<b>3.0 Extracellular Vesicle Delivery of Klotho Transcripts Rejuvenates Aged Stem Cell Progeny .....</b>	<b>48</b>
<b>3.1 Abstract .....</b>	<b>48</b>
<b>3.2 Introduction .....</b>	<b>49</b>

<b>3.3 Results.....</b>	<b>51</b>
<b>3.3.1 Circulating extracellular vesicles modulate the bioenergetics of target cells in an age-dependent manner .....</b>	<b>51</b>
<b>3.3.2 Aging causes a significant loss of CD63+ EVs but not of CD81+ and CD9+ EVs .....</b>	<b>52</b>
<b>3.3.3 EV nucleic acid content is compromised with aging.....</b>	<b>53</b>
<b>3.3.4 Klotho transcripts are abundant in young EVs, but their content is decreased with age .....</b>	<b>54</b>
<b>3.3.5 Klotho mRNA cargoes of circulating EVs enhance muscle functional recovery after injury.....</b>	<b>56</b>
<b>3.4 Discussion .....</b>	<b>57</b>
<b>3.5 Methods .....</b>	<b>59</b>
<b>3.5.1 Serum and muscle progenitor cell isolation.....</b>	<b>59</b>
<b>3.5.2 Immunofluorescence imaging .....</b>	<b>59</b>
<b>3.5.3 Analysis of cellular bioenergetics.....</b>	<b>59</b>
<b>3.5.4 EV isolation and characterization .....</b>	<b>60</b>
<b>3.5.5 SPR imaging and analysis .....</b>	<b>60</b>
<b>3.5.6 Raman Spectroscopy.....</b>	<b>60</b>
<b>3.5.7 ELISA.....</b>	<b>61</b>
<b>3.5.8 Functional and histological analysis of muscle regeneration of injured animals .....</b>	<b>61</b>
<b>3.5.9 Steps to ensure rigor .....</b>	<b>62</b>
<b>3.6 Data Availability.....</b>	<b>62</b>

<b>3.7 Code Availability .....</b>	<b>62</b>
<b>3.8 Acknowledgments.....</b>	<b>62</b>
<b>3.9 Author information-Affiliations.....</b>	<b>63</b>
<b>3.10 Author Contributions.....</b>	<b>64</b>
<b>3.11 Figures .....</b>	<b>65</b>
<b>4.0 Conclusions, Discussion and Future Directions .....</b>	<b>71</b>
<b>4.1 Circulating Klotho Regulates Cellular Senescence and Mitochondria in MuSCs .</b>	<b>71</b>
<b>4.2 Epigenetic Modifications of Klotho Promoter are Important for Skeletal Muscle Healing.....</b>	<b>74</b>
<b>4.3 Paracrine Function of Klotho in Promoting Intercellular Communication .....</b>	<b>75</b>
<b>4.4 Concluding Thoughts .....</b>	<b>77</b>
<b>Appendix A Supplementary Information to Section 2 .....</b>	<b>78</b>
<b>Appendix B Supplementary Information to Section 3 .....</b>	<b>103</b>
<b>Bibliography .....</b>	<b>116</b>

## List of Tables

<b>Appendix Table 1 Skeletal muscle contractile characteristics.....</b>	<b>85</b>
<b>Appendix Table 2 Primary antibody details. ....</b>	<b>105</b>
<b>Appendix Table 3 Secondary antibody details.....</b>	<b>106</b>

## List of Figures

<b>Figure 1. <math>\alpha</math>-Klotho is increased in young muscle after injury, but the response is absent with age.....</b>	<b>36</b>
<b>Figure 2. Genetic and muscle-specific loss of <math>\alpha</math>-Klotho impairs skeletal muscle regeneration. ....</b>	<b>38</b>
<b>Figure 3. <math>\alpha</math>-Klotho expression in quiescent and activated MuSCs. ....</b>	<b>40</b>
<b>Figure 4. Loss of <math>\alpha</math>- Klotho drives mitochondrial dysfunction and disrupts mitochondrial DNA integrity. ....</b>	<b>42</b>
<b>Figure 5. Mitochondrial structure and function are impaired in Kl<math>\pm</math> mice, but are rescued with SS-31. ....</b>	<b>43</b>
<b>Figure 6. <math>\alpha</math>-Klotho supplementation improves aged MPC bioenergetics and muscle regeneration.....</b>	<b>45</b>
<b>Figure 7. Hypothesis schematic. ....</b>	<b>47</b>
<b>Figure 8. Aged muscle progenitor cells (MPCs) cultured in the presence of young serum display and extracellular vesicle-dependent increase in MyoD expression and bioenergetics. ....</b>	<b>65</b>
<b>Figure 9. Aging drives a noticeable loss of CD63+ EV subpopulation.....</b>	<b>66</b>
<b>Figure 10. Aging results in a distinct biochemical fingerprint of circulating EVs. ....</b>	<b>67</b>
<b>Figure 11. Klotho mRNAs are preferentially contained within EVs in an age-dependent manner. ....</b>	<b>68</b>
<b>Figure 12. Klotho mRNA within EVs contribute to the functional regeneration of aged animals. ....</b>	<b>70</b>

Appendix Figure 1. Antibody validation. ....	78
Appendix Figure 2. $\alpha$ -Klotho is also expressed in female muscle with a contusion injury..	79
Appendix Figure 3. Aging results in a blunted <i>Klotho</i> response following injury in female mice.....	79
Appendix Figure 4. $\alpha$ -Klotho expression in MuSCs and FAPs. ....	80
Appendix Figure 5. Decreased $\alpha$ -Klotho expression in MPCs is associated with increased cellular senescence. ....	81
Appendix Figure 6. $\alpha$ -Klotho expression does not affect mitochondrial quantity or morphology.....	82
Appendix Figure 7. Expression of $\alpha$ -Klotho affects the bioenergetics profile of the cells but does not affect the mtDNA copy number.....	83
Appendix Figure 8. SS31 rescues the bioenergetics profile of <i>Kl<sup>+/-</sup></i> MPCs to wild-type control levels but does not significantly alter muscle strength in the absence of injury. ....	84
Appendix Figure 9. Representative gating strategy used to flow sort MuSCs and FAPs....	84
Appendix Figure 10. In-cell western blot supporting analysis in Figure 2G.....	103
Appendix Figure 11. The impact of EV age on target cell Klotho protein expression. ....	103
Appendix Figure 12. Quantification of relative abundance Klotho mRNA EVs using digital PCR. ....	103
Appendix Figure 13. Whole body endurance of aged animals. ....	104

## Acknowledgements

In ‘*reel*’ life, the Avengers were brought together by Nick Fury to form a super-team of super-heroes. Iron Man alone could not have saved the planet in the face of danger. ‘Real’ life is no different. It is full of challenges and a team is needed to effectively resolve them. Every day in lab, we face a different battle, and facing them becomes easier when we have a team with whom we can share the load. A cohesive teamwork is paramount for the success of any project. I have been extremely lucky to have superheroes in real life who have provided me with great support and guidance to accomplish this gargantuan task of completing my doctoral thesis.

First, I am grateful to my thesis advisor Dr. Fabrisia Ambrosio. She is the living example of a great mentor and scientist. Her excitement and drive for answering the unanswerable is contagious, and I for sure have caught that attribute of hers. Thank you, Ricardo, for being my first teacher in the lab. I am grateful to our lab manager, Sunita, who does all the work in the background driving projects and always wishes the best for every member in the lab. I cannot thank Abish and Zachary enough for helping with every project of mine. Together, we are called the “mouse-mafia” of the lab, and I could not be happier, for it resulted in amazing stories. Lia, my first undergraduate student trainee and my friend for life, has been a great support throughout the process of getting my thesis out the door. I thank you for everything you have done. Projects would not be as exciting without other graduate students in the lab—Sruthi and soon-to-be Dr. Hikaru, a big shout out to you for being amazing peers (and friends). The discussions I have had with you regarding science (and food) have been very stimulating.

I thank my committee members-Dr. Aaron Barchowsky, Dr. Radosveta Koldamova and Dr. Claudette St. Croix for being an amazing mentoring team. Your support and guidance have

made this thesis an even better story. I cannot thank Dr. Gwendolyn Sowa and Dr. Michael Boninger enough for playing a role in sending me to Milan for training. My vision for stepping into the field of translational science was established in Milan while working at Don Gnocchi Foundation. Of course, Dr. Marzia Bedoni and her team—Silvia, Alice, Cristiano and Andrea—made it even easier for me venture into this new avenue of my career. I have found great scientists, colleagues, and forever friends in them.

Getting through a doctoral program is only possible with the help of friends and family outside the work environment. They become the best sounding boards of one’s life. I thank all my friends, particularly Ankit, Lidija, Ruby, Nairita, Bharat, Evan, George and Sneha, for they became my support system here. My grandparents, who always motivated me to study more and enjoy the process of getting through a doctoral program—thank you so much for being pillars of wisdom. My in-laws, Jayshree and N. Ramani, thank you for always treating me as your own daughter and being an amazing support. To my parents, Lipi and Anjan—words cannot describe how thankful I feel towards you. You have and still do support me with every endeavor. You have been the biggest and warmest cheerleaders of my life. Thank you. Lastly, I dedicate this thesis to my husband, Suraj. Even though we reside miles away from each other, your support was the only reason I could pull through this intense training. You are my best friend, my soulmate, and my biggest critic. It has always been fun getting generous feedback from you on my work from your mechanical engineering brain. Thank you and love you!

‘Thank you. Obrigada. धन्यवाद. ありがとうございます. Grazie. நன்றி. ଧନ୍ୟବାଦ’

“Iron Man: We’re the Avengers...how do we cope with something like that?  
Captain America: Together”

## 1.0 Introduction

### 1.1 Aging in Skeletal Muscle

The world's aging population is growing at a rapid rate. In US alone, ~50 million people are greater than 65 years of age (1). This number is expected to increase to 72 million by 2030 (2). While the increase in average lifespan is encouraging, it cannot be discounted that, together with the aging process typically comes a multitude of age-associated pathologies, such as an increased incidence of diabetes, cardiovascular diseases, Alzheimer's diseases, and also blunted skeletal muscle performance (3-5). This raises an interesting scientific and philosophical question, "*Is aging a disease?*" Aging in itself, of course, is not the problem. However, the manifestation of a myriad of diseases implicates the aging process as an important public health consideration.

Aging causes a gradual loss of muscle integrity and, hence, function (6, 7). Aging is accompanied by a decreased capacity to heal after an acute injury. Physical fitness and skeletal muscle strength are both strong predictors of mortality and all-cause morbidity(8), and an impaired regenerative response is a major contributor to declines in functional mobility and increased morbidity in elderly population (9). Skeletal muscle aging is typically defined by a shift from a functional myofiber repair following injury to a quick-fix default towards fibrosis, leading to abovementioned impairments (10). This leads to weakness (11), susceptibility to recurrent muscle injury(12), and a prolonged recovery period (13).

Skeletal muscle regeneration is primarily dictated by the action of muscle satellite, or stem, cells (MuSCs)(14). Upon an injury, MuSCs that are originally in a quiescent state become activated and begin to proliferate and differentiate to form functional myofibers that, under the

right conditions, will restore the original architecture of a young healthy muscle (14). However, a decline in MuSC function with aging contributes to the impaired healing response (15). Elegant studies using heterochronic parabiosis, in which the circulatory systems of young and aged animals are surgically joined, have demonstrated that factors in the circulatory system of young have a beneficial impact on the tissue regenerative potential of aged animals (14, 16-18). Although these studies have identified some “rejuvenating factors” that have elicited a systemic benefit on different organs, the identification of a tissue-specific factor remains unresolved. For example, Growth Differentiation Factor 11 (GDF11), oxytocin, and C-C Motif Chemokine Ligand 11 (CCL11) have been identified as circulatory factors that play a role in muscle and neural maintenance and regeneration (19-21). The role of GDF11 remains controversial. One study suggested that GDF11 declines with age and causes muscle wasting, and that upregulation of GDF11 reverses the phenotype (19). However, since then, several studies have suggested that GDF11 is actually a *negative* regulator of skeletal muscle regeneration, and that overexpression leads to muscle atrophy and cachexia (22, 23). Oxytocin has also been suggested to play a role in MuSC regulation and skeletal muscle regeneration (20). However, no studies to date have established oxytocin’s impact on skeletal muscle functional recovery after injury. Villeda et al demonstrated that increasing circulating levels of CCL11 negatively regulate neurogenesis and cognitive function(21). Another study by Griffin et al listed CCL11 as one of the chemokines present in the early stage of myogenesis, a phenomenon that leads to skeletal muscle development (24). However, no studies to date have established a physiological impact of circulating CCL11 in the skeletal muscle regenerative cascade. Collectively, these findings suggest that there is much to be gained from a better understanding of the impact of circulating factors on aged skeletal muscle regeneration.

## **1.2 Hallmarks of Aging in Skeletal Muscle**

There are several factors that contribute to an attenuated anatomical and physiological skeletal muscle function. Some of the factors that drive these age-related declines in skeletal muscle include altered metabolism, circulating hormones, and genetics (25). The progressive loss of physiological functions in humans occur at the cellular and molecular level. In 2013, Lopez-Otin et al systemically reviewed nine ‘hallmarks of aging’ that contribute to the declines in aging tissue (26). Here, we focus on the following hallmarks of aging that have been shown to play a critical role in the maintenance of skeletal muscle functioning, including: (i) Cellular senescence, (ii) mitochondrial dysfunction, (iii) epigenetic alterations, and (iv) altered inter-cellular communication,

### **1.2.1 Cellular senescence**

Senescence was first identified by Hayflick and Moorhead in 1961 during a serial passage of human fibroblasts (27). The investigative team observed an accumulation of debris and an absence of mitotic figures with arrested population growth over time. These two investigators were the first to posit that cellular senescence may be a driver of aging process (27). Although senescence plays an important role in the developmental process and tissue homeostasis, it also occurs as a response to stressed state of a cell that may be triggered by pathophysiological factors (28, 29).

One of the characteristic features of cellular senescence is cell growth arrest, which is initiated by the tumor suppressor pathways, p53 and p16/Rb (30, 31). Senescence leads to DNA damage resulting in an increased formation of  $\gamma$ H2Ax and 53BP1 in chromatin (29). These

processes eventually lead to the activation of the p53 pathway (29, 32, 33)). In skeletal muscle, increased chronic p53 activity in p53<sup>+/mt</sup> mice has been shown to induce muscle atrophy and increased paternally-expressed gene 3 (PW1) expression, thereby driving disrupted satellite cell differentiation (34). An evaluation of force producing capacity by the gastrocnemius muscle of p53<sup>-/-</sup> mice revealed a significantly decreased fatigue resistance (35). Studies in skeletal muscle have also identified p16 as a key regulator of satellite cell self-renewal capacity, and activation of the p16-associated senescence pathway disrupts skeletal muscle homeostasis, causing a cascade of events that lead to muscle degeneration (36). Conversely, inhibition of the p16 pathway enhances skeletal muscle function in aging mice (37, 38). While MuSCs generally senesce with increasing age through upregulation of the p16-pathway (38), depletion of senescent cells enhances the ability of non-senescent MuSCs to form functional muscle fibers (39). Together, these findings suggest that senescence impairs MuSC function, but that the removal of these senescent cells restores muscle metabolism and function (40).

### **1.2.2 Mitochondrial dysfunction in aging skeletal muscle**

Mitochondria play a major role in maintaining cellular homeostasis, and loss of mitochondrial function has been regarded as a contributor to tissue dysfunction (41). With age, mitochondrial electron transport chain complexes display blunted activity and increased accumulation of reactive oxygen species (ROS)(42). Accumulation of these oxidants may subsequently lead to pathological conditions such as increased insulin resistance (43), intolerance to muscle contractile activity (44), and increased muscle wasting (45, 46).

ROS accumulation increases damage to components of the mitochondrial membranes that are rich in unsaturated fatty acids (47). In particular, peroxidation of mitochondrial membrane lipids

blunt mitochondrial function, a phenomenon shown to increase with age (48). Cardiolipin, for example, is a phospholipid present in the inner mitochondrial membrane in close proximity to ROS generation sites and, thus, is an easy target for oxidative attack (48). Similarly, mitochondrial DNA (mtDNA) is located near the site of mitochondrial ROS generation, and is therefore highly vulnerable to oxidative damage (49, 50). It has been suggested that mtDNA damage can be transferred to daughter cells upon division, which has downstream effects on cellular health (47, 51).

Aged skeletal muscle displays an increased oxidative damage to DNA and a decreased mtDNA content (52). The oxidative capacity of skeletal muscle declines with age, and such mitochondrial dysfunction is currently regarded as an intrinsic factor that drives biological aging(46). The muscle of aged animal models demonstrates a decline in ATP production and content along with increases in mtDNA deletions (53, 54). Nuclear Magnetic Resonance (NMR) imaging-based analyses have revealed a decline in mitochondrial function in healthy elderly humans (55). However, synthetic peptides, such as SS-31, enhance skeletal muscle function by reversing cardiolipin peroxidation (56). Taken together, these findings suggest that maintenance of mitochondrial function is paramount for sustained skeletal muscle function throughout the lifespan.

### **1.2.3 Epigenetic alterations**

Epigenetic modifications occur throughout the lifespan of all tissues and include alterations in DNA methylation patterns, histone modifications and chromatin remodeling(57). Studies have demonstrated that skeletal muscle cells retain the ‘memory’ of their environmental niche and transfer the molecular information to the daughter cells through DNA methylation (58).

During the skeletal muscle regenerative cascade, activated MuSCs express cell-cycle regulatory genes that are controlled by methylation of lysine 4 on histone 3 (H3K4me3)(59). The MuSC switch from quiescence to activation are also controlled by Wnt/b-catenin signaling pathway, which induces histone modifications by activating H3K4me2 and suppressing H3K9me2 on Myf5 and MyoD gene promoters (60). Epigenetic changes are highly dynamic and are influenced by a number of factors, including aging. Excessive global DNA methylation in aged MuSCs has been regarded as one of the underlying causes for an impaired self-renewal capacity which can be reversed by using a demethylation agent such as 5-aza-20-deoxycytidine (5AZA) on aged MuSCs (61). Self-renewal capacity of MuSCs is an important factor in regulating the skeletal muscle health and function, a property that declines with age (62). Taken together, these findings suggest that aging can induce epigenetic modifications in skeletal muscle that can eventually lead to an impaired muscle regenerative response. However, these alterations can be reversed to improve skeletal muscle performance.

#### **1.2.4 Altered inter-cellular communication**

The decline in the regenerative capacity of skeletal muscle has been attributed to changes in the MuSC microenvironment, or niche, including circulating factors and hormones, extracellular matrix composition and inflammation (63). Circulating hormones such as interleukin 6 (IL6), growth hormones (GH) and insulin-like growth factor 1(IGF-1) all decline with age (64, 65). GH acts on muscle myoblasts through the GH receptors that stimulate the production of IL4, a factor critical for myogenic progression (66, 67). GH also regulates myogenesis by stimulating the production of IGF-1 via the p38/MAPK signaling pathway (68). Other endocrine hormones, such as testosterone and estrogen, promote the differentiation capacity of MuSCs via the protein

kinase C and IGF-1 signaling pathways, respectively (69, 70). IL6, an anti-inflammatory myokine increases with age, a process that has been shown to impair myogenic differentiation (71).

Senescent cells release pro-inflammatory cytokines that activate the NF- $\kappa$ B pathway, which, in turn, leads to increased levels of IL-1 $\beta$  and tumor necrosis factors (TNF) (72, 73). In aged mice muscle, the NF- $\kappa$ B DNA binding capacity increases (74). NF- $\kappa$ B activation has also been shown to inhibit myogenesis, which has downstream effects on muscle architecture (75, 76). Conversely, NF- $\kappa$ B inhibition with systemic administration of sodium salicylate improves muscle regeneration of aged mice (77). AU-binding factor 1 (AUF1) is a known inhibitor of senescence (78). AUF1 has been shown to be an important factor that controls inflammatory response, regulates mRNA degradation of the cytokines and also maintains telomere lengths (78). Interestingly, chronic muscle contractions are able to stimulate systemic production of AUF1 isoforms in the skeletal muscle of rodents, a phenomenon associated with improved muscle plasticity (79).

Skeletal muscle releases myokines that perform a regulatory role in the skeletal muscle regenerative cascade as paracrine mediators (63). Aging can alter the muscle secretome and inhibit the regenerative process by affecting the function of MuSCs. For instance, Chakkalakal et al showed that aging increased fibroblast-growth factor-2 levels, which resulted in a decreased level of sprouty 1 expression in MuSCs (80). Such declines drive a negative feedback for the self-renewal capacity of the MuSCs that could lead to an impaired regenerative response of the muscle(80). The muscle secretome also contains extracellular matrix (ECM) components, miRNAs, and extracellular vesicles (EVs)(81, 82).

EVs are nano-vesicles that are secreted by all cells and tissues that encapsulate bioactive molecules such as proteins, mRNAs, miRNAs, double-stranded DNA and other non-coding

RNAs (83, 84). EVs are increasingly recognized as important paracrine mediators of intercellular communication (85). Although, EVs have been identified as key mediators of intercellular communication in physiological and pathological states, their role in the context of aging muscle is poorly understood. EVs secreted from differentiated MuSCs promote the myogenic differentiation process (82). Differentiated myotubes have been shown to release miRNAs in the EVs that inhibit Sirtuin 1 expression, which stimulates the differentiation of myoblasts (86). Although the overall muscle secretome of humans declines with age (87), the mechanistic impact of these age-related alterations warrants further investigation.

### **1.3 $\alpha$ -Klotho Attenuates Skeletal Muscle Hallmarks of Aging (Summary of our Findings)**

Heterochronic parabiosis studies, in which the circulatory systems of young and old mice are surgically joined, have clearly shown a positive impact of the young circulatory system on the overall health of the older mice (10, 14, 16-18). Genetic studies have identified one such factor,  $\alpha$ -Klotho, that plays a vital role in extending lifespan and delaying aging-associated declines in tissue functioning (88-91). Although, deficiency of  $\alpha$ -Klotho can result in an impaired kidney and cognitive function (92), the role of  $\alpha$ -Klotho in age-related declines in skeletal muscle function has not been widely investigated. Given the potential role of  $\alpha$ -Klotho in regulating hallmarks of aging, such as cellular senescence, mitochondrial function, epigenetic modifications and intercellular communication (93)—processes important for MuSC function—the studies proposed in this thesis are based on the central hypothesis that circulating  *$\alpha$ -Klotho plays a key role in maintenance of skeletal muscle health over time by targeting key hallmarks of aging.*

The overarching goal of this thesis is to elucidate the role of  $\alpha$ -Klotho in regulating skeletal muscle regeneration. The proposed studies have tested the central hypothesis that **decline in  $\alpha$ -Klotho expression with aging drives MuSC mitochondrial dysfunction resulting in impaired muscle regenerative response.** Furthermore, **we hypothesize that serum EVs deliver  $\alpha$ -Klotho to recipient cells in an age-dependent manner, and that such declines in EV-  $\alpha$ -Klotho mRNA contribute to MuSC dysfunction and impaired skeletal muscle regeneration.** These hypotheses were tested through two specific aims:

*Specific Aim 1 (Section 2): To interrogate a role of  $\alpha$ -Klotho in driving MuSC mitochondrial function and muscle regeneration.*

*Specific Aim 2 (Section 3): To evaluate the effect of a loss of Klotho mRNA within EVs on MuSC-mitochondrial function and skeletal muscle regeneration.*

## **2.0 Age-Related Declines in $\alpha$ -Klotho Drive Progenitor Cell Mitochondrial Dysfunction and Impaired Muscle Regeneration**

Data presented in this chapter were published in *Nature Communications*, volume 9, Article number: 4859 (2018)

Amrita Sahu, Hikaru Mamiya, Sunita N Shinde, Amin Cheikhi, Lia L. Winter, Nam Viet Vo, Donna Stolz, Vera Roginskaya, Wan-Yee Tang, Claudette St. Croix, Laurie H. Sanders, Michael Franti, Bennett Van Houten, Thomas A. Rando, Aaron Barchowsky & Fabrisia Ambrosio

### **2.1 Abstract**

While young muscle is capable of restoring the original architecture of damaged myofibers, aged muscle displays a markedly reduced regeneration. We show that expression of the “anti-aging” protein,  $\alpha$ -Klotho, is up-regulated within young injured muscle as a result of transient Klotho promoter demethylation. However, epigenetic control of the Klotho promoter is lost with aging. Genetic inhibition of  $\alpha$ -Klotho in vivo disrupted muscle progenitor cell (MPC) lineage progression and impaired myofiber regeneration, revealing a critical role for  $\alpha$ -Klotho in the regenerative cascade. Genetic silencing of Klotho in young MPCs drove mitochondrial DNA (mtDNA) damage and decreased cellular bioenergetics. Conversely, supplementation with  $\alpha$ -Klotho restored mtDNA integrity and bioenergetics of aged MPCs to youthful levels in vitro and enhanced functional regeneration of aged muscle in vivo in a temporally-dependent manner.

These studies identify a role for  $\alpha$ -Klotho in the regulation of MPC mitochondrial function and implicate  $\alpha$ -Klotho declines as a driver of impaired muscle regeneration with age.

## 2.2 Introduction

Aging is associated with impaired skeletal muscle regenerative capacity after an acute injury, resulting in declines in force-producing capacity. The impaired regenerative response of aged muscle is characterized by a shift from functional myofiber repair following injury to fibrotic deposition (94). This increased fibrosis has been attributed to muscle stem (satellite) cell (MuSCs) dysfunction (94).

In response to muscle injury, MuSCs become activated from a quiescent state to repair damaged myofibers (95, 96). While MuSC activation in young muscle restores the original architecture of the damaged myofibers, aging is associated with MuSC dysfunction, as evidenced by increased apoptosis (97), decreased proliferation (10), impairment of autophagy(98), and a decreased resistance to stress (99). Aged MuSCs also display a manifold increase in expression of aging-associated senescence markers, including p16<sup>Ink4a</sup> and p21<sup>Cip1</sup>(37). Though aged MuSCs clearly display cell-autonomous deficits that contribute to an impaired regenerative response(37, 100-102), it was recently suggested that extrinsic changes in the muscle microenvironment may provide the initial geroconversion trigger in MuSCs (103). Indeed, several studies have demonstrated that rejuvenation of the systemic muscle microenvironment largely restores the healing capacity of aged skeletal muscle (10, 94, 104, 105), leading to interest in the identification of circulating “anti-geronic” proteins and an improved mechanistic understanding by which such proteins may transpose a youthful regenerative phenotype onto aged skeletal muscle.

To this end, genetic studies have identified a powerful aging suppressor gene, *Klotho*, which is found within the circulatory systems of mice and humans (92, 106). *Klotho* deficiency results in the onset of numerous aging phenotypes, including decreased activity levels, gait disturbances, cognitive impairment, sarcopenia, as well as an impaired wound repair process (92, 107-112). Three homologs of *Klotho*,  $\alpha$ ,  $\beta$  and  $\gamma$ , have been identified (reviewed in (113)). In tissues such as the skin, small intestine and kidney, declines in  $\alpha$ -*Klotho* have been shown to promote cellular senescence (114) and stem cell dysfunction (107).

In this study, we tested the hypothesis that age-related declines in  $\alpha$ -*Klotho* drive dysfunctional muscle progenitor cell (MPC) mitochondrial bioenergetics, ultimately resulting in an impaired tissue regeneration. Our findings demonstrate that young skeletal muscle displays a robust increase in local  $\alpha$ -*Klotho* expression following an acute muscle injury with transient demethylation of the *Klotho* promoter. However, aged muscle displays no change in *Klotho* promoter methylation and no increase in  $\alpha$ -*Klotho* expression following injury. Levels of  $\alpha$ -*Klotho* in MPCs derived from aged mice are decreased relative to those of young animals, and genetic knockdown of  $\alpha$ -*Klotho* in young MPCs confers an aged phenotype with pathogenic mitochondrial ultrastructure, decreased mitochondrial bioenergetics, mitochondrial DNA damage, and increased senescence. Further supporting a role for  $\alpha$ -*Klotho* in skeletal muscle vitality, mice heterozygously deficient for *Klotho* (*Kl*<sup>+/-</sup>) have impaired MPC bioenergetics that is consistent with a defective regenerative response following injury. Indeed, the regenerative defect of *Kl*<sup>+/-</sup> mice is rescued at the cellular and organismal level when mitochondrial ultrastructure is restored through treatment with the mitochondria-targeted peptide, SS-31(56, 115, 116). Finally, we demonstrate that systemic delivery of exogenous  $\alpha$ -*Klotho* rejuvenates MPC bioenergetics and enhances functional myofiber regeneration in aged animals in a temporally-dependent manner.

Together, these findings reveal a role for  $\alpha$ -Klotho in the regulation of MPC mitochondrial function and skeletal muscle regenerative capacity.

## 2.3 Results

### 2.3.1 Aged muscle displays a blunted $\alpha$ -Klotho response to injury

To determine whether  $\alpha$ -Klotho is up-regulated locally in response to an acute muscle injury, we performed immunofluorescence analysis of  $\alpha$ -Klotho in the skeletal muscle in young (4-6 months) and aged (22-24 months) male mice under conditions of homeostasis and following a cardiotoxin-induced injury.  $\alpha$ -Klotho was virtually undetectable in healthy, uninjured muscle, regardless of age (Figure 1A, B, E). In contrast, strong expression of  $\alpha$ -Klotho was observed at the regenerating site of young muscle 14 days post injury (Figure 1C, E; confirmation of antibody specificity is presented in Appendix A Figure 1). Aged muscle, however, displayed no appreciable increase in  $\alpha$ -Klotho expression following an acute injury (Figure 1D, E). Serum  $\alpha$ -Klotho levels followed a similar expression pattern according to age and injury status (Figure 1F). RT-qPCR findings revealed that Klotho transcript expression increases significantly at three and seven days post-injury in the skeletal muscle of young male mice (Figure 1G). Despite the fact that  $\alpha$ -Klotho protein is still detected in young muscle at 14 days post-injury (Figure 1C, E), gene expression approached baseline levels at this later time point. On the other hand, aged counterparts display unaltered gene expression across all the time points tested (Figure 1G). The  $\alpha$ -Klotho response to injury was not unique to a cardiotoxin injury, as we found that young mice exposed to a severe contusion injury displayed a robust  $\alpha$ -Klotho response at the protein level 14

days after injury (Appendix A Figure 2). Young female mice displayed a similar, yet blunted, increase in *Klotho* expression in response to injury, but the response is lost with aging (Appendix A Figure 3).

Epigenetic silencing of the  $\alpha$ -*Klotho* gene contributes to the impaired regenerative potential of dystrophic skeletal muscle, and a differentially methylated region (DMR) of 110 nucleotides within the *Klotho* promoter region was identified in the muscles of aged mdx mice (117). Therefore, we measured methylation levels of the DMR after injury in young and aged muscle of mice. An acute injury to young muscle triggered demethylation of the DMR in the *Klotho* promoter three and seven days after injury (Figure 1H). Injury-induced demethylation was, however, absent in the *Klotho* promoter within aged muscle (Figure 1H).

To examine whether modifying enzymes for DNA methylation contribute to methylation changes in the *Kl* promoter, we used a chromatin immunoprecipitation (ChIP) assay to measure the enrichment of DNMT3a methyltransferases in the *Klotho* promoter region. There was a decrease of DNMT3a binding to the *Klotho* promoter in the injured young muscle that, at the timepoints evaluated, reached a nadir three days after injury, and was increased by day 14 (Figure 1I). In contrast, the injury-induced decrease in DNMT3a binding was delayed and blunted in injured aged muscle (Figure 1I). Consistent with the finding that dimethylated histone H3 lysine 9 (H3K9me2) bound to the *Klotho* promoter in dystrophic skeletal muscle represses *Klotho* (117), H3K9me2 binding to the *Klotho* promoter region was decreased after injury in young muscle (Figure 1J). Taken together, these findings suggest that acute injury drives the reactivation of *Klotho* by reducing DNA methylation and H3K9 dimethylation in the promoter of young muscle, but that *Klotho* remains epigenetically repressed after injury in aged muscle.

### 2.3.2 Genetic inhibition of $\alpha$ -Klotho impairs muscle regeneration

To directly implicate a functional role for  $\alpha$ -Klotho in skeletal muscle regeneration, we next evaluated the regenerative response to acute muscle injury in adult mice that are heterozygously deficient for Klotho (Kl<sup>+/-</sup> mice). As expected, Kl<sup>+/-</sup> mice displayed a significantly decreased local  $\alpha$ -Klotho expression at the site of injury (Figure 2A, B). Kl<sup>+/-</sup> mice also displayed a decreased regenerative index, smaller myofiber cross-sectional area, and increased fibrosis when compared to age- and sex-matched wild type counterparts (Figure 2A-E). These findings are consistent with a recent study of muscle regeneration in  $\alpha$ -Klotho hypomorphs (118). Together, the data demonstrate that  $\alpha$ -Klotho is necessary for effective skeletal muscle regeneration after injury.

Given our findings of a significantly increased Klotho expression within the injured muscles of young mice (Figure 1C, E, G), we next evaluated the contribution of local  $\alpha$ -Klotho in functional muscle regeneration. The tibialis anterior (TA) muscles of young mice were injected with GFP-tagged SMARTpool® lentiviral particles carrying shRNA to  $\alpha$ -Klotho, whereas control counterparts were injected with an equal volume of the non-targeting control (NTC) lentivirus. After four weeks, TAs were injured via a local cardiotoxin injection, and regeneration was evaluated two weeks after injury. As expected, muscles treated with shRNA to  $\alpha$ -Klotho displayed a significant decrease in  $\alpha$ -Klotho expression at the site of injury (Appendix A Figure 1B). Circulating  $\alpha$ -Klotho was also significantly decreased (Appendix A Figure 1D). This suggests that muscle-derived  $\alpha$ -Klotho may contribute to the increased circulating levels observed in young mice after injury (Figure 1F).

Histological analysis revealed that knock down of  $\alpha$ -Klotho expression resulted in a decreased number of regenerating fibers, a decrease in the percentage of myofiber area/total area,

and an increased adiposity (Figure 2F-I). There was, however, no difference in the fibrosis across groups (Figure 2K). The cross-sectional area of regenerating (centrally-nucleated) fibers in muscles treated with shRNA to  $\alpha$ -Klotho was also significantly smaller than NTC controls (Figure 2L), further confirming a defective regenerative response. Unexpectedly, we also observed the presence of a number of large, non-regenerating myofibers at the injury site of muscles treated with shRNA to  $\alpha$ -Klotho (Figure 2F). To evaluate the structural integrity of these myofibers, we performed second harmonic generation (SHG) imaging, which allows for 3-dimensional visualization of myofiber structure and organization. Consistent with histological findings, SHG analysis revealed that muscles treated with shRNA to  $\alpha$ -Klotho contain a decreased number of centrally-nucleated fibers (Figure 2M, N). This decreased evidence of active regeneration was concomitant with pathologic myofiber architecture and integrity (Figure 2M and Supplemental Movies 1 and 2). Most importantly, the impaired regenerative response and disrupted myofiber structure was concomitant with a decreased functional recovery after injury (Figure 2O).

### **2.3.3 $\alpha$ -Klotho is expressed by MuSCs and their progeny**

The fact that  $\alpha$ -Klotho expression in young muscle is elevated at 3 days after injury (Figure 1G)—a time point that corresponds with MuSC activation—led us to next investigate whether MuSCs express  $\alpha$ -Klotho and whether  $\alpha$ -Klotho is necessary for the MuSC response to injury. We accessed RNAseq data from a recent study (119), which is stored on the Gene Expression Omnibus (GEO) publicly accessible database. Analysis of archived data revealed a 10-fold increase in Klotho expression of freshly sorted MuSCs as compared to whole muscle lysates (Figure 3A). Structured illumination microscopy (SIM) confirmed robust  $\alpha$ -Klotho in

muscle progenitor cells (MPCs) isolated from young mice (Figure 3B, C). MPCs were cultured for no more than three passages prior to analysis and were confirmed to be >90% MyoD+. MPCs isolated from aged muscle, however, displayed a markedly decreased  $\alpha$ -Klotho protein expression (Figure 3B, C). We also evaluated  $\alpha$ -Klotho expression in MuSCs isolated by fluorescence activated cell sorting (120). As observed in MPCs, we found that young MuSCs displayed a robust  $\alpha$ -Klotho expression, but that  $\alpha$ -Klotho expression was decreased in aged MuSCs (Appendix A Figure 4).

Tissues previously shown to express high levels of  $\alpha$ -Klotho, such as the kidney, contain a membrane-bound form of  $\alpha$ -Klotho (~120kDa), which functions as an obligate co-receptor for fibroblast growth factor-23 (FGF23)(121). However, upon proteolytic cleavage of the extracellular domain,  $\alpha$ -Klotho is released from the cells, where it functions as a humoral factor(92). To determine whether MPCs secrete  $\alpha$ -Klotho, we performed ELISA of the conditioned media from MPCs isolated from young and old muscle. Conditioned media derived from young MPCs contained significantly more  $\alpha$ -Klotho than did the condition medium from aged MPCs (Figure. 3D), suggesting that MuSCs secrete  $\alpha$ -Klotho but that this declines with age.

Immunohistochemical analysis of young muscle three days after injury revealed that 96.7% of MyoD+ cells express  $\alpha$ -Klotho (Figure 3E). MyoD is a marker of activated MuSCs and is required for myogenic lineage progression(122).. We accessed and analyzed MuSCs RNAseq data housed on the GEO repository (119)and found that activated MuSCs display significantly increased Klotho expression when compared to quiescent MuSC counterparts that were isolated from 1% PFA-perfused mice (Figure 3F). These findings suggest that  $\alpha$ -Klotho expression is increased in the transition from MuSC quiescence to activation. To investigate this more directly, we compared  $\alpha$ -Klotho expression in freshly sorted (quiescent) MuSCs and MuSCs that were

maintained in culture for three days, thereby promoting activation *in vitro* (123). Activated MuSCs displayed a 4.5-fold increase in  $\alpha$ -Klotho, when compared to quiescent counterparts (Figure 3G, H). Conditioned media derived from activated MuSCs also contained significantly more  $\alpha$ -Klotho, when compared to conditioned media derived from quiescent MuSCs (Figure 3I). We also isolated MuSCs from uninjured young muscle and young muscle three days post-injury, yielding a population of quiescent and activated MuSCs, respectively (Appendix A Fig. 4C). As observed when MuSCs were activated *in vitro*, there was a significant increase in  $\alpha$ -Klotho expression in MuSCs that were activated *in vivo* (Figure 3J, K). As a comparison, fibroadipogenic progenitor cells (FAPs), which also play a critical role in the skeletal muscle regenerative cascade (124), displayed no change in  $\alpha$ -Klotho over three days of activation in culture, nor was  $\alpha$ -Klotho expression increased when FAPS were isolated from acutely injured muscle (Figure 3 G, H, J, K, Appendix A Figure 4D). The conditioned media from activated FAPs also contained significantly less  $\alpha$ -Klotho when compared to the conditioned media from activated MuSCs (Figure 3I). Therefore, at least some of the  $\alpha$ -Klotho protein detected in muscle after injury could come from MPCs themselves, although other neighboring cell populations may also express and secrete  $\alpha$ -Klotho in response to an acute injury. Indeed, it was recently demonstrated that  $\alpha$ -Klotho derived from macrophages promotes muscle regeneration (125).

We next asked whether  $\alpha$ -Klotho is necessary for normal MuSC lineage progression. MPCs isolated from the skeletal muscle of KI<sup>+/-</sup> mice displayed a small, but significant, decrease in the percentage of MyoD<sup>+</sup> cells when compared to age-matched wild type counterparts. There was, however, no difference in Pax7 expression across groups (Figure 3L-N). These findings are consistent with a previous report demonstrating that  $\alpha$ -Klotho hypomorphs display a decreased number of MyoD<sup>+</sup> cells as compared to control counterparts(118). *In vivo*, lentiviral shRNA

inhibition of  $\alpha$ -Klotho resulted in a decreased MyoD expression at the site of injury (Figure 3O, P). Taken together, these data suggest that a loss of  $\alpha$ -Klotho disrupts MuSC lineage progression.

#### **2.3.4 Loss of $\alpha$ -Klotho in MPCs drives mitochondrial dysfunction**

Previous studies have implicated  $\alpha$ -Klotho as being involved in multiple processes associated with inhibition of senescence (114). Senescence is actively repressed in young MuSCs, but this capacity declines with aging, resulting in a failure of MuSCs to activate and proliferate in response to injury (38). Therefore, we investigated whether the decreased MuSC activation in  $\alpha$ -Klotho-deficient muscles may be attributed to cellular senescence. To confirm an inhibitory role for  $\alpha$ -Klotho in myogenic cell senescence, we used small interference RNA (siRNA) inhibition, which resulted in a ~3-fold decrease in  $\alpha$ -Klotho (Appendix A Figure 1G, H). As expected, knockdown of  $\alpha$ -Klotho induced a senescent phenotype in young MPCs, as evidenced by the percentage of senescence associated (SA)- $\beta$ gal positive cells, increased cytosolic HMGB1 levels (an indicator of cellular stress) and decreased cellular proliferation (Appendix A Figure 5). These findings mimicked the phenotype of MPCs isolated from aged muscle (Appendix A Figure 5).

Given that senescent cells are known to have higher levels of DNA damage (126), we used LXRepair multiplex technology(127, 128) to evaluate the DNA base excision repair (BER) enzyme activities of OGG1 and APE1, which work on two common oxidative DNA lesions, 8-oxodG and abasic sites, respectively. When compared to scramble siRNA-treated young MPCs, there was no significant decline in base excision repair (BER) in the nucleus of cells treated with siRNA to  $\alpha$ -Klotho (Appendix Figure 5G, H). However, just 48 hours of  $\alpha$ -Klotho supplementation to siRNA-treated MPCs from young animals dramatically stimulated the activity of these BER enzymes (Appendix A Figure 5G, H). These data suggest that  $\alpha$ -Klotho's role in

MPC senescence may be attributed to induction of key enzymes in the BER pathway, which is rapid and can occur even within a couple of hours(129).

While  $\alpha$ -Klotho's role in cellular senescence has been demonstrated in multiple systems, the mechanisms underlying this role are incompletely understood. Cellular senescence is associated with altered mitochondrial morphology and dysregulated bioenergetics that can lead to aging and aging-associated pathologies(26, 130) Thus, regulation of MPC senescence by  $\alpha$ -Klotho raised the intriguing possibility that  $\alpha$ -Klotho may play regulate MPC mitochondrial structure and function. Using an antibody against the mitochondrial membrane protein, Tom20, we observed no difference in mitochondrial morphology, as determined by sphericity, the number of mitochondria per cell, or mitochondrial volume according to age or  $\alpha$ -Klotho levels (Appendix A Figure 6A, C-F). This was further supported qualitatively using STimulation Emission Depletion (STED) microscopy to visualize the mitochondrial network (Appendix A Figure 6B). These findings suggest that a loss of  $\alpha$ -Klotho does not affect mitochondrial morphology or mass. However, detailed analysis by transmission electron microscopy (TEM) revealed a striking alteration of ultrastructural integrity of the mitochondrial cristae and endoplasmic reticulum, in addition to lipid droplet accumulation when young MPCs were treated with siRNA to  $\alpha$ -Klotho (Figure 4A).

In light of the loss of mitochondrial ultrastructural integrity resulting from decreased  $\alpha$ -Klotho expression, we next evaluated whether loss of  $\alpha$ -Klotho drives MPC mitochondrial dysfunction. Indeed, recent reports have shown a critical role for mitochondria in MuSC function(131, 132). The bioenergetic profiles of young and aged MPCs were studied using a Seahorse XF<sup>96</sup> Flux analyzer, which measures oxygen consumption rate (OCR), a measure of oxidative phosphorylation. OCR was measured again after injection of oligomycin, FCCP, 2-

deoxyglucose (2-DG), and rotenone. These data demonstrate that, when normalized to total number of cells, MPCs from older animals display dramatically decreased levels of basal OCR as compared to young counterparts (Figure 4B; Appendix A Figure 7). A similar age-associated deficit in the OCR of freshly isolated and cultured MuSCs was recently reported (133). When young MPCs were treated with siRNA to  $\alpha$ -Klotho, basal OCR was reduced to ~25% values of scramble-treated counterparts (Figure 4C, Appendix A Figure 6). MPCs isolated from uninjured  $Kl^{+/-}$  mice display a similarly blunted bioenergetic profile (Figure 4D). Though there was no appreciable decrease in reserve capacity in aged MPCs, young MPCs treated with siRNA to  $\alpha$ -Klotho and MPCs isolated from  $Kl^{+/-}$  mice both showed a ~25% decrease in the reserve capacity (Figure 4E-G; Appendix A Figure 7). Reserve capacity represents the spare bioenergetic capacity, is calculated as the difference between the basal and maximal OCR, and indicates the ability of a cell to respond to stress(134). Taken together, these data support the hypothesis that age-related declines in  $\alpha$ -Klotho drive impaired MPC mitochondrial bioenergetics.

One factor that could contribute to decreased mitochondrial function with decreased  $\alpha$ -Klotho is oxidative damage, which could manifest itself as mtDNA damage (135). Therefore, we next examined mtDNA integrity. Using a qPCR-based assay that we have successfully applied to different cell types including mouse tissue and human peripheral lymphocytes (136-138), we evaluated mtDNA damage in MPCs isolated from young or aged mice. The method used is based on the principle that a wide variety of types of DNA damage have the propensity to block DNA polymerase progression (135). Therefore, this assay detects numerous kinds of base DNA damage or DNA repair intermediates such as abasic sites, as well as single and double DNA strand breaks.

There was no difference in steady-state mtDNA copy number across groups (Appendix A Figure 7C, D), consistent with immunocytochemical analysis showing no difference in

mitochondrial mass (Appendix A Figure 6C). However, we found that MPCs isolated from aged mice displayed higher levels of mtDNA damage as compared to young counterparts (Figure 4H). Accordingly, young MPCs receiving siRNA to  $\alpha$ -Klotho and MPCs isolated from  $Kl^{+/-}$  mice displayed increased numbers of mtDNA lesions when compared to scramble-treated and wild type controls, respectively (Figure 4I, J).

### 2.3.5 Loss of $\alpha$ -Klotho impairs mitochondrial bioenergetics

What is the mechanism by which  $\alpha$ -Klotho regulates mitochondrial function? The disrupted mitochondrial cristae structure within cells displaying decreased  $\alpha$ -Klotho expression (Figure 4A) suggests that  $\alpha$ -Klotho is necessary for the maintenance of mitochondrial matrix integrity. Loss of matrix integrity disrupts mitochondrial respiration and induces the accumulation of reactive oxygen species (ROS). ROS accumulation, in turn, drives mtDNA damage and, ultimately, cellular senescence (139). This led us to ask whether  $\alpha$ -Klotho may preserve mitochondrial function through maintenance of mitochondrial ultrastructure. TEM analysis reveals a significantly greater number of vacuolated mitochondria with disrupted cristae in the MPCs of  $Kl^{+/-}$  mice (Figure 5A, B).

Cardiolipin is an anionic phospholipid that is confined almost exclusively to the inner mitochondrial membrane where it is synthesized. It is required for the mitochondrial respiratory supercomplex assembly and activity, the disruption of which enhances the generation of mitochondrial reactive oxygen species (ROS) (140). We found that cardiolipin content is depleted in MPCs isolated from  $Kl^{+/-}$  mice, as compared to wild type counterparts (Figure 5C, D). However, treatment with SS-31, a mitochondrially-targeted peptide that mitigates cardiolipin peroxidation (140), restored  $Kl^{+/-}$  MPC ROS generation, mtDNA damage and cellular

bioenergetics to levels comparable to wild type counterparts (Figure 5A-I, Appendix A Figure 8). Administration of SS-31 to  $Kl^{+/-}$  mice also resulted in an increased number of MyoD<sup>+</sup> cells at the site of injury, an enhanced regenerative index, and an increased myofiber cross-sectional area (Figure 5J-N). Accordingly,  $Kl^{+/-}$  mice treated with SS-31 display an increased strength recovery after injury that parallels that of wild type counterparts (Figure 5O). Of note, treatment of wild type mice with SS-31 did not alter strength recovery after injury when compared to saline-injected counterparts. Taken together, these findings suggest that the defect in MPC mitochondrial bioenergetics and the accumulation of mtDNA lesions accompanying a loss of  $\alpha$ -Klotho are mediated by disruption of mitochondrial ultrastructure, ultimately resulting in dysfunctional muscle regeneration.

### **2.3.6 Muscle regeneration is enhanced by $\alpha$ -Klotho supplementation**

Given the established hormonal role of  $\alpha$ -Klotho, we next investigated whether supplementation of  $\alpha$ -Klotho may restore mitochondrial function in aged MPCs. We found that when MPCs isolated from aged skeletal muscle were cultured in the presence of recombinant  $\alpha$ -Klotho for 48 hours, the aged mitochondrial phenotype was improved, as determined by decreased mtDNA damage, increased OCR, and increased reserve capacity (Figure 6A-C).

These encouraging *in vitro* findings led us to next probe whether  $\alpha$ -Klotho supplementation may enhance skeletal muscle regeneration *in vivo*. To do this,  $\alpha$ -Klotho was administered to aged mice via osmotic pump. Osmotic pumps were implanted three days prior to injury and were maintained for 14 days post-injury. At the dose tested, we observed a significant increase in local  $\alpha$ -Klotho within the injured muscle areas (Figure 6D, E). Systemic administration of  $\alpha$ -Klotho in aged muscle resulted in an increased number of regenerating fibers

after injury, as determined both by histology and SHG imaging (Figure 6D, F-H). These findings were consistent with an approximately 3.5-fold increase in the number of MyoD<sup>+</sup> cells at the site of injury in animals that received supplementation with  $\alpha$ -Klotho (Figure 6I, J). However, osmotic pump delivery of  $\alpha$ -Klotho yielded no significant increase in myofiber cross sectional area or total muscle area, when compared to saline counterparts.

Given that osmotic pump administration delivers  $\alpha$ -Klotho continuously, we next tested the hypothesis that the timing of  $\alpha$ -Klotho administration may be critical for functional tissue regeneration. To do this, we performed daily intraperitoneal injections of recombinant  $\alpha$ -Klotho to aged mice either from 1-3 days post injury (dpi) or from 3-5 dpi (i.e. the timepoints at which we found *Klotho* to be highly expressed in young muscle (Figure 1G)). Similar to our findings using osmotic pumps,  $\alpha$ -Klotho delivery both from 1-3 dpi and 3-5 dpi resulted in an increased number of regenerating fibers when compared to vehicle controls (Figure 6K, L). Both treatment groups also displayed an increased myofiber area, though the magnitude of the improvement was greater in mice receiving  $\alpha$ -Klotho over 3-5 dpi (Figure 6M). Importantly, only animals receiving  $\alpha$ -Klotho over 3-5 dpi displayed an improved functional recovery (Figure 6N, O, Supplementary Table 1).

Taken together, the data suggest that  $\alpha$ -Klotho is required for an adequate regenerative response to an acute injury, and that supplementation with  $\alpha$ -Klotho via the circulatory system promotes MuSC commitment and myofiber regeneration in aged mice when administered at the appropriate time point. These findings implicate declines in this longevity protein as a contributor to a defective muscle regenerative response with aging and raise the possibility of systemic administration of  $\alpha$ -Klotho as a therapeutic approach to promote the healing of aged skeletal muscle after injury.

## 2.4 Discussion

Though aged muscle typically demonstrates a shift from functional myofiber repair following injury, to a quick-fix default towards fibrosis (10), these age-related declines are reversible. Heterochronic parabiosis, in which circulatory systems of young and old animals are surgically joined, has clearly shown that systemic factors in young animals have a positive impact on the health of older animals (10, 19, 94, 104). Here, we tested the hypothesis that  $\alpha$ -Klotho, a circulating hormone and paracrine factor associated with the attenuation of tissue aging is critical for effective MPC function and muscle regeneration after injury. Unexpectedly, we found that  $\alpha$ -Klotho is highly up-regulated at both the mRNA and protein level locally within the acutely injured muscles of young skeletal muscles. However, the response is markedly attenuated in aged muscles. At the cellular level, we uncovered a role for  $\alpha$ -Klotho in the maintenance of mitochondrial ultrastructure, mtDNA damage, and MPC bioenergetics (Figure 7). Though skeletal muscle  $\alpha$ -Klotho expression under conditions of homeostasis is low (92), the data indicate that expression of  $\alpha$ -Klotho within injured muscle is required for functional regeneration(118). As an alternative, systemic supplementation with  $\alpha$ -Klotho at physiologically-relevant time points may promote muscle regeneration in aged mice.

Previous studies have demonstrated that decreased  $\alpha$ -Klotho levels impair the wound healing response of the skin and small intestine through regulation of stem cell function (107). In dystrophic muscle,  $\alpha$ -Klotho levels are epigenetically repressed at the level of the *Klotho* promoter via DNA methylation and histone modification (117). Our observation that *Klotho* is silenced in normal muscle but poised to lose the repressive marks following an injury, presents a novel mechanism for regulating the contribution of local *Klotho* expression to regeneration after acute injury. It is intriguing that failure to de-repress the *Klotho* promoter in the injury response

contributes to the deficiency of aged muscle regeneration. This may have implications for mechanisms of degeneration or failed regeneration in other tissues where  $\alpha$ -Klotho has been demonstrated to decline with age.

The impaired tissue healing previously observed in  $\alpha$ -Klotho knockout mice is associated with decreased cellular proliferation (107, 141), decreased resistance to stress (141, 142), fibrosis formation (117), and increased senescence (114). Mitochondrial dysfunction is a hallmark of the aged tissue phenotype (143), and, increasingly, mitochondria are emerging as a nexus that modulates cell-wide signaling pathways governing these cellular processes. Among these, Wnt/TGF $\beta$ , insulin growth factor (IGF)-1, and fibroblast growth factor (FGF) signaling, for example, have been shown to be responsive to signals emanating from the mitochondria, predominantly through ROS production (144-147). It is noteworthy that these pathways have been implicated both in the anti-aging effects of  $\alpha$ -Klotho (107, 121, 148) and in age-related declines in muscle regeneration (80, 94, 98, 100, 149). A recent report demonstrated that  $\alpha$ -Klotho inhibits Wnt signaling in aged MuSCs (118). However, a direct role of  $\alpha$ -Klotho on cellular mitochondrial function has remained poorly understood. While an impaired mitochondrial morphology with decreased  $\alpha$ -Klotho levels has been previously demonstrated in  $\alpha$ -Klotho knockout mice (150), it is difficult to discern whether the mitochondrial defects are a primary result of  $\alpha$ -Klotho deficiency, or if they represent a secondary consequence of cumulative tissue dysfunction in these progeroid mice.

It is plausible that the main actions of  $\alpha$ -Klotho and FGF23 on phosphorous homeostasis that are lost in aging and in  $Kl^{+/-}$  mice promotes mitochondrial hyperpolarization and subsequent ROS production due to increased phosphate levels (151). The studies presented here employed gain- and loss-of-function paradigms to demonstrate a direct role for  $\alpha$ -Klotho in the maintenance

of MPC mitochondrial morphology, genome integrity and bioenergetics. Decreased levels of  $\alpha$ -Klotho in MPCs and skeletal muscle were associated with vacuolated mitochondria possessing compromised cristae structure. This loss of architecture may lead to reorganization and oxidation of cardiolipin that, in turn, converts cytochrome c into an oxidant-generating peroxidase (140). The reversal of the aged or  $Kl^{+/-}$  mitochondrial phenotype with SS-31 supports this mechanism, as SS-31 binding to cardiolipin, protects the structure of mitochondrial cristae, prevents cardiolipin interactions with cytochrome c, and promotes oxidative phosphorylation (140). SS-31 administration has also been shown to rejuvenate aged skeletal muscle mitochondrial energetics and performance (56). It was recently shown that restoration of mitochondrial function by replenishing nicotinamide adenine dinucleotide (NAD<sup>+</sup>) levels protects aged MuSCs from senescence and enhances myogenicity (133), further supporting the link between MuSC mitochondrial function and muscle regenerative capacity.

Consistent with induction of an aged phenotype when  $\alpha$ -Klotho expression is inhibited in young MPCs *in vitro*, depletion of  $\alpha$ -Klotho *in vivo* impairs myofiber regeneration and drives fibrosis after an acute injury event.  $\alpha$ -Klotho has been shown to regulate fibrosis formation under conditions of renal pathology, skin lesions and muscular dystrophy (107, 117, 152). The *in vivo* data suggest that, with acute injury,  $\alpha$ -Klotho plays an important role in regulating physiological muscle regenerative cascade. It appears that only a portion of this role is attributed to  $\alpha$ -Klotho within the muscle itself as local inhibition of  $\alpha$ -Klotho results in an attenuated regenerative defect when compared to whole body knockdown. The fact that administration of  $\alpha$ -Klotho enhanced MuSC lineage progression and myofiber regeneration in aged skeletal muscle suggests that supplementation via the circulation may be an effective means to compensate for the regenerative deficit observed in aged animals.

## 2.5 Materials and Methods

### 2.5.1 Animals

C57BL/6 young (4-6 months) and old (22-24 months) mice were received from the Jackson laboratories and NIA rodent colony, respectively. *Kl*<sup>+/-</sup> mice were obtained from MMRRC, UC Davis and were genotyped prior to inclusion in the studies. All procedures were approved by the Institutional Animal Care and Use Committee of the University of Pittsburgh. Animals were ear-tagged, randomly assigned to intervention group, and compared to age-matched littermate controls whenever possible. Mice were evaluated prior to inclusion in the study, and animals with obvious health problems were eliminated. Animal experiments were repeated across a minimum of two separate cohorts of the experimental groups. All primary endpoints were prospectively selected prior to analyses and investigators performing endpoint analysis were blinded to the experimental group whenever possible.

### 2.5.2 Histological analysis of muscle regeneration

Wild-type male C57BL/6 young, *Kl*<sup>+/-</sup> mice, or old mice received injuries to bilateral Tibialis Anterior (TA) muscles via an intramuscular injection of cardiotoxin (10  $\mu$ L of 1 mg/mL). Fourteen days following the injury, TAs were harvested for histological analysis of  $\alpha$ -Klotho, fibrosis (picrosirius red), degenerating myofibers (IgG) and myofiber regeneration (laminin). Second Harmonic Generation (SHG) imaging was performed on isolated TA muscles treated with a non-targeting control or lentiviral knockdown of  $\alpha$ -Klotho, as well as pump-administered

animals in order to visualize collagen and myofibers within the muscle 14 days post injury, as we previously described(153).

### **2.5.3 Primary muscle cell isolation**

MPCs were isolated from young, *Kl<sup>+/-</sup>*, and aged mice, as previously described (154). MuSCs were sorted using FACS for surface markers CD31-, CD45-, Sca1- and VCAM+ (120). A modified protocol was used to isolate MuSCs and FAPs as CD31-, CD45-,  $\alpha$ -7 integrin+ for MuSCs and CD31-, CD45- and  $\alpha$ -7 integrin- for FAPs (155). Gating strategy was based on sorting MuSCs and FAPs over a negative population of CD31 and CD45 (Appendix A Figure 9).

### **2.5.4 Primary muscle cell imaging**

Immunofluorescence staining ( $\alpha$ -Klotho, Tom20 (mitochondrial marker), ki67, MyoD, Pax7 and HMGB1) and senescence-associated beta-galactosidase staining was performed in isolated cells. Transmission electron microscopy of fixed cells was performed, as previously described (154). Structured illumination microscopy was performed in young and old cells stained for  $\alpha$ -Klotho and DAPI.

### **2.5.5 ELISA**

The levels of  $\alpha$ -Klotho protein were measured by a colorimetric sandwich enzyme immunoassay (SEH757Mu, Cloud-Clone Corp), according to manufacturer's instructions. Each sample was measured in duplicate.

### **2.5.6 Hanging-Wire Test**

Strength endurance was tested using the hang-wire test, as in (156). The Hang Impulse (HI) score was calculated as bodyweight (grams) x time hung (seconds). Male mice were used for all testing using C57Bl/6 mice. Wild type and *Kl<sup>+/-</sup>* were females for testing.

### **2.5.7 Inhibition of and supplementation with $\alpha$ -Klotho**

MPCs were treated with 25 nmol of silencing RNA (siRNA) to  $\alpha$ -Klotho (GE Dharmacon, Product no.SO2462181G) for 48 hours. As a control, young MPCs were treated with a non-targeting (scramble) siRNA. Aged MPCs were treated with 0.05  $\mu$ g/mL exogenous  $\alpha$ -Klotho (R & D systems, Product no. aa 34-981), added to the culture media for 48 hours.

### **2.5.8 Epigenetic regulation of $\alpha$ -Klotho**

At baseline, three, seven, and fourteen days after injury, TAs were snap frozen using liquid nitrogen for gene expression, methylation specific PCR (MSPCR), and chromatin immunoprecipitation (ChIP) analysis, essentially as previously described (157).

### **2.5.9 Analysis of MPC bioenergetics and mitochondrial DNA damage**

Oxygen consumption rate (OCR) and extracellular acidification rate (ECAR) were measured in real time using a Seahorse XFe96 Extracellular Flux Analyzer (Billerica, MA) as previously described (134). The basal OCR was measured by averaging the OCR values before

treating the cells with oligomycin. Total reserve capacity was calculated by the differences of OCR between treatment with FCCP and 2DG and basal values. Mitochondrial DNA damage was quantified as previously described (136, 138).

#### **2.5.10 SS-31 administration**

Isotonic saline or SS-31 (3 mg/kg dissolved in saline at 0.3 mg/mL) was administered daily via an i.p. injection to wild-type and *Kl<sup>+/-</sup>* animals for the entire duration of injury (56). For *in vitro* experiments, 100 nM of SS-31 was administered to MPCs isolated from *Kl<sup>+/-</sup>* animals for 48 hours. Dosing was based on studies demonstrating the effectiveness in a mouse model of chronic cardiomyopathy (158) as well as *in vitro* dose ranging studies performed in C2C12s to evaluate inhibition of stress-induced mitochondrial membrane hyperpolarization and ROS generation.

#### **2.5.11 In-vivo lentiviral knockdown of $\alpha$ -Klotho**

*In-vivo*  $\alpha$ -Klotho knockdown was done using lentiviral vectors for a SMARTpool of  $2.0 \times 10^5$  TU/TA or  $3.82 \times 10^6$  TU/TA shRNA to  $\alpha$ -Klotho per TA muscle. Given that there was no significant difference in the local  $\alpha$ -Klotho expression between the two treatment groups, samples across the two treatment groups were pooled for analysis. Control animals received equal volumes of empty lentiviral vector. Knockdown was maintained for three weeks, after which time bilateral TAs were injured. Histology or SHG imaging was performed 14 days after injury.

### **2.5.12 Supplementation of $\alpha$ -Klotho in vivo**

Mini osmotic pumps containing either saline or  $\alpha$ -Klotho (324 pg/ml in saline vehicle) were inserted subcutaneously into aged mice. After 2 days, bilateral TA muscles were injured by intramuscular CTX injection (as above). Osmotic pumps remained implanted until euthanasia 14 days post injury. Isotonic saline or  $\alpha$ -Klotho (10  $\mu$ g/kg body weight) was administered to aged animals via daily intraperitoneal injections over days 1-3 post-injury or 3-5 days post-injury. The TAs were then harvested 14 days post injury and preserved for histology or SHG analysis. Blood serum was also collected to evaluate circulating  $\alpha$ -Klotho levels via ELISA. The activity of  $\alpha$ -Klotho was confirmed as previously described (159).

### **2.5.13 Data Availability**

The data supporting the results of this paper can be made available by the corresponding author upon reasonable request.

## **2.6 Acknowledgements**

The study was supported by NIA R01AG052978 (F.A.), NIEHS R01 AG052978 (F.A. and A.B.), grant NIEHS R01 ES023696 (F.A. and A.B.), grant R56 grant AG052978-01 (F.A. and B.V.H.) and the William N. & Bernice E. Bumpus Foundation Innovation Award (L.H.S.). The authors thank Gregory Gibson, Mike Calderon, and Callen Wallace from the Center of Biological Imaging, University of Pittsburgh for their guidance with high-resolution microscopy,

Evan Howlett and Dr. Claudia Gonzalez Hunt for their help with analyzing mtDNA damage, as well as Zachary Clemens and Abish Pius for their help with data collection and analysis. Finally, we acknowledge the NIH-supported microscopy resources in the Center for Biologic Imaging (Grant #1S10OD019973-01).

## **2.7 Author Information-Affiliations**

Department of Physical Medicine and Rehabilitation, University of Pittsburgh, Pittsburgh, 15213, PA, USA

A. Sahu, H. Mamiya, S. N. Shinde, A. Cheikhi, L. L. Winter & F. Ambrosio

Department of Environmental and Occupational Health, University of Pittsburgh, Pittsburgh, 15261, PA, USA

A. Sahu, A. Barchowsky & F. Ambrosio

Department of Bioengineering, University of Pittsburgh, Pittsburgh, 15260, PA, USA

H. Mamiya, L. L. Winter & F. Ambrosio

Division of Geriatric Medicine, Department of Medicine, University of Pittsburgh, Pittsburgh, 15213, PA, USA

A. Cheikhi

Department of Orthopaedic Surgery, University of Pittsburgh, Pittsburgh, 15213, PA, USA

N. V. Vo & F. Ambrosio

Department of Pathology, University of Pittsburgh, Pittsburgh, 15261, PA, USA

N. V. Vo

Department of Cell Biology, University of Pittsburgh, Pittsburgh, 15261, PA, USA

D. Stolz & C. St. Croix

Department of Pharmacology & Chemical Biology, University of Pittsburgh Cancer Institute,  
University of Pittsburgh, Pittsburgh, 15232, PA, USA

V. Roginskaya, B. Van Houten & A. Barchowsky

Department of Environmental Health and Engineering, Johns Hopkins Bloomberg School of  
Public Health, Baltimore, 21218-2608, MD, USA

W. Y. Tang

Department of Neurology, Duke University School of Medicine, Durham, 27704, NC, USA

L. H. Sanders

Research Beyond Borders: Boehringer-Ingelheim Pharmaceuticals, Ridgefield, 06877, CT, USA

M. Franti

Department of Neurology and Neurological Sciences, Stanford University School of Medicine,  
Stanford, CA, 94305, USA

T. A. Rando

The Paul F. Glenn Center for the Biology of Aging, Stanford University School of Medicine,  
Stanford, CA, 94305, USA

T. A. Rando

Center for Tissue Regeneration, Restoration and Repair, Veterans Affairs Hospital, Palo Alto,  
CA, 94036, USA

T. A. Rando

McGowan Institute for Regenerative Medicine, University of Pittsburgh, Pittsburgh, 15219, PA,  
USA

F. Ambrosio

## 2.8 Contributions

F.A. and A.S. provided the concept, idea and experimental design for the studies. F.A. wrote the manuscript. A.S., H.M. and S.N.S. provided data collection, analyses, interpretation, and review of the manuscript. A.C. provided data analyses, interpretation and review of the manuscript. L.L.W. provided data collection and analyses. V.R. provided data collection. N.V.V. and W.Y.T. provided data interpretation and review of the manuscript. D.S. provided data interpretation. C.S.C. provided data analysis and interpretation. L.H.S. and B.V.H. provided data analysis, interpretation, and manuscript review. M.F. provided consultation with research design. T.A.R and A.B. provided consultation with data interpretation and review of the manuscript.

## 2.9 Figures

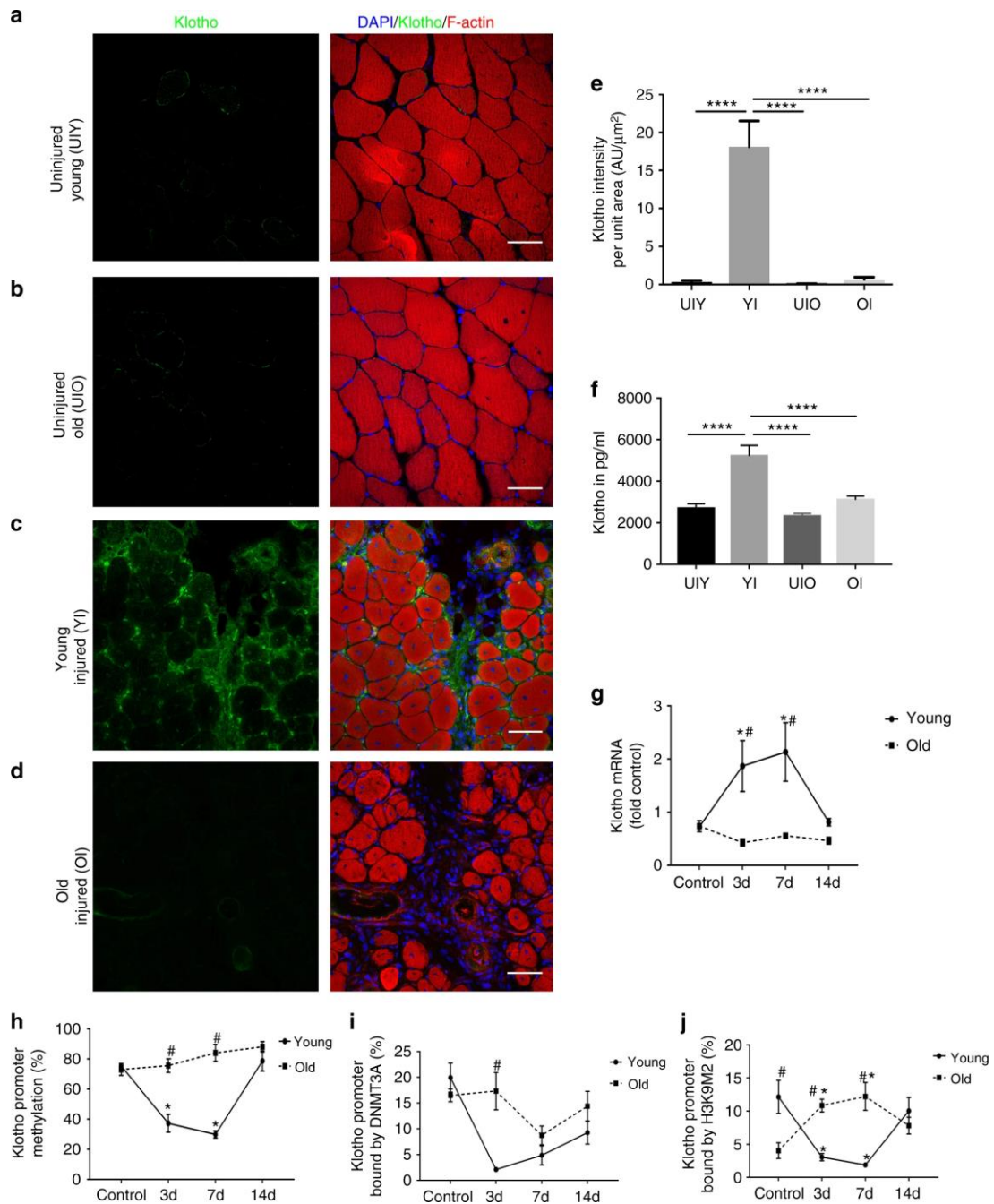


**Figure 1.  $\alpha$ -Klotho is increased in young muscle after injury, but the response is absent with age.**

(A-D) Immunofluorescent imaging of  $\alpha$ -Klotho and F-actin in skeletal muscle from uninjured young (UIY; 4-6 months) and old mice (UIO; 22-24 months) as well as 14 days post injury (dpi) in young (YI) and old (OI) mice (scale=50  $\mu$ m)

(E) Quantification of  $\alpha$ -Klotho across the four comparison groups, UIY, UOI, YI, and OI. Experimental cohorts were performed in duplicate, n=3/group/cohort. \*\*\*\*p<0.0001 (F) ELISA analysis of serum obtained from UIY, UOI, YI and OI mice. (n=8-11/group; \*\*\*\*p<0.0001). (G) RT-PCR analysis of  $\alpha$ -Klotho in young and old muscles at 0 (control), 3, 7, and 14 dpi (n=4/age/time-point) (H) MSPCR analysis of young and old muscle at 0 (control), 3, 7 and 14 dpi. (n=4/age/timepoint). (I) ChIP analysis of DNMT3a in young and old muscle at 0 (control), 3, 7 and 14 dpi (n=4/age/timepoint). (J) ChIP analysis of H3K9me2 in the Klotho promoter in young and old muscle at 0 (control), 3, 7 and 14 dpi (n=4/age/timepoint). (\*p<0.05 compared to young, sex-matched uninjured muscles; #p<0.05 indicates a significant difference between young and aged groups at the respective time-point. (E-G) One-way ANOVA with Tukey's post hoc test. (H-J) Two-way ANOVA with Tukey's post hoc test. Data represented as mean + SEM.

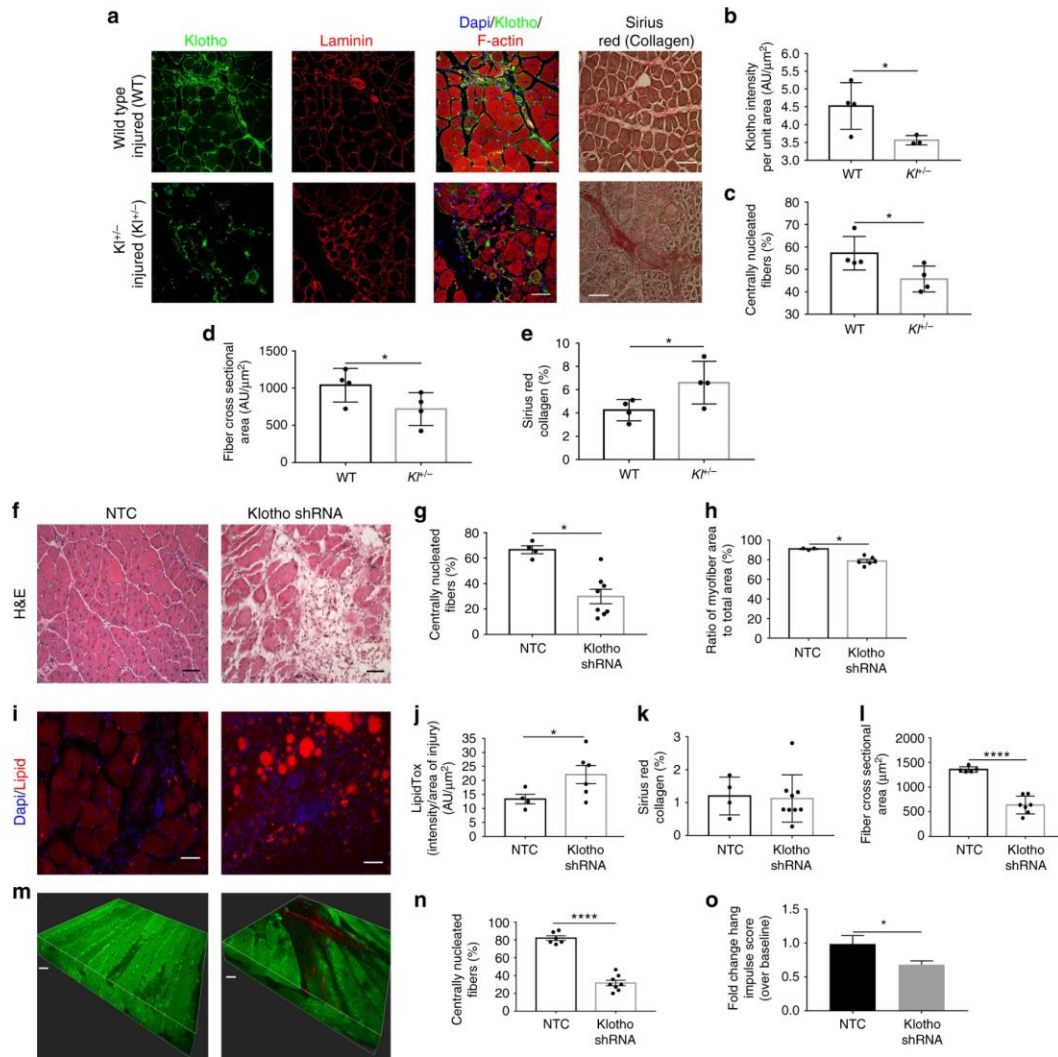


**Figure 2. Genetic and muscle-specific loss of  $\alpha$ -Klotho impairs skeletal muscle regeneration.**

(A) Immunofluorescence of  $\alpha$ -Klotho, laminin, F-actin and Sirius red stain and in wild type and  $Kl^{+/-}$  mice 14 dpi. Scale: 50  $\mu\text{m}$ . (B) Quantitation of  $\alpha$ -Klotho in wild type versus  $Kl^{+/-}$  mice 14 dpi. (n=3-4/group; \* $p < 0.05$ , one-tailed Student's t-test). (C, D, E) Quantitation of the % of centrally nucleated fibers (n=4/group; \* $p < 0.05$ , Mann-Whitney test), fiber cross-sectional area (n=4/group; \* $p < 0.05$ , one-tailed Student's t-test) and collagen (Sirius red) deposition (n=4/group; \* $p < 0.05$ , Student's t-test with Welch's correction). (F) Representative Hematoxylin & Eosin stain of non-targeting control (NTC) and shRNA to  $\alpha$ -Klotho ( $0.2\text{-}3.82 \times 10^6$  TU/TA) Scale: 50  $\mu\text{m}$ . (G, H) Quantification of the % centrally nucleated fibers and ratio of myofiber area to total area, respectively, in NTC and Klotho shRNA-treated mice at 14 dpi (n=4-8/group; \* $p < 0.05$ , Mann-Whitney U test). (I) Representative immunofluorescence imaging of lipid in NTC and  $\alpha$ -Klotho shRNA treated muscle at 14 dpi. Scale: 50  $\mu\text{m}$ . (J) Quantification of lipid in NTC and Klotho shRNA treated muscle 14 dpi (n=4-6/group; \* $p < 0.05$ , one-tailed Student's t-test). (K) Quantification of collagen deposition (Sirius red) in NTC and Klotho shRNA groups (n=4-8/group;  $p > 0.05$ ,

Student's t-test). (L) Quantification of fiber cross-sectional area of regenerating muscle fibers in NTC and  $\alpha$ -Klotho shRNA treated muscle (n=5-7/group; \*\*\*\*p<0.0001, Student's t-test). (M) Representative second harmonic generation (SHG) images of tibialis anterior (TA) muscles injected with NTC or  $\alpha$ -Klotho shRNA. Scale: 30  $\mu$ m. (N) SHG quantification of the regeneration index in NTC and Klotho shRNA treated mice at 14 dpi (n=6-8/group; \*\*\*\*p<0.0001, one-tailed Student's t-test). (O) Hang impulse (calculated as hanging time x mouse weight) at 14 dpi represented as a fold-change from baseline score pre-injury (n=6/group; \*p<0.05, one-tailed Student's t-test). Data represented as mean + SEM.

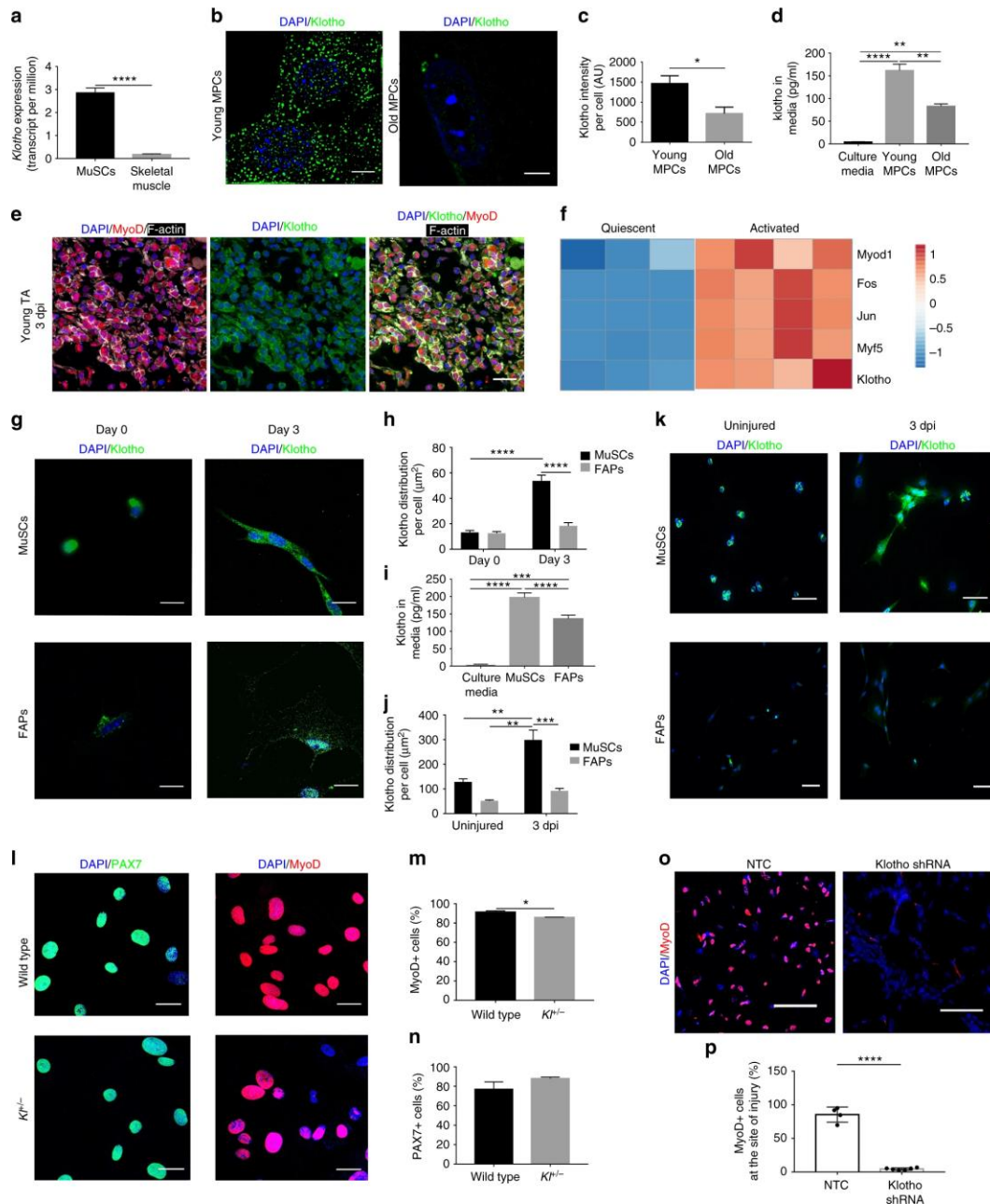


**Figure 3.  $\alpha$ -Klotho expression in quiescent and activated MuSCs.**

(A) Klotho expression in isolated MuSCs versus whole muscle lysates as per RNAseq analysis in transcripts per million (TPM) ( $n=4/\text{group}$ ;  $****p<0.0001$ , one-tailed Student's t-test). (B) Representative structured illumination microscopy of  $\alpha$ -Klotho in young and old MPCs. Scale: 5  $\mu\text{m}$ . (C) Quantification of  $\alpha$ -Klotho in young and old MPCs ( $*p<0.05$ , student t-test). (D) ELISA analysis of  $\alpha$ -Klotho in culture media alone, as well as conditioned media from young and old MPCs ( $n=3/\text{group}$ ;  $**p<0.01$ ,  $****p<0.0001$ , one-way ANOVA with Tukey's post hoc test). (E) Immunofluorescent co-localization of MyoD, F-actin and  $\alpha$ -Klotho 3 dpi. Scale: 50  $\mu\text{m}$  (F) Heat-map representation of  $\alpha$ -Klotho as well as markers of MuSC activation (MyoD1, Fos, Jun, Myf5) in quiescent and activated cells from

RNASeq analysis of cells from a recent report. (G) Immunofluorescence staining of  $\alpha$ -Klotho and DAPI in sorted MuSCs and fibroadipogenic progenitors (FAPs) fixed immediately after isolation (Day 0) or after activation in culture (Day 3). Scale: 12.5  $\mu$ m. (H). Quantification of  $\alpha$ -Klotho expression in MuSCs and FAPs at Day 0 and Day 3 (\*\*\*\* $p$ <0.0001, two-way ANOVA with Tukey's post hoc test). (I). Quantification of  $\alpha$ -Klotho in the conditioned media of MuSCs and FAPs sorted from uninjured muscle. Conditioned media was obtained after 3 days in culture (n=3/group; \*\*\*\* $p$ <0.0001, one-way ANOVA with Tukey's post hoc test). (J) Quantification of  $\alpha$ -Klotho in MuSCs and FAPs isolated from uninjured muscle and muscle 3 dpi (\*\* $p$ <0.01, \*\*\* $p$ <0.001, two-way ANOVA with Tukey's post hoc test). (K) Immunofluorescence imaging of  $\alpha$ -Klotho and DAPI in MuSCs and FAPs sorted from uninjured muscle and muscle 3 dpi. Scale: 50  $\mu$ m. (L) Immunofluorescent imaging of Pax7 and MyoD in MPCs isolated from wild type and Kl<sup>+/-</sup> mice. Scale: 50  $\mu$ m. (M) Quantification of the % of MyoD<sup>+</sup> cells in MPCs from wild type and Kl<sup>+/-</sup> mice (\* $p$ <0.05, one-tailed Student's t-test). (N) Quantification of the % of Pax7<sup>+</sup> cells in MPCs from wild type and Kl<sup>+/-</sup> mice (\* $p$ <0.05, one-tailed Student's t-test). (O) Immunofluorescent imaging of MyoD and DAPI in the injured muscles of non-targeting control (NTC) and shRNA to  $\alpha$ -Klotho 14 dpi. Scale: 25  $\mu$ m (P) Quantification of the percentage of MyoD<sup>+</sup> nuclei within the injured muscles of non-targeting control (NTC) and shRNA to  $\alpha$ -Klotho 14 dpi (n=4-6/group; \*\*\*\* $p$ <0.0001, one-tailed Student's t-test). Data represented as mean + SEM.

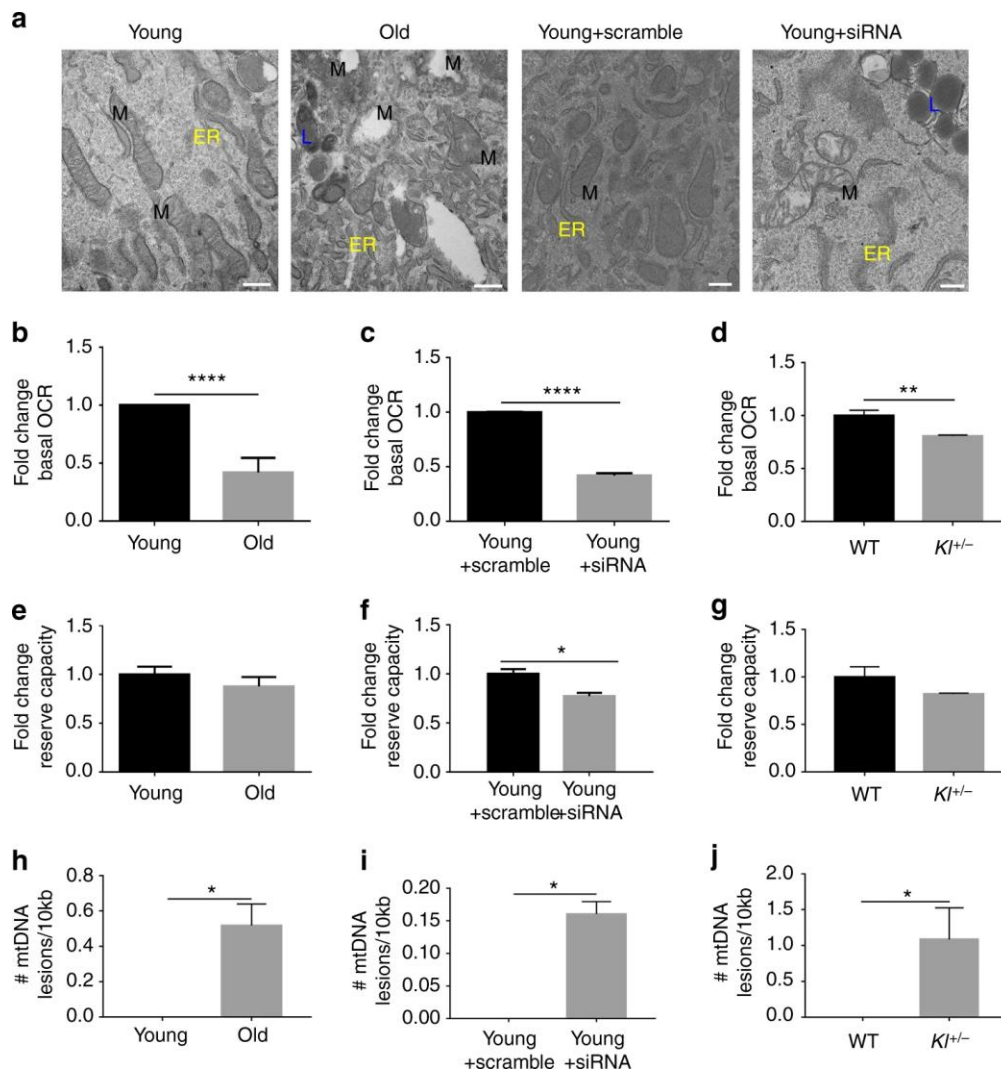


**Figure 4. Loss of  $\alpha$ -Klotho drives mitochondrial dysfunction and disrupts mitochondrial DNA integrity.**

(A) TEM images of young, old, young+scramble and young+siRNA MPCs showing mitochondria (M), lipid droplet accumulation (L), as well as endoplasmic reticuli (ER). Scale: 400 nm. (B, C) Seahorse analysis of young, old, young+scramble and young+siRNA MPCs quantifying the basal oxygen consumption rate (OCR) (D) Seahorse analysis of basal OCR on MPCs isolated from wild-type and KI<sup>+/-</sup> mice. (E, F) Seahorse analysis of reserve capacity (calculated as the difference between basal and maximum OCR) of young, old, young+scramble and young+siRNA MPCs. (G) Seahorse analysis of reserve capacity of MPCs isolated from wild-type and KI<sup>+/-</sup> mice. (H, I) RT-PCR based analysis of mtDNA damage in young, old, young+scramble and young+siRNA MPCs. (J) RT-PCR analysis of mtDNA damage in MPCs isolated from wild-type and KI<sup>+/-</sup> mice. (\*p<0.05, \*\*p<0.01, \*\*\*\*p<0.0001, one-tailed Student's t-test). Data represented as mean + SEM.

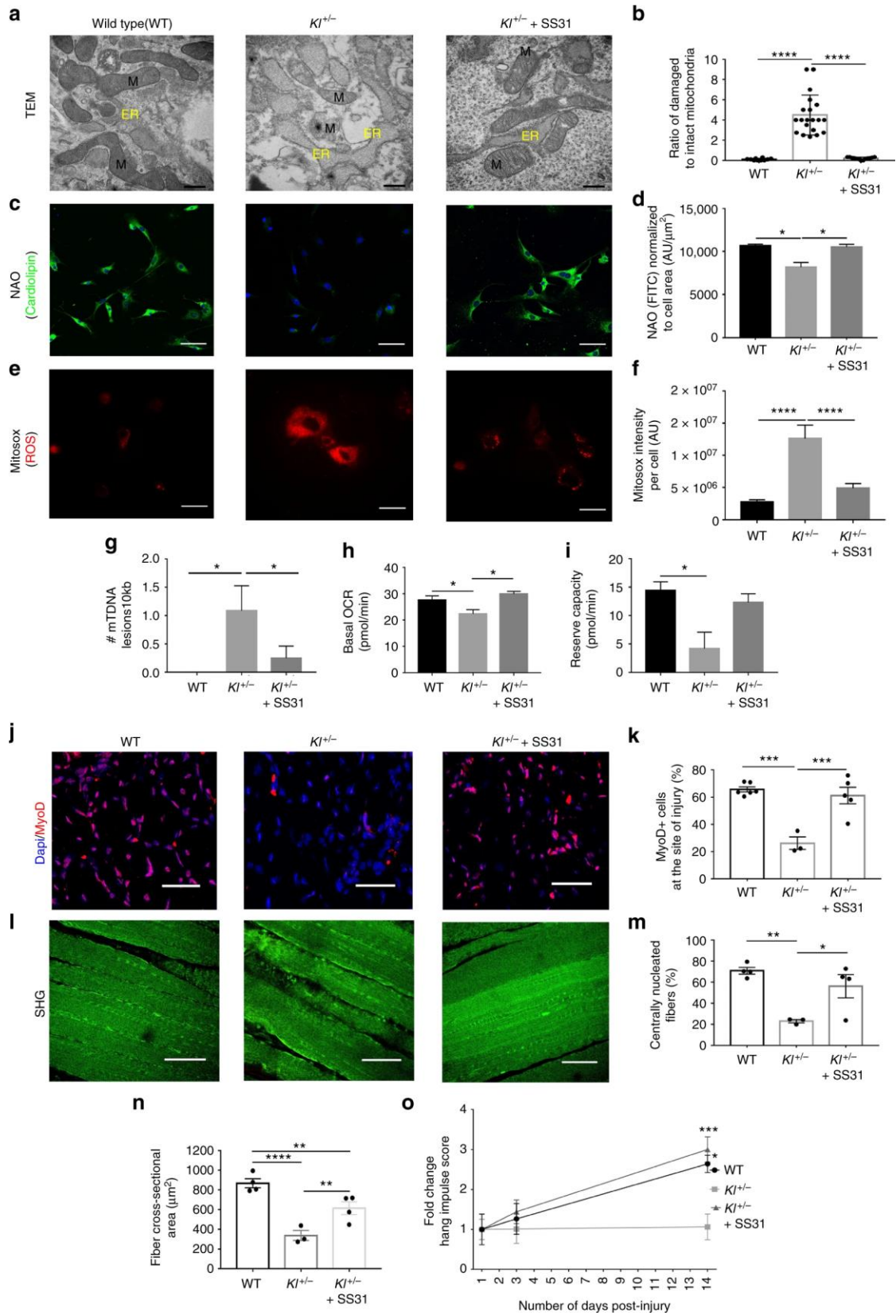
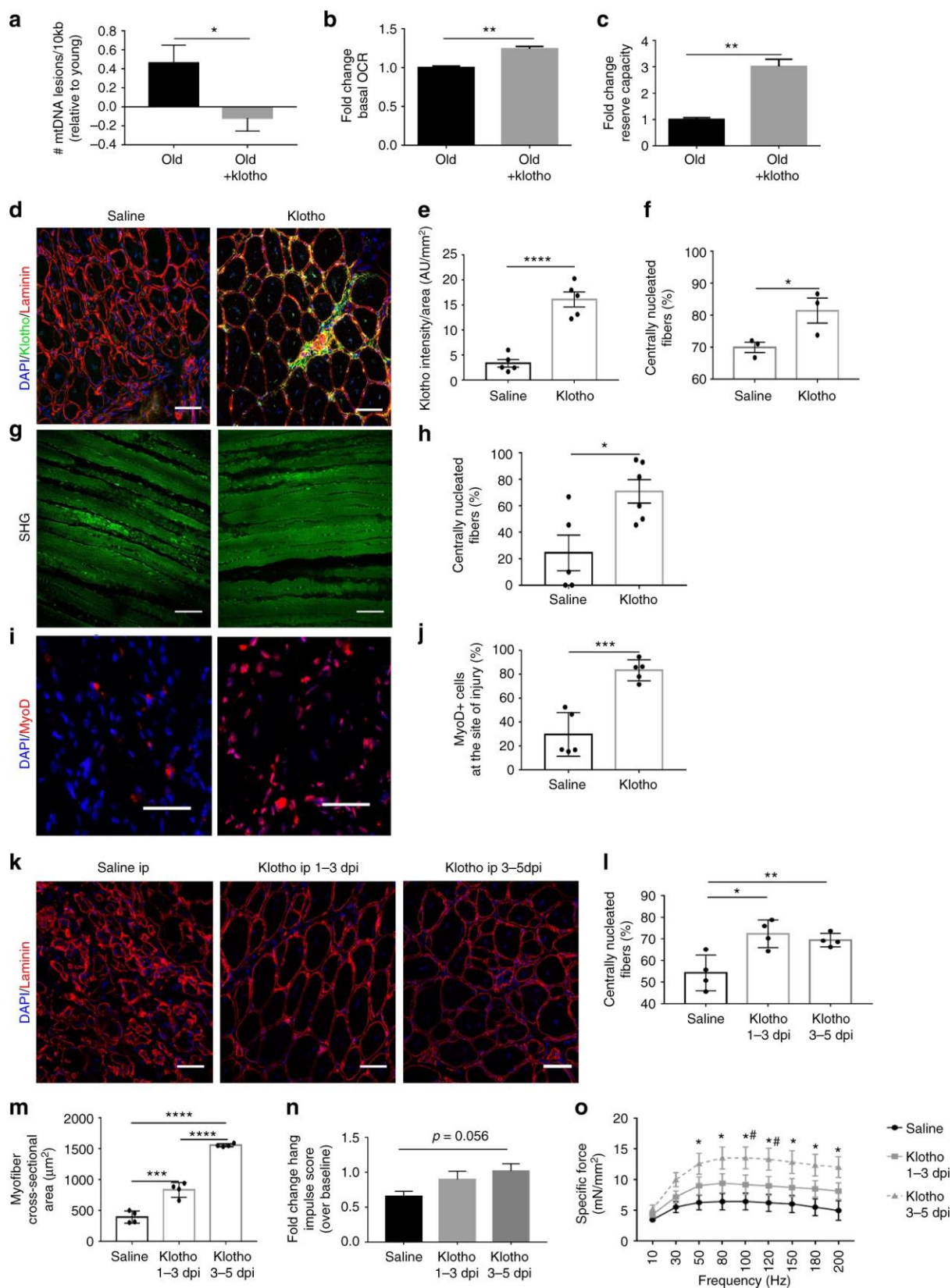


Figure 5. Mitochondrial structure and function are impaired in  $KI^{+/-}$  mice, but are rescued with SS-31.

(A, B) Representative TEM images and analysis of damaged mitochondria of wild-type (WT), K1+/- and K1+/- + SS-31 groups (10-20 images were analyzed to quantify >100 mitochondria/group; \*\*\*\*p<0.0001, one-way ANOVA with Tukey's post hoc test). Scale: 500 nm. (C, D) Representative immunofluorescent images and quantification of cardiolipin content, by Nonyl Acridine Orange staining (NAO, Red) in WT, K1+/- and K1+/- + SS-31 MPCs (\*p<0.05, one-way ANOVA with Tukey's post hoc test). Scale: 50  $\mu$ m. (E, F) Representative immunofluorescent images from live imaging and quantification of ROS as determined by MitoSox staining (Green) on live cells from WT, K1+/- and K1+/- + SS-31 group (\*\*\*\*p<0.0001, one-way ANOVA with Tukey's post hoc test). Scale: 50  $\mu$ m. (G) RT-PCR-based analysis of mtDNA damage on WT, K1+/- and K1+/- + SS-31 MPCs (n=3/group; \*p<0.05, one-way ANOVA with Tukey's post hoc test). (H, I) Seahorse analysis of basal OCR and reserve capacity of WT, K1+/- and K1+/- + SS-31 MPCs (n=4-6/group; \*p<0.05, one-way ANOVA with Tukey's post hoc test). (J, K) Quantification of MyoD+ cells at the site of injury of TA muscles from WT, K1+/- and K1+/- + SS-31 groups (n=3-6/group; \*\*\*p<0.001, one-way ANOVA with Tukey's post hoc test). Scale: 25  $\mu$ m. (L, M) Representative SHG images and analysis of the percentage of centrally nucleated fibers from WT, K1+/- and K1+/- + SS-31 mice at 14 dpi (n=3-4/group; \*p<0.05, \*\*p<0.01, one-way ANOVA with Tukey's post hoc test). Scale: 50  $\mu$ m. (N) Quantification of myofiber cross-sectional area from WT, K1+/- and K1+/- + SS-31 groups (n=3-4/group; \*p<0.05, \*\*p<0.01, one-way ANOVA with Tukey's post hoc test). (O) Hang impulse (calculated as hanging time x mouse weight) at 14 dpi, represented as a fold-change from 1 dpi score during the wire hang test (n=3-6/group; \*p<0.05, \*\*\*p<0.001, two-way ANOVA with Tukey's post hoc test). Each mouse was used as its own control in order to account for baseline variability (shown in Appendix A Figure 8). Data represented as mean + SEM.



**Figure 6.  $\alpha$ -Klotho supplementation improves aged MPC bioenergetics and muscle regeneration.**

(A) RT-PCR-based analysis of mtDNA damage in old and MPCs and in old MPCs that received supplementation with recombinant  $\alpha$ -Klotho in the culture medium for 48 hours ((n=3/group; \*p<0.05, one-tailed Student's t-test). (B, C) Seahorse analysis of basal OCR and reserve capacity of age and aged+  $\alpha$ -Klotho MPCs (n=6-8/group; \*\*p<0.01). (D, E) Representative immunofluorescent images and quantification of  $\alpha$ -Klotho expression in aged muscle 14 dpi after systemic supplementation of  $\alpha$ -Klotho via an osmotic pump, as compared to saline-infused control muscles (n=3/group; \*p<0.05). Scale: 50  $\mu$ m. (F) Quantification of the percentage of centrally nucleated fibers as per histological analysis across saline and  $\alpha$ -Klotho infused animals 14 dpi (n=3/group; \*p<0.05). (G, H) Representative SHG imaging and quantification of the percentage of centrally nucleated fibers of saline versus  $\alpha$ -Klotho infused animals at 14 dpi (n=5-6/group; \*p<0.05). Scale: 35  $\mu$ m. (I, J) Representative images and quantification of MyoD+ cells at the site of injury 14 dpi in animals receiving osmotic pump delivery of saline or  $\alpha$ -Klotho (n=5/group; \*\*\*p<0.001). Scale: 25  $\mu$ m. (K) Representative immunofluorescent images showing laminin and DAPI in animals receiving i.p. administration of saline,  $\alpha$ -Klotho 1-3 dpi and  $\alpha$ -Klotho 3-5 dpi. Scale: 50  $\mu$ m. (L) Quantification of percentage of centrally nucleated fibers in aged animals receiving i.p. administration of saline,  $\alpha$ -Klotho 1-3 dpi and  $\alpha$ -Klotho 3-5 dpi (n=4/group; \*p<0.05, \*\*p<0.01). (M) Quantification of fiber cross-sectional area across the three i.p. injection groups (n=4/group; \*\*\*p<0.001, \*\*\*\*p<0.0001). (N) Fold-change hang impulse score over baseline scores across the 3 i.p. injection groups (n=6/group). (O) Force-frequency curves obtained from in-situ contractile testing analysis of specific force (n=6-8/group, \*p<0.05 when comparing  $\alpha$ -Klotho 3-5 dpi with saline control, #p<0.05 when comparing  $\alpha$ -Klotho 3-5 dpi with  $\alpha$ -Klotho 1-3 dpi group; two way ANOVA with repeated measures). (A-J) one-tailed Student's t-test. (K-N) one-way ANOVA with Tukey's post hoc test. Data represented as mean + SEM.

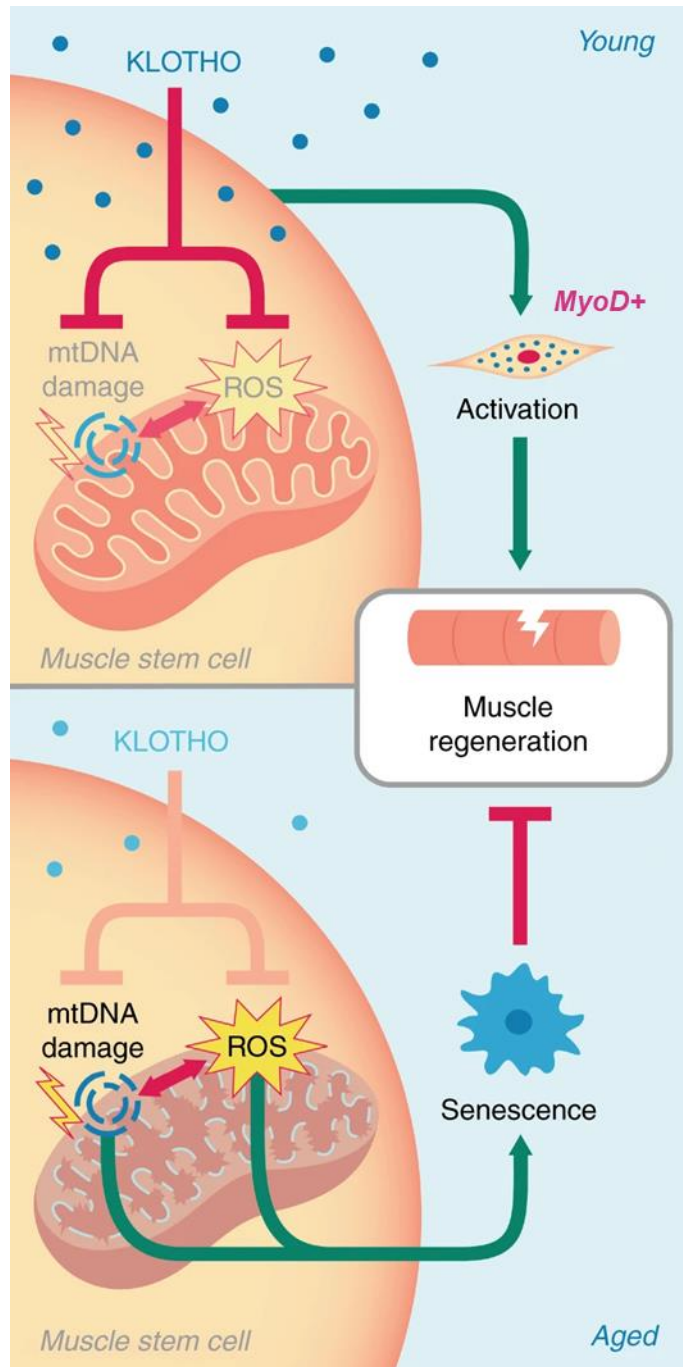


**Figure 7. Hypothesis schematic.**

Youthful levels of the circulating hormone  $\alpha$ -Klotho are critical for the maintenance of muscle stem cell (MuSC) mitochondrial ultrastructure, thereby limiting mtDNA damage and mitochondrial ROS production. This maintenance of healthy mitochondria within MuSCs is required for muscle stem cell activation and contribution to functional skeletal muscle regeneration. However, age-related declines in  $\alpha$ -Klotho causes disrupted mitochondrial ultrastructure, increased mtDNA damage, and ROS accumulation, resulting in cellular senescence and impaired skeletal muscle regeneration.

### **3.0 Extracellular Vesicle Delivery of Klotho Transcripts Rejuvenates Aged Stem Cell Progeny**

Data presented here has been prepared for submission to *Nature* and is currently in the re-submission process.

Contributing Authors:

Amrita Sahu, Amin Cheikhi, Sunita Shinde, Zachary Clemens, Abish Pius, Hikaru Mamiya, Silvia Picciolini, Cristiano Carlomagno, Alice Gualerzi, Marzia Bedoni, Bennett Van Houten, Aaron Barchowsky, Fabrisia Ambrosio

#### **3.1 Abstract**

While heterochronic parabiosis studies have linked age-related impairments of tissue regeneration to changes in circulating factors, none have evaluated whether circulating extracellular vesicles (EVs) mediate these alterations over time. Here, we employed an unsupervised machine learning approach on Raman scattering-based analyses for population-level profiling of EVs isolated from young and aged mice. Although EV protein content was essentially unaltered, nucleic acid content declined with age. Further interrogation revealed that the transfer of Klotho mRNAs from young EVs to target muscle stem cell progeny enhances mitochondrial integrity, but that Klotho mRNA content was significantly decreased in aged EVs. In vivo, intramuscular transplantation of young EVs improved functional regeneration in aged mice. However, this benefit was diminished when EVs were derived from Klotho<sup>+/-</sup> mice. Collectively, these studies

demonstrate that Klotho transcripts within circulating EVs mediate intercellular communications crucial for the regenerative cascade.

### **3.2 Introduction**

Circulating factors play crucial roles in regulating tissue homeostasis and organismal aging. One empirical approach to identify these factors and the effects they have on target tissues involves the surgical joining of a young and an old mouse, or heterochronic parabiosis.

Heterochronic parabiosis couples the circulatory systems of the two animals such that the aged parabiont is exposed to circulatory factors from the young parabiont, and vice versa (17). This model has provided valuable insight into the influence of age-associated humeral factors on stem cell function and tissue regeneration. Notably, studies demonstrate that young mice exposed to blood from aged mice decreased muscle regeneration, whereas old mice exposed to blood from young mice displayed improved muscle stem cell (MuSC) regenerative capacity (94, 104). These studies imply a non-cell autonomous, systemic regulation of muscle aging.

Accumulating evidence suggests that a large portion of the circulating secretome is packaged within membranous nanovesicles, or extracellular vesicles (EVs). EVs are couriers of genetic material and proteins that have the potential to traffic between anatomically remote sites (160, 161). Emerging evidence suggests that mRNA cargoes within EVs can target and reprogram cells in a range of tissues to regulate physiological functions or pathophysiological processes (84). EVs have been identified in most bodily fluids including plasma, serum, urine, saliva, and cerebrospinal fluid (161-167). However, whether EVs serve as carriers of transcripts that

propagate the “rejuvenating” effects of heterochronic parabiosis on the regeneration of aged muscle has yet to be elucidated.

One blood-borne factor that might be instrumental in mediating the crosstalk between the circulation and muscle cells is the longevity protein,  $\alpha$ -Klotho (Klotho)(92). Epidemiological studies have positively associated circulating Klotho with skeletal muscle strength and function (110, 111, 168). In contrast, skeletal muscle aging and a decline in Klotho levels were concomitant with mitochondrial dysfunction (169), as well as a decrease in MuSC regenerative capacity (118, 169). Thus far, the beneficial effects of Klotho have been primarily ascribed to its circulating protein form (170). Whether and how Klotho contained within circulating EVs may attenuate age-related alterations in tissue maintenance and regeneration has not been investigated.

Here, we show that depletion of EVs eliminates the beneficial effect of young serum on the bioenergetics of target MuSC progeny, and that the impact of EVs on target cell mitochondrial function is a result of Klotho mRNA transfer. Machine learning classifiers further reveal that aging disrupts EV population heterogeneity through a selective loss of CD63<sup>+</sup> extracellular vesicles, which we demonstrate preferentially contain Klotho mRNAs. *In vivo*, we show that Klotho mRNA content within EVs supports muscle regeneration after acute injury. While transplantation of young EVs enhanced the functional recovery of aged muscle, this benefit was lost when young EVs were derived from Klotho<sup>+/-</sup> mice. Using this gain- or loss-of-function approach, we demonstrate that Klotho transcripts within CD63<sup>+</sup> EVs mediate intercellular communications crucial for the regenerative cascade.

### 3.3 Results

#### 3.3.1 Circulating extracellular vesicles modulate the bioenergetics of target cells in an age-dependent manner

Circulating factors are critical determinants of skeletal muscle regeneration, and previous studies have shown that exposure of aged MuSCs to young serum *in vitro* increases myogenic potential (94, 104). Consistent with these previous reports, we found that expression of MyoD, a master regulator of myogenesis (171), is increased in aged MuSC progeny when cultured in the presence of young serum (Figure 8A, B). Given that impaired mitochondrial function has been shown to contribute to aberrant myogenic lineage specification of MuSCs (133, 169, 172), we also evaluated the impact of young versus aged serum on mitochondrial respiration. Aged muscle progenitor cells cultured in the presence of young serum displayed a significantly increased basal oxygen consumption rate when compared to cells exposed to aged serum (Figure 8C). Young serum also improved mitochondrial integrity of aged progenitor cells, as demonstrated by a 1.5-fold increase in the mitochondrial inner membrane phospholipid, cardiolipin (Figure 8D, E). Cardiolipin plays a key role in the maintenance of mitochondrial membrane integrity, as well as the modulation of oxidative phosphorylation (173). These findings support the hypothesis that serum-derived components preserve target cell mitochondrial ultrastructure and bioenergetics in an age-dependent manner.

EVs are membrane-enclosed paracrine mediators that have been shown to be capable of mitochondrial quality control and activation of the metabolic machinery within recipient cells (174). To determine whether EVs contribute to the observed effects of young serum on muscle progenitor cell mitochondrial function, we depleted young and aged serum of circulating EVs (Figure 8F). Immunocytochemical analysis of MyoD and live cell assessment of respiration

revealed that the beneficial effect of young serum on target cell MyoD expression and bioenergetics was lost in the absence of circulating EVs (Figure 8G-I).

### **3.3.2 Aging causes a significant loss of CD63+ EVs but not of CD81+ and CD9+ EVs**

The above findings suggest that circulating EVs may regulate the bioenergetics of target muscle progenitor cells, but that aging disrupts this information flow. The transfer of information between EVs and their target cells is mediated by a wide range of EV cargoes, including cytosolic proteins, membrane proteins, mRNAs, noncoding RNAs, and even DNA (160). However, age-associated changes in the circulating EV structure and cargo have not yet been thoroughly investigated. Therefore, we performed an in-depth analysis of young and aged EVs that were isolated using size-exclusion chromatography (qEVsingle, iZON columns). Nanoparticle tracking analysis using the NanoSight apparatus (Product# NS300) confirmed that the size of isolated EVs was less than 200 nm in diameter (Figure 9A), which falls within the size-range for small- to mid-sized EVs (175). Interestingly, aged serum yielded a significantly higher concentration of nanoparticles when compared to young serum (Figure 9A).

NanoSight quantifies the total concentration of nanoparticles in a non-discriminant manner, thereby including microvesicles, exosomes and apoptotic bodies. Therefore, we used an in-cell western blot technique to evaluate the expression of the three well-established EV markers, CD63, CD81 and CD9 (175). These data suggest that aging creates a notable preferential shift in the membrane composition of CD63 expression when compared to CD81 and CD9 (Figure 9B-D, Appendix B Figure 1). The findings were further confirmed with a label-free approach for multiplexed detection of CD63 using surface plasmon resonance imaging (SPRi) (Figure 9E).

To address the physiological relevance of age-related changes in EV composition, we evaluated the direct effect of young or aged EVs on target muscle progenitor cell responses. Consistent with serum co-culture experiments described above, we found that aged cells cultured in the presence of young EVs, but not old EVs, displayed increased MyoD expression and mitochondrial cardiolipin content (Figure 9G, H). These findings suggest that EVs and/or EV cargoes are internalized by recipient progenitor cells to modulate cellular responses, and that functional communication is disrupted with aging.

### **3.3.3 EV nucleic acid content is compromised with aging**

To better understand whether age-related alterations in EV cargo underlie alterations in target cell responses, we next performed Raman spectroscopy analysis of young and aged EVs. This method allows for bulk characterization of EV biochemical composition according to light scattering properties (176). Qualitative EV differences as a function of age were evaluated by subtracting the aged EV spectra from the young, and the resulting Raman spectral peaks were assigned to functional chemical groups, as previously described (177). Interestingly, there were no appreciable differences in the protein content of EVs according to age, which we further confirmed by a bicinchoninic acid assay (Figure 10A-C). However, aged EVs displayed a marked decrease ( $\Delta$  Intensity > 0.2) in the Raman shift bands that are attributable to nucleic acids and a concomitant increase in lipid content. These findings suggest that aging drives remodeling of EV genetic cargo and membrane composition, respectively. A hybrid model of unsupervised (Principal Component Analysis) and supervised (Linear Discriminant Analysis) dimension reduction techniques were then used to graphically express the differential variance of EVs

according to age (Figure 10D, E). Taken together, the label-free and non-invasive Raman fingerprints revealed a distinct biochemical profile of aged EV cargoes.

### **3.3.4 Klotho transcripts are abundant in young EVs, but their content is decreased with age**

We next sought to identify specific alterations in the EV cargo that may contribute to changes in target cell responses. The data presented thus far suggest that aging disrupts EV composition and the transfer of mitochondrially-targeted information to recipient MuSC progeny. Our recent studies have shown that Klotho, considered to be a “longevity” protein, supports mitochondrial function in MuSCs (169). While young MuSCs highly express and secrete the Klotho protein, MuSC Klotho levels significantly decline with increasing age (169). We posited that the transfer of EV cargo alters Klotho protein within recipient cells, thereby regulating mitochondrial function.

To test this hypothesis, aged muscle progenitor cells were cultured either in the presence or absence of young serum-derived EVs. Immunofluorescence imaging revealed that Klotho protein in target cells increased by ~40% when cells were exposed to young EVs (Figure 11 A, B). ELISA analysis of conditioned media further demonstrated that cells cultured in the presence of young EVs displayed increased Klotho expression and secretion (Figure 11 C), suggesting that EVs also promoted Klotho secretion by recipient cells. Cells cultured with aged EVs, however, displayed significantly decreased Klotho protein levels when compared to cells cultured with young EVs (Appendix B Figure 2).

To more directly implicate Klotho signals originating from the EVs, we sought to test the impact of EVs isolated from Klotho<sup>-/-</sup> mice on Klotho protein levels in target muscle progenitors. However, we found that EVs from Klotho<sup>-/-</sup> mice were toxic to the cells, presumably because of the severe progeroid phenotype of these mice (92). We then cultured cells in the presence of EVs

isolated from the serum of either *Klotho*<sup>+/-</sup> mice or age- and sex-matched wild type control mice. Indeed, the increased *Klotho* protein levels observed when aged cells were incubated with young *Klotho*<sup>+/+</sup> EVs was blunted when the EVs were isolated from young *Klotho*<sup>+/-</sup> mice (Figure 11D).

Given these data, we asked whether EVs carry and transmit the *Klotho* protein in an age-dependent manner. While EVs within urine have been shown to express the *Klotho* protein (178), *Klotho* protein within serum-derived EVs has not been previously reported. Surface Plasmon Resonance imaging (SPRi) analysis revealed that circulating EVs do indeed contain *Klotho* protein on their membranes (Figure 11 E, F). However, levels were unaltered with aging (Figure 11 E, F). These findings suggest that *Klotho* protein within EVs is not likely to explain the age-related changes in EV function on target cells.

The Raman spectroscopy-based finding that aged EVs display a marked decline in nucleic acids content prompted us to next test whether the increase in *Klotho* protein by target muscle progenitors may be a result of the transfer of genetically encoded information by EVs. Valadi and colleagues first demonstrated that mRNAs packaged within the EVs are functional and capable of being translated when in the presence of the requisite protein machinery of the target cells (84). To detect and quantify *Klotho* mRNA within peripheral EVs, we designed a set of *Klotho* oligonucleotides to probe for *Klotho* transcripts. Digital PCR revealed that young EVs contained abundant levels of *Klotho* mRNAs, but that aged EVs exhibited approximately 25% decrease in *Klotho* mRNA content (Figure 11 G). Moreover, EVs isolated from serum of *Kl*<sup>+/-</sup> mice expressed ~70% less *Klotho* mRNA content compared to wild type controls (Figure 11 H).

To more directly test whether EV-derived *Klotho* mRNA is a source of *Klotho* protein within target cells, we evaluated whether treatment of young EVs with a small interference RNA to *Klotho* would abate the *Klotho* response of recipient progenitors. Digital PCR confirmed a

decrease in Klotho mRNA of approximately 20% when EVs were treated with siRNA to Klotho (Appendix B Figure 3). After 48 hours of co-culture, we found that Klotho protein in aged muscle progenitors exposed to siRNA treated EVs was significantly lower than that from cells cultured in the presence of EVs treated with a scramble siRNA (Figure 11 I).

To rule out the possibility that the effect of EVs on progenitor cell Klotho protein expression may result from the transmission of some transcriptional regulator that promotes endogenous Klotho mRNA expression in target cells, we delivered young EVs to muscle progenitor cells isolated from Klotho<sup>-/-</sup> mice, which lack a functional endogenous Klotho locus. Just as was observed in wild type cells, Klotho<sup>-/-</sup> cells cultured in the presence of young EVs displayed a significant increase in Klotho protein, and the effect was blunted following treatment with siRNA (Figure 11 J). Taken together, these findings support the hypothesis that circulating EVs increase Klotho protein within target cells via the transfer of Klotho mRNA.

### **3.3.5 Klotho mRNA cargoes of circulating EVs enhance muscle functional recovery after injury**

Next, we designed a series of studies to evaluate whether EVs isolated from the circulation may contribute, upon transplantation, to the skeletal muscle regenerative cascade after an acute injury. To induce a muscle injury, aged animals received cardiotoxin injections to bilateral tibialis anterior muscles. The average functional defect one day after injury is approximately 50% of baseline levels (Appendix B Figure 4), as determined by hanging grid impulse score (179). To minimize variability in the extent of injury in experimental groups, only those animals with a functional deficit within the 25-75% percentile one-day post-injury score were randomized to receive either an intramuscular injection of EVs or an equal volume of saline at three days after injury (Figure 12 A, Appendix B Figure 4). We chose three days post injury since this is a time

point of both peak MuSC activation and Klotho expression (169). *In situ* contractile testing of TA muscles two weeks after injury revealed an increase in peak tetanic force in muscles that received EV transplantation (Figure 12 B-D). Histological analysis revealed that treatment with EVs also resulted in an increase in the cross-sectional area of regenerating fibers (Figure 12 B-D), consistent with the enhanced force generation. To directly test whether these enhanced regenerative features were due to the presence of Klotho transcripts in the EVs, we also injected EVs isolated from young Klotho<sup>+/-</sup> animals into injured muscles. Results revealed that the transplantation of Klotho<sup>+/-</sup> EVs failed to enhance the functional recovery of aged muscle (Figure 12 E).

### 3.4 Discussion

The studies presented here show that EVs regulate mitochondrial integrity and function in target cells through the transfer of Klotho transcripts. Aging, however, creates a shift in EV subpopulation heterogeneity, resulting in decreased storage of Klotho mRNAs. The consequence is impaired mitochondrial function of target MuSC progeny, ultimately contributing to a dysfunctional regenerative response.

While it has been challenging to associate surface marker expression with a specific tissue source, it is clear that EV subpopulations induce distinct effects on recipient cells. The current understanding is that RNAs are actively apportioned to specific EV subpopulations (180). In the context of miRNAs, for example, specific short motifs underlie selective sorting into exosomes (a subpopulation of EVs)(180). Further studies are needed to understand the mechanisms by which Klotho mRNA could be apportioned to a subpopulation of EVs. Moreover, the precise

mechanisms controlling the observed age-related decline in Klotho mRNA cargoes within EVs have yet to be elucidated. We posit that the impact of aging on mRNA storage may be a reflection of the overall “stressed” state of an aged organism. In support of this hypothesis, Eldh et al proposed that exosomes released by oxidatively stressed murine mast cells display altered mRNA cargoes when compared to unstressed counterparts, though exosomal protein content remained unaltered (181). In the acute state, the exosomes released from stressed cells were shown to induce a beneficial effect on distal target cells (181). Under chronic conditions such as aging, however, signals communicated by circulating EVs may become less supportive—and potentially deleterious—in nature.

The *in vivo* studies presented suggest that the transplantation of circulating EVs enriched with Klotho mRNAs enhance skeletal muscle regeneration in aged mice. While our studies focused on evaluating the impact of age-related alterations in bioenergetics of MuSC progeny, it is also possible that neighboring cell populations (ie. fibro-adipogenic progenitors, inflammatory cells, and/or fibroblasts) may have also been the targets of exogenous EVs. Future studies should evaluate whether these neighboring cell populations may be differentially responsive to EV cargo, and Klotho mRNAs mediate these responses. In addition, the development of novel approaches to enhance the localization and retention of transplanted EVs are warranted.

## **3.5 Methods**

### **3.5.1 Serum and muscle progenitor cell isolation**

Serum of young and aged C57/BL6 mice (obtained from Jackson laboratories and NIA Rodent colony, respectively), as well as *Klotho*<sup>+/+</sup>, *Klotho*<sup>+/-</sup> and *Klotho*<sup>-/-</sup> mice (original breeders obtained from MMRCC, UC Davis) were isolated blood obtained from animals using a cardiac puncture. Skeletal muscle progenitor cells were isolated from aged C57/BL6 (22-24 months) and *Klotho*<sup>-/-</sup> male mice (8 weeks), using a previously described protocol(169).

### **3.5.2 Immunofluorescence imaging**

Immunofluorescence staining for *Klotho* (R&D systems, MAB1819) and MyoD (SCBT, sc-760) as well as nonyl acridine orange (NAO) staining (Thermofisher, A1372) for cardiolipin content was performed on aged cells across experimental groups. Muscle sections were analyzed for fiber cross-sectional area using an antibody against Laminin (Abcam, ab11575). Imaging was performed at 20X magnification on Zeiss-Axiovision microscope.

### **3.5.3 Analysis of cellular bioenergetics**

Oxygen consumption rate (OCR) was measured in real time using a Seahorse XFe96 Extracellular Flux Analyzer (Billerica, MA) as previously described(134).

### **3.5.4 EV isolation and characterization**

EVs were isolated from serum of young, aged, Klotho<sup>+/+</sup> and Klotho<sup>+/-</sup> animals using size-exclusion chromatography (qEVsingle-35 nm iZON columns) according to manufacturer's instructions. The EVs were characterized for size by Nanoparticle Tracking Analysis on aNanoSight NS300. EVs were then characterized for CD63 (SCBT 5275), CD81(SCBT 23962) and CD9 (SCBT 13118) markers using in-well western blot. EV marker CD63 was further confirmed using SPRi.

### **3.5.5 SPR imaging and analysis**

EVs were injected into the flow cell of the SPRi instrument XelPleX (Horiba Scientific SAS). The EVs were then injected over a gold chip (SPRi-Biochip, Palaiseau, France) onto which antibodies against CD63 and Klotho were spotted using a micro-spotter (SPRi Arrayer, Horiba). EzSuite software and OriginLab software were used to analyze the collected sensograms.

### **3.5.6 Raman Spectroscopy**

Young and aged EVs isolated by size-exclusion chromatography were concentrated by an ultracentrifugation step (100,000 g x 70min). These EVs were then analyzed by means of Raman spectroscopy (LabRAM, Horiba Jobin Yvon S.A.S. Lille, France) following a previous published protocol (176).

### **3.5.7 ELISA**

Aged muscle progenitor cells were cultured at 10,000 cells per well of an 8-well chamber slide, for 24 hours prior to treatment with young EVs. The conditioned media was collected 48 hours post-administration and levels of Klotho protein in conditioned media were measured by a colorimetric sandwich enzyme immunoassay (SEH757Mu, Cloud-Clone Corp), according to manufacturer's instructions. The protein concentration was then normalized to total number of cells per well.

### **3.5.8 Functional and histological analysis of muscle regeneration of injured animals**

All experiments were performed with prior approval from the Institutional Animal Care and Use Committee of the University of Pittsburgh. Wild-type male C57BL/6 (22-24 months) and Klotho<sup>+/-</sup> mice (4-7 months) mice received injuries to bilateral Tibialis Anterior (TA) muscles via an intramuscular (i.m.) injection of cardiotoxin (10  $\mu$ L of 1 mg/mL). Three days post-injury, the animals received 20-30  $\mu$ L of bilateral i.m. injections of EVs, and in situ contractile testing was performed using a previously described protocol two weeks after injury (153). The overall muscle endurance of mice was tested at one- and 13-days post injury using a modified hanging-grid test (169, 179). The hang time for each mouse was normalized to mouse weight (179). TAs were harvested for histological analysis of myofiber regeneration using an antibody against Laminin (Abcam, ab11575). All animals were randomly assigned to intervention group based on their baseline hang-impulse scores and were compared to age-matched littermate controls whenever possible.

### **3.5.9 Steps to ensure rigor**

For all experiments, investigators performing endpoint analyses were blinded to the treatment group. To do this, animals were ear-tagged for in vivo analyses, and samples were number-coded. Animals with obvious health problems were eliminated prior to inclusion in the study. All animals meeting criteria for inclusion were then randomly assigned to treatment groups.

### **3.6 Data Availability**

The data supporting the results of this paper can be made available by the corresponding author upon reasonable request.

### **3.7 Code Availability**

The OriginLab plugin “Principal Component Analysis for Spectroscopy” was used to generate PCAs for Raman Spectroscopy data.

### **3.8 Acknowledgments**

These studies were supported by NIA R01AG052978 (FA) and UPMC Enterprises (FA). The authors thank the genomics core at the University of Pittsburgh for processing samples for digital PCR.

### 3.9 Author information-Affiliations

Department of Physical Medicine and Rehabilitation, University of Pittsburgh, Pittsburgh, 15213, PA, USA

A. Sahu, A. Cheikhi, S. N. Shinde, Z. Clemens, A. Pius, H. Mamiya & F. Ambrosio

Department of Environmental and Occupational Health, University of Pittsburgh, Pittsburgh, 15261, PA, USA

A. Sahu, A. Barchowsky & F. Ambrosio

Division of Geriatric Medicine, Department of Medicine, University of Pittsburgh, Pittsburgh, 15213, PA, USA

A. Cheikhi

Department of Bioengineering, University of Pittsburgh, Pittsburgh, 15260, PA, USA

H. Mamiya & F. Ambrosio

Laboratory of Nanomedicine and Clinical Biophotonics (LABION), Fondazione Don Carlo Gnocchi, Milan, Italy

S. Picciolini, C. Carlomagno, A. Gualerzi & M. Bedoni

Department of Pharmacology & Chemical Biology, University of Pittsburgh Cancer Institute, University of Pittsburgh, Pittsburgh, 15232, PA, USA

B. Van Houten & A. Barchowsky

McGowan Institute for Regenerative Medicine, University of Pittsburgh, Pittsburgh, 15219, PA, USA

F. Ambrosio

### **3.10 Author Contributions**

F.A., A.S and A.C. provided the concept, idea and experimental design for the studies. F.A., A.S. and A.C wrote the manuscript. A.S., A.C., S.N.S, Z.C, A.P and H.M. provided data collection, analyses, interpretation and review of the manuscript. S.P., C.C., A.G. provided data collection and analyses. M.B. provided data interpretation and manuscript review. B.V.H. provided data analysis, interpretation and manuscript review. A.B. provided consultation with data interpretation and review of the manuscript. F.A. provided funding for the studies.

### 3.11 Figures

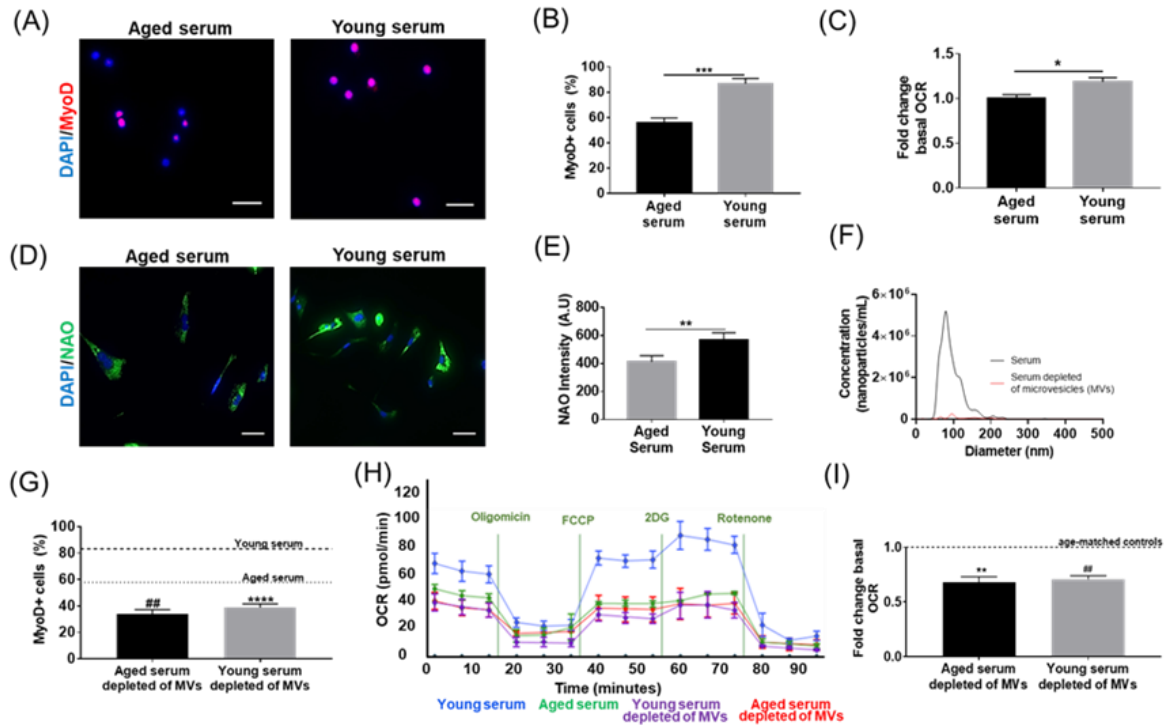


**Figure 8. Aged muscle progenitor cells (MPCs) cultured in the presence of young serum display and extracellular vesicle-dependent increase in MyoD expression and bioenergetics.**

(A) Immunofluorescent imaging of MyoD and DAPI in aged MPCs cultured with serum from aged or young mice. Scale: 25  $\mu\text{m}$ . (B) Quantification of MyoD across the groups ( $***p < 0.001$ , one-tailed Mann Whitney test,  $n=73-88$  cells/group). (C) Seahorse analysis of oxygen consumption rates (OCR,  $*p < 0.05$ , one-tailed Student's t test). (D) Immunofluorescent imaging of cardiolipin (NAO) in aged MPCs cultured with young or aged serum. Scale: 50  $\mu\text{m}$  (E) Quantification of cardiolipin content across groups ( $*p < 0.05$ , one-tailed Mann Whitney test). (F) Representative nanoparticle tracking curve for nanoparticle concentration of young serum and young serum depleted of EVs diluted 1:1000. (G) Quantification of MyoD in aged MPCs cultured with EV-depleted serum ( $****p < 0.0001$   $##p < 0.01$  when compared to age-matched controls, one-tailed Student's t test). (H) Representative bioenergetics profile of three independent experiments of aged cells treated with young and aged serum with or without EVs. (I) Seahorse analysis of aged MPCs treated with young and aged serum depleted of EVs ( $**p < 0.01$   $##p < 0.01$  when compared to age-matched controls, one-tailed Student's t test). Seahorse data are represented as the fold change of mean + sem of the three time points prior to oligomycin treatment, performed in 3-8 wells per experiment across three independent experimental setup.

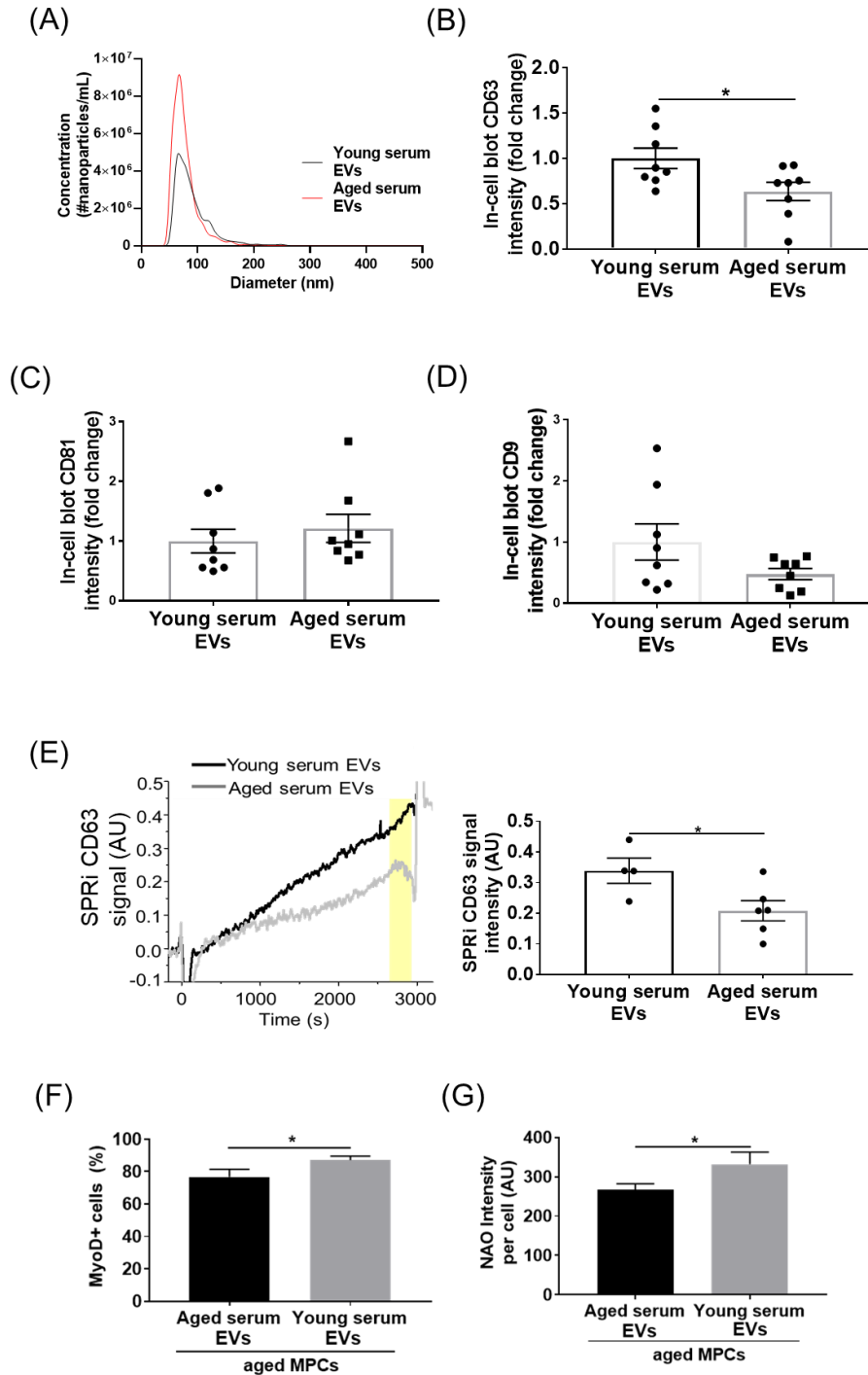


**Figure 9. Aging drives a noticeable loss of CD63+ EV subpopulation.**

(A) Histogram of concentration of nanoparticles in young and aged serum EVs. (B-D) Quantification of CD63, CD81 and CD9 expression per EV using in-cell western blot (\* $p < 0.05$ , one-tailed Mann Whitney test,  $n = 8$ /group). (E) Quantification of EV CD63 expression using Surface Plasmon Resonance imaging. Yellow bar indicates end of injection of EVs (\* $p < 0.05$ , one-tailed Student's t-test,  $n = 4-6$ /group). (F, G) Quantification of MyoD-positive aged muscle progenitor cells (MPCs) and cardiolipin content of aged MPCs upon exposure to young and aged EVs. (\* $p < 0.05$ , one-tailed Student's t-test, 97-183 cells/group).

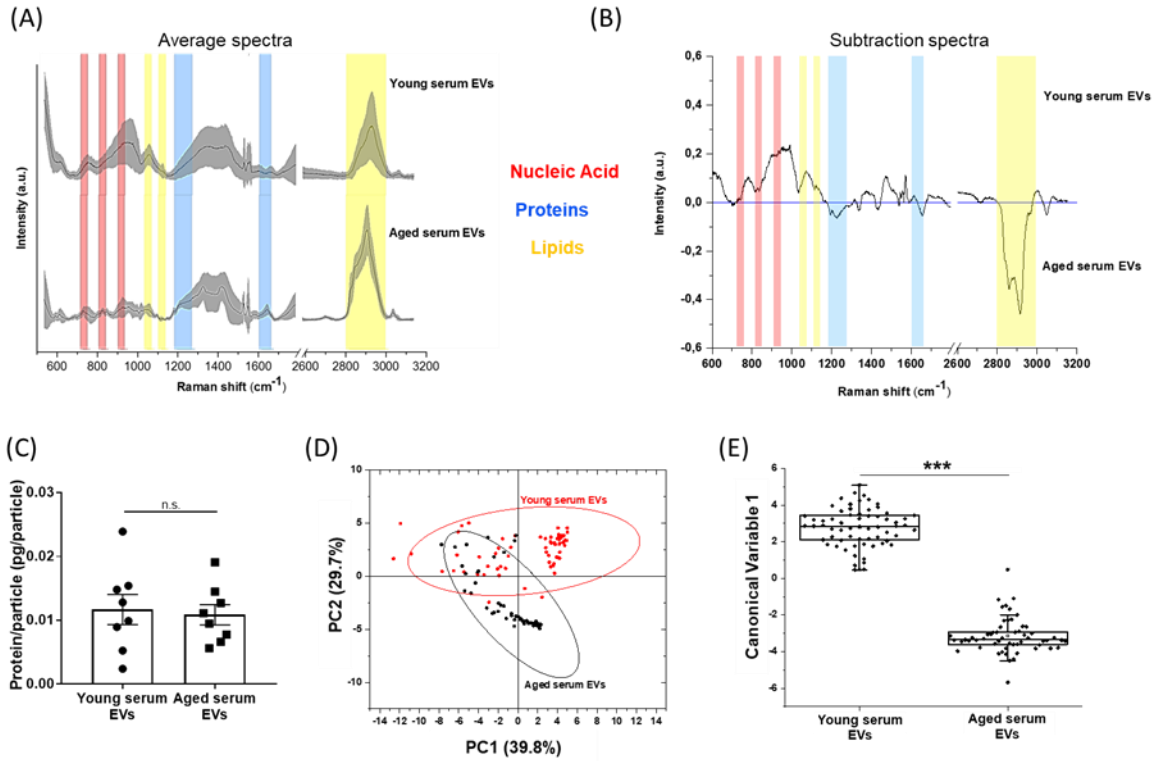


**Figure 10. Aging results in a distinct biochemical fingerprint of circulating EVs.**

(A) Average Raman spectra with standard deviation (grey band) of young and aged serum EVs. (B) Subtraction spectrum of the differences between the average spectra acquired for young and aged serum EVs. (C) Quantification of protein content per nanoparticle isolated using BCA assay. (D) Principal Component Analysis (PCA) with confidence interval of 95% and (E) Linear Discriminant Analysis of data acquired from aged and young serum EVs ( $n=5/\text{group}$ ;  $***p<0.001$ , Mann Whitney test).

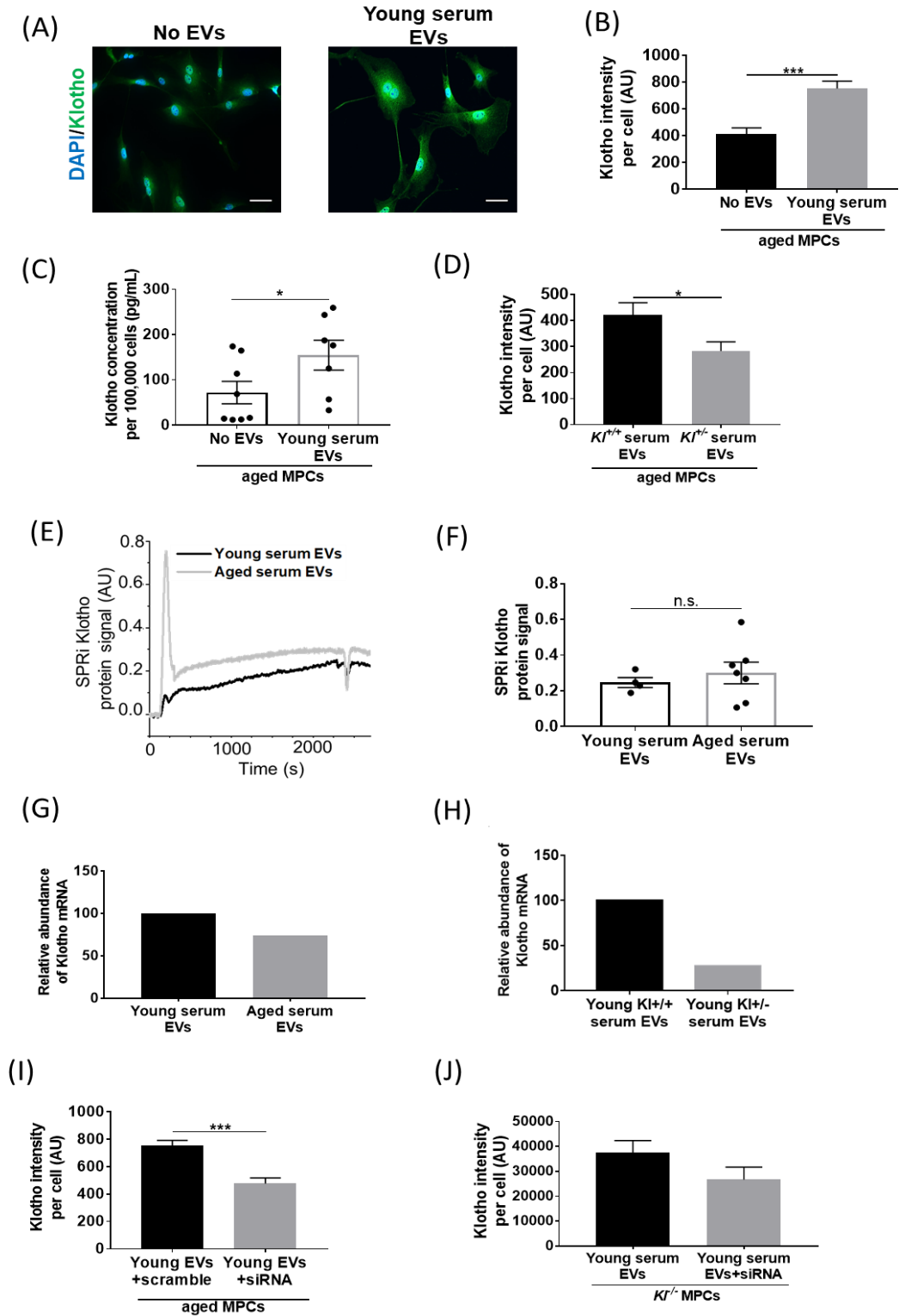


**Figure 11. Klotho mRNAs are preferentially contained within EVs in an age-dependent manner.**

(A) Immunofluorescent imaging of Klotho and DAPI in aged muscle progenitor cells (MPCs) cultured in the presence or absence of young EVs in culturing media. Scale: 50  $\mu$ m. (B) Quantification of Klotho in aged MPCs treated with

and without EVs. (\*\* $p < 0.001$ , one-tailed Mann Whitney test,  $n=66-119$  cells/group). (C) ELISA based quantification of Klotho in conditioned media of aged MPCs treated with and without young EVs. ( $*p < 0.05$ , one-tailed Student's  $t$  test,  $n=7-8$ /group). (D) Quantification of Klotho in aged MPCs receiving EVs isolated from  $Kl^{+/+}$  and  $Kl^{-/-}$  serum. ( $*p < 0.05$ , one-tailed Welch's  $t$  test,  $n=126-144$ /group) (E, F) Surface Plasmon Resonance imaging (SPRi) analysis of Klotho protein in young and aged serum EVs. ( $p > 0.05$ , one-tailed Student's  $t$  test,  $n=4-7$ /group). (G) Quantification of Klotho mRNA in young and aged EVs based on digital PCR. Data represent the total Klotho mRNA abundance after pooling of four different samples. (H) Quantification of Klotho mRNA in  $Kl^{+/+}$  and  $Kl^{-/-}$  serum EVs based on digital PCR. Data represent the total Klotho mRNA abundance after pooling of four different samples. (I) Quantification of Klotho protein in aged MPCs receiving young EVs and young EVs treated with siRNA to Klotho (\*\* $*p < 0.001$ , one-tailed Mann Whitney test,  $n=68-104$  cells/group). Datasets of  $Kl^{-/-}$  MPCs treated with young EVs and EVs treated with non-targeting siRNA were pooled since there was no statistical difference between the two groups. (J) Quantification of Klotho protein in  $Kl^{-/-}$  MPCs receiving young EVs and young EVs treated with siRNA to Klotho ( $p=0.08$ , one-tailed Mann Whitney test).

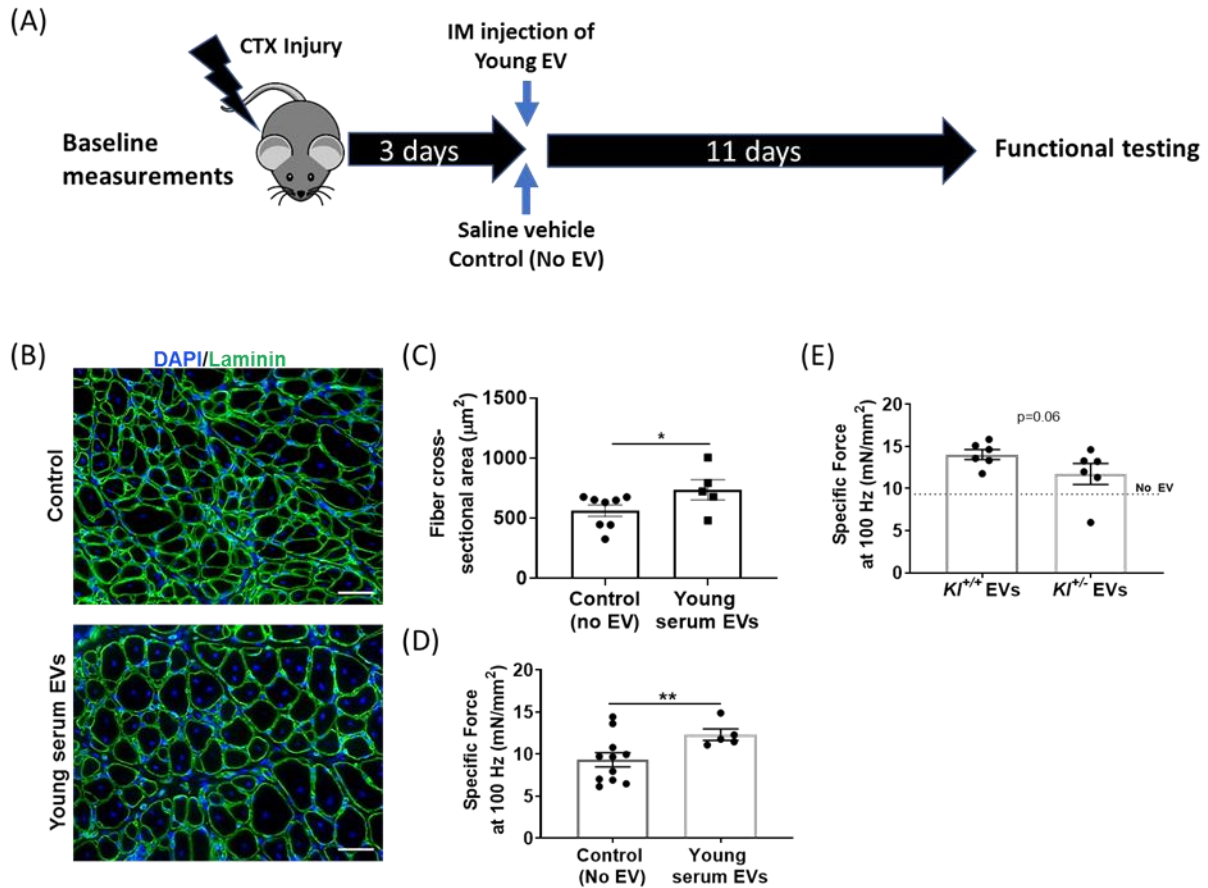


**Figure 12. Klotho mRNA within EVs contribute to the functional regeneration of aged animals.**

(A) Schematic of the in vivo administration of EVs to injured aged mice. (B, C) Histological analysis of fiber cross-sectional area of injured TAs of aged mice receiving young EVs. (\*p < 0.05, Mann-Whitney test, n = 5-8/group). (D) Quantification of specific tetanic force at 100 Hz for control aged animals and aged animals receiving intramuscular injection of young EVs when compared to saline-injected controls. (\*p < 0.05, Mann-Whitney test, n = 5-11/group). (E) Specific peak tetanic force of aged animals receiving EVs isolated from *Kltho*<sup>+/+</sup> or *Kltho*<sup>+/-</sup> serum (p = 0.06, one-tailed Student's t test, n = 6/group).

## **4.0 Conclusions, Discussion and Future Directions**

### **4.1 Circulating Klotho Regulates Cellular Senescence and Mitochondria in MuSCs**

Klotho plays a crucial role in regulating cellular senescence and oxidative stress (91). In vascular and epithelial cells, induction of senescence is inhibited with administration of Klotho (182). Likewise, our studies demonstrated that the aging-associated senescence are reduced by administration of Klotho. Senescence and mitochondrial dysfunction are both hallmarks of aging and are tightly intertwined. However, it was only in 2016 that Wiley et al. demonstrated a direct link between the two (183). They demonstrated that mitochondrial dysfunction can lead to mitochondrial dysfunction-associated senescence (MiDAS), ultimately driving an aged phenotype.

Mitochondria are well recognized as an organelle that becomes increasingly dysfunctional over time (184), and such declines have been implicated as leading to aging-associated impairment in tissue/organ function. For example, Peterson et al. demonstrated that reduction in mitochondrial oxidative and phosphorylation activity could be a potential cause for increase in insulin resistance in healthy elderly individuals (43, 185). Additionally, studies in both humans and rodent models have shown that mitochondrial DNA mutations also increase with age (41) (Nuo Sun, Mol Cell, 2017). Dysfunctional mitochondria are known drivers of impaired tissue and cellular ‘quality’ in skeletal muscle (186). Mitochondrial function of MuSCs also plays a pivotal role in driving stem cell fate during myogenesis (132, 172). Aging in skeletal muscle results in a decline in mitochondrial enzymes such as citrate synthase, a decline in bioenergetics profile, and an increase in ROS production (52, 56, 187-190).

Mitochondria serve as a cell-governing system that maintains cellular function by modulating several signaling pathways. For example, Wnt/TGF $\beta$ , insulin growth factor (IGF)-1, phosphatidylinositol 3-kinase (PI3K)/serine-threonine kinase (Akt) and fibroblast growth factor (FGF) signaling pathways have been shown to be regulators of mitochondrial functions (191-196). Interestingly, Klotho has also been involved in regulating oxidative stress through each of the above mentioned pathways (197-199). For instance, inhibition of IGF-1/PI3K pathway by Klotho upregulation resulted in resistance to oxidative stress (199). Klotho also negatively regulates the PI3K/Akt pathway by enhancing the superoxide neutralizer manganese superoxide dismutase (200). Upregulation of circulating Klotho also reduces blood pressure and oxidative stress in mice (201). The activation of the Akt signaling pathway by the FGF21/FGF23/Klotho complex leads to improved cellular function due to enhanced nitrous oxide production (202). FGF23 was also positively associated with Klotho protein and the FGF23 activity-degradation of ROS axis was maintained only in the presence of Klotho (202). The Klotho-FGF23 complex could, hence, be postulated as a regulator of mitochondrial activity by controlling ROS production. However, a direct mechanism of Klotho on cellular mitochondrial function in skeletal muscle has not been widely investigated. In our studies, we show a direct role of Klotho in maintaining muscle progenitor mitochondrial ultrastructure, mtDNA, and bioenergetics. Genetic inhibition of Klotho in muscle progenitors resulted in vacuolated mitochondria and compromised cristae architecture.

Our studies reveal that the *Klotho*<sup>+/-</sup> mice have disrupted mitochondria, leading to impaired skeletal muscle function. However, these declines are reversible with treatment of SS-31, which we find restores mitochondrial ultrastructure and bioenergetics in muscle stem cell progeny. SS-31 is a mitochondrial protectant that binds to cardiolipin and protects mitochondrial

cristae thereby promoting oxidative phosphorylation (116). Our findings further suggest that the disrupted ultrastructure of mitochondria and impaired bioenergetics state of MuSCs are enhanced with administration of recombinant Klotho. Likewise, restoration of mitochondrial function by replenishment of nicotinamide adenine dinucleotide (NAD<sup>+</sup>) levels has been shown to protect aged MuSCs from senescence and enhances myogenicity (133, 203, 204). These findings further support the association between mitochondrial function of MuSCs and functional skeletal muscle regenerative cascade. Given that MuSCs are primary regulators of the skeletal muscle regenerative cascade, an improvement in MuSC mitochondrial function is a likely target to enhance aged muscle function.

Although heterochronic exchange of circulating systems have shown a beneficial effect of youthful circulation on aged tissue regeneration, no study has yet linked this benefit to an enhanced mitochondrial function. Findings from this thesis revealed that exposure to young serum improved mitochondrial function of aged muscle progenitors. However, the beneficial effect was blunted when EVs were depleted from the serum. These findings are consistent with a previous study showing that exposure to fibroblast derived EVs restored OXPHOS in recipient cells (205). Accordingly, here we show that EVs derived from young mouse serum enhanced mitochondrial cardiolipin content in aged muscle progenitors, a phospholipid that is often regarded as the site for OXPHOS. Hence, we posit that EVs are key players in driving mitochondrial function of recipient cells such as muscle progenitors, which is consistent with the fact that EVs are paramount for mitochondrial quality control and stem cell regulation (206, 207).

Klotho protein was detectable in EVs, but the levels were not altered according to age. However, we found that young EVs contained ~25% higher amount of Klotho mRNA compared to aged EVs, and that administration of young EVs to aged muscle progenitors significantly

enhanced reduced cardiolipin content. Klotho mRNA contained within young EVs could, hence, be playing a key role in the regulation of mitochondria. Klotho administration has already been shown to attenuate the mtDNA damage in different tissue types (208, 209). Future studies to implicate specific EV-cargo, such as Klotho mRNA, that may be responsible for such mitochondrial regulation, are warranted.

#### **4.2 Epigenetic Modifications of Klotho Promoter are Important for Skeletal Muscle Healing**

Patterns of epigenetic alterations of mtDNA dynamically change over time (210). For instance, a knockout of DNMT3a altered mtDNA methylation status and disrupted mitochondrial respiratory capacity(210). Another study revealed that elevated DNMT3a levels display abnormal mitochondria in skeletal muscle fiber (211). Although mtDNA methylation is a newly found phenomenon, these studies suggest that the non-random methylation patterns of mtDNA is partly responsible for causing mitochondrial dysfunction.

Declining levels of Klotho have been shown to result in a dysfunctional stem cell population (88, 107, 212). Such declines in stem cell function lead to impairment in the wound healing response of skin and small intestine (107). Wehling-Henricks et al demonstrated that the Klotho promoter is epigenetically repressed via DNA methylation and histone modifications in a dystrophic mouse model (117, 125). Likewise, our data demonstrated that the Klotho promoter is de-repressed in response to injury in young animals, but that epigenetic control is lost with aging, thereby contributing to an impaired skeletal muscle regeneration. This raises the question, “*Could epigenetic regulation of the Klotho promoter be a viable therapeutic option?*”

One study in rhesus monkey suggested that epigenetic modification of the Klotho promoter leads to decreased expression of Klotho gene and protein in brain white matter due to inefficient DNA repair mechanisms and age-related declines in uncharacterized neuronal factors (213). Moreover, epigenetic silencing of Klotho gene has been implicated in playing a pervasive role in oncogenesis, which is intriguing in the light of Klotho's anti-tumorigenic properties (214, 215). In chronic kidney diseases, hypermethylation of Klotho promoter is accompanied with induction of DNMT1 and DNMT3a, and reversal of these modifications significantly improved renal function (216). Hypermethylation of the Klotho promoter has also been shown to functional loss of the Klotho gene by an aberrant activation of the canonical Wnt/ $\beta$ -pathway (214). Altogether, these findings suggest that de-repression of Klotho promoter plays a role in alleviating impaired tissue responses in dystrophy, cancer and kidney diseases. Such epigenetic alterations of Klotho promoter could indeed be a potential mechanism for reversing age-related declines in skeletal muscle function.

#### **4.3 Paracrine Function of Klotho in Promoting Intercellular Communication**

Circulating levels of Klotho have been associated with various age-related pathologies, but a mechanistic understanding of Klotho's paracrine role on stem cell functioning has been lacking. Through the studies presented here, a potential paracrine role of Klotho in regulating hallmarks of aging skeletal muscle has been illustrated by: (a) demonstrating the beneficial impact of systemic Klotho protein levels on muscle function and (b) implicating Klotho mRNA within the cargo of circulating EVs as a potential regulator muscle function. In these studies, we tested the hypothesis that Klotho is a "rejuvenating factor" that acts as a paracrine mediator critical for

effective muscle progenitor function and skeletal muscle regeneration after injury. Our studies demonstrated that Klotho, although expressed in low amounts under conditions of homeostasis, is rapidly upregulated after an acute skeletal muscle injury in young animals and plays an important role in the regenerative cascade. We found that Klotho is highly upregulated locally and systemically in acutely injured young skeletal muscle, but that the response is attenuated with aging. Our studies further demonstrated that systemic upregulation of Klotho enhances muscle stem cell myogenic lineage progression and functional skeletal muscle regeneration, suggesting that systemic supplementation with Klotho may overcome the blunted regenerative response of aging animals. However, caution must be taken when administering Klotho to aged animals for enhancing skeletal muscle function, as both dosing and timing of administration appear to be crucial. Indeed, we found that daily injections of Klotho protein severely hampered the skeletal muscle performance (217).

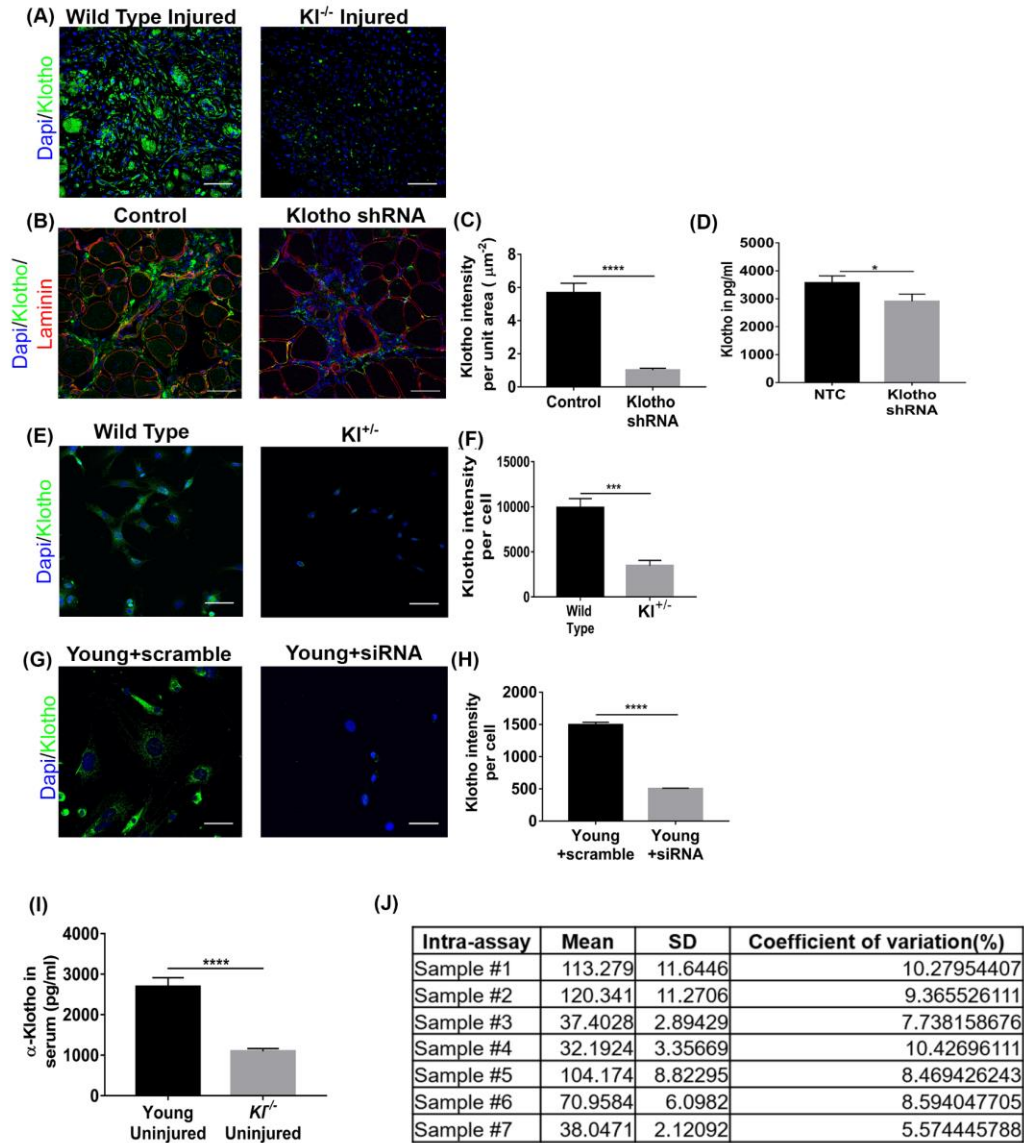
Thus far, it is evident from our studies that Klotho plays a paracrine role in dictating the regenerative machinery of skeletal muscle. Despite Klotho's crucial role, the protein is highly unstable and prone to degradation. Therefore, we next asked, "Are there mechanisms to protect and maintain Klotho-associated information in the blood?" To answer this, we next evaluated whether extracellular vesicles (EVs) may store and protect Klotho cargo in the circulation. To increase the Klotho content in the EVs, mesenchymal stem cells were treated with Klotho membrane protein plasmid, and the EVs released in the conditioned media were shown to contain an increased Klotho protein(218). Administration of these loaded EVs enhanced the proliferating capacity of endothelial progenitor cells, which subsequently supported tissue-engineered blood vessels. Engineering EVs with Klotho mRNA has, to the best of our knowledge, not been

previously explored. This opens a promising avenue of research to test EV engineering with Klotho mRNA as means to promote cellular and tissue healing.

#### **4.4 Concluding Thoughts**

In the field of aging research, aging is defined by nine hallmarks of aging as described by Lopez-Otin et al (26). Experimental amelioration of these hallmarks is be able to, in theory, block the aging process. Since the hallmarks are clearly interdependent, affecting one hallmark would have downstream effects on every other hallmark. The overarching aim of these studies was to explore an interventional therapeutic that could ameliorate one or more hallmarks of aging in the context of skeletal muscle regeneration. Since several epidemiological studies associated declining Klotho expression with reduced muscle strength and decreased overall organismal health of aging individuals(110, 111, 219, 220), we wondered whether Klotho treatment could be used to reverse or delay aging-associated impaired skeletal muscle function. Indeed, the mechanistic findings in these studies suggested that Klotho-based replacement therapies may be a promising approach for enhancing healing capacity of the geriatric population by targeting at least four hallmarks of aging namely, (i) cellular senescence, (ii) mitochondrial dysfunction, (iii) epigenetic alterations and (iv) altered intercellular communication. Additional studies describing the functional role of Klotho treatment in mitigating these and other hallmarks are warranted. The long-term goal is promotion of an enhanced lifespan and, more importantly, health-span.

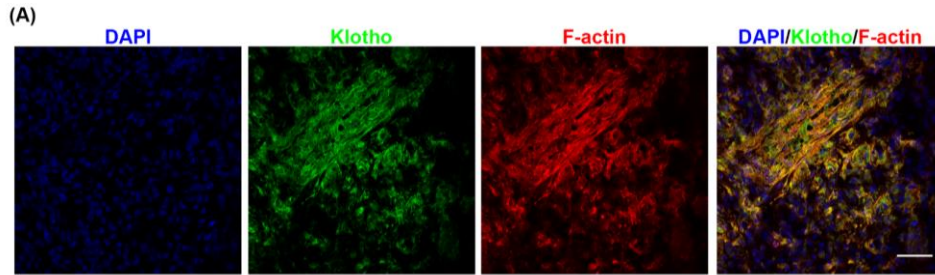
## Appendix A Supplementary Information to Section 2



**Appendix Figure 1. Antibody validation.**

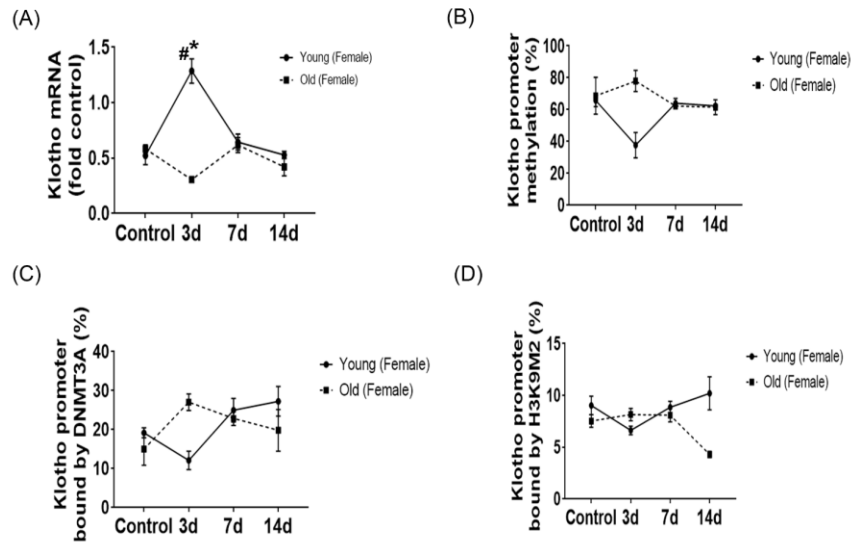
(A) To validate the antibody (MAB1819, R&D Systems) used for histology, muscle sections were co-stained for Klotho and DAPI in wild type and *Kl<sup>-/-</sup>* mice. Minimal  $\alpha$ -Klotho was detected in the *Kl<sup>-/-</sup>* mice. Knockdown of  $\alpha$ -Klotho by lentiviral shRNA revealed  $\sim$ 3-fold decrease in expression in the muscle (B, C) and a decline in circulating Klotho (D). (E, F) MPCs isolated from wild type and *Kl<sup>+/-</sup>* mice were co-stained for  $\alpha$ -Klotho and DAPI. Immunofluorescence imaging revealed that MPCs from *Kl<sup>+/-</sup>* mice expressed  $\sim$ 50% less  $\alpha$ -Klotho. (G, H) In the MPCs,  $\alpha$ -Klotho knockdown using a siRNA, revealed  $\sim$ 3-fold decrease in  $\alpha$ -Klotho expression. (I) The ELISA kit (Cloud-Clone Corp, SEH757Mu, Lot#L170622859) was validated by comparing serum levels of  $\alpha$ -Klotho from young uninjured (n=8) and *Kl<sup>-/-</sup>* mice

(n=6). Serum from *Kl<sup>-/-</sup>* mice revealed some non-specific binding of the target protein. (J) Intra-assay precision was determined by the coefficient of variation for 7 samples repeated in quintuplicate (\* $p \leq 0.05$ , \*\*\* $p < 0.001$ , \*\*\*\* $p < 0.0001$ , student t-test). (A, B, E, G) Scale: 50 $\mu$ m. Data represented as mean  $\pm$  SEM.



**Appendix Figure 2.  $\alpha$ -Klotho is also expressed in female muscle with a contusion injury.**

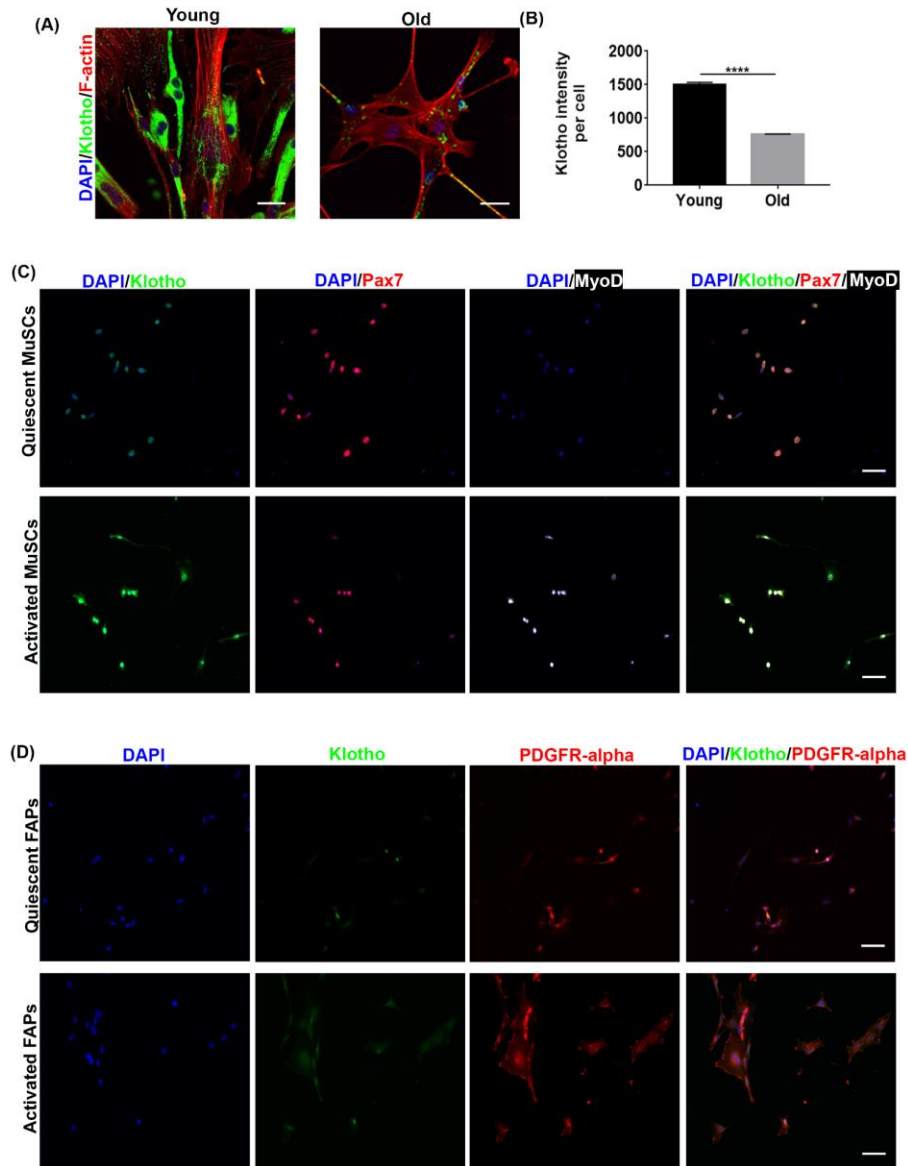
(A) To confirm that  $\alpha$ -Klotho's response to injury is not unique to male mice or cardiotoxin injury, TA muscle sections from a female contusion model were co-stained for  $\alpha$ -Klotho and F-actin and imaged using confocal microscopy (Scale: 50  $\mu$ m).



**Appendix Figure 3. Aging results in a blunted *Klotho* response following injury in female mice.**

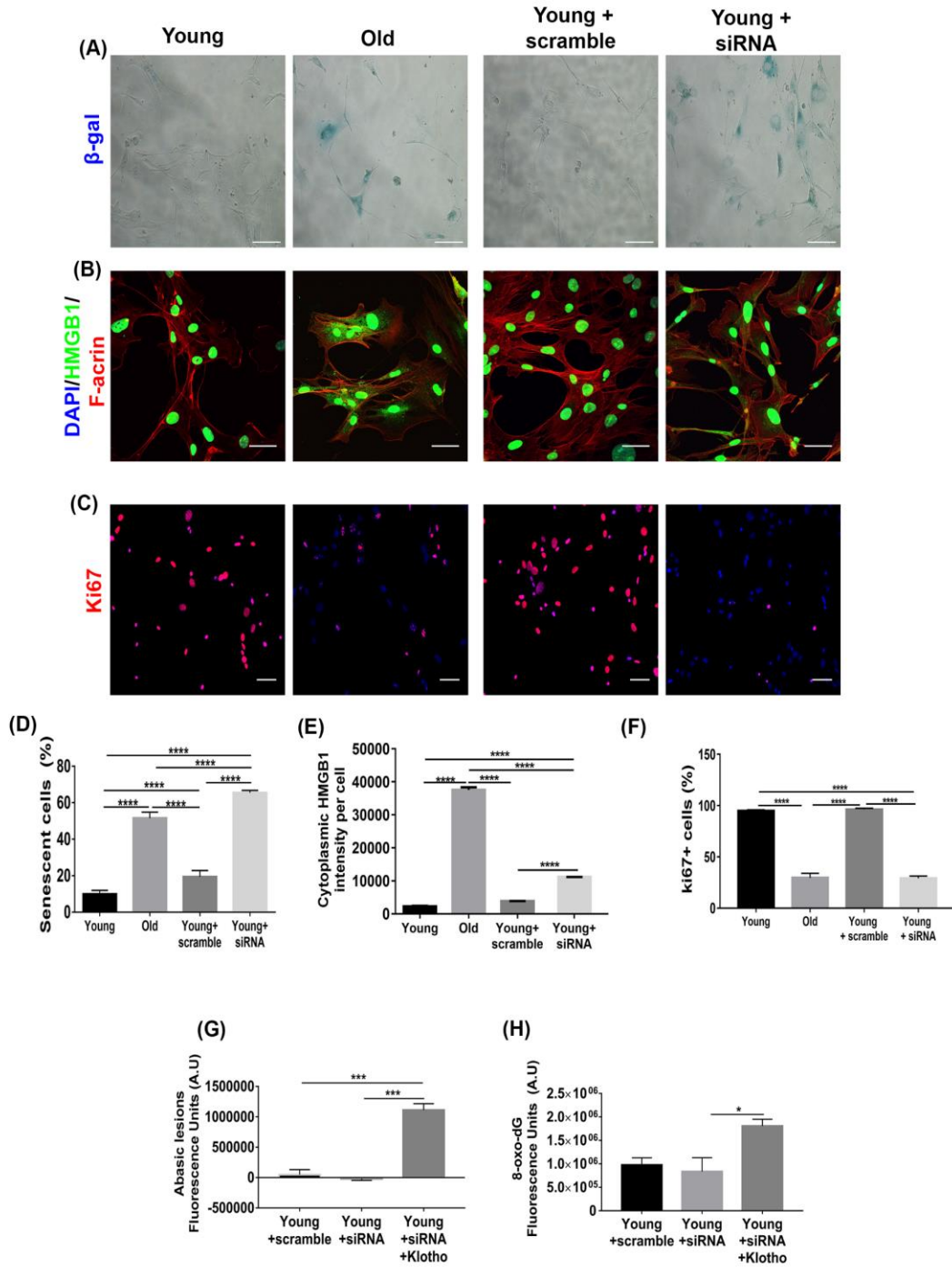
(A) *Klotho* expression is increased in young females 3 days post injury (dpi), after which time levels return to the basal state. However, this response is blunted with aging. (B) Demethylation of the *Klotho* promoter occurs 3 dpi in young female mice, but the response is absent in aged female muscle. (C) There was a decrease in the DNMT3a binding in the young females which is returned to basal binding at 7 and 14 dpi. The reverse trend was observed in aged females. (D) H3K9M2 binding to *Klotho* promoter declined at 3dpi and then increased by 14 dpi. However, aged females displayed a decreased H3K9M2 binding to *Klotho* promoter at 14 dpi. (n=3/group/time point, \* $p \leq 0.05$  compared to

young uninjured muscles; # $p \leq 0.05$  indicates a significant difference between young and aged groups at the respective time-point, two-way ANOVA with tukey's post hoc test). Data represented as mean  $\pm$  SEM.



#### Appendix Figure 4. $\alpha$ -Klotho expression in MuSCs and FAPs.

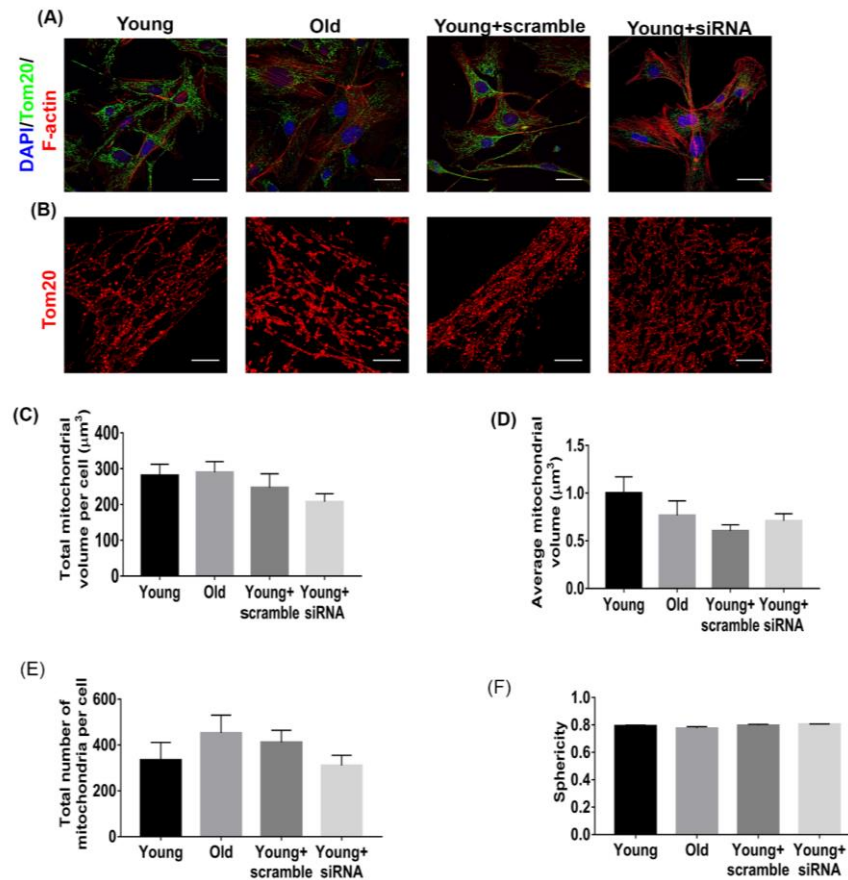
(A, B) The intensity of  $\alpha$ -Klotho was quantified in a purified population of flow-sorted muscle stem cells (MuSCs), which were subsequently cultured for 6 days. Aged MuSCs display significantly less  $\alpha$ -Klotho when compared to young counterparts (Scale: 50  $\mu$ m; \*\*\*\* $p < 0.0001$ , Student's t-test). (C) Flow sorted MuSCs express Pax7, MyoD and  $\alpha$ -Klotho. (D) Confirmation of flow sorted FAPs expressing PDGFR $\alpha$  and  $\alpha$ -Klotho. Scale: 50  $\mu$ m. Data represented as mean  $\pm$  SEM.



**Appendix Figure 5. Decreased  $\alpha$ -Klotho expression in MPCs is associated with increased cellular senescence.**

Aged MPCs display increased senescence as evidenced by an increase in senescence-associated  $\beta$ -galactosidase expression (A, D; Scale: 100  $\mu$ m) and increased cytoplasmic expression of HMGB1 (B, E; Scale: 50  $\mu$ m). When young cells were treated with 25nmol of silencing RNA (siRNA) to  $\alpha$ -Klotho, the average percentage of senescent cells was significantly higher when compared to young controls, as determined by SA- $\beta$  gal and cytoplasmic HMGB1. There was no difference in the senescence profiles between old MPCs and young MPCs treated with siRNA to  $\alpha$ -Klotho. (C, F) Inhibition of  $\alpha$ -Klotho in young MPCs decreased cellular proliferation (Ki67 positivity) (Scale: 50  $\mu$ m). Klotho

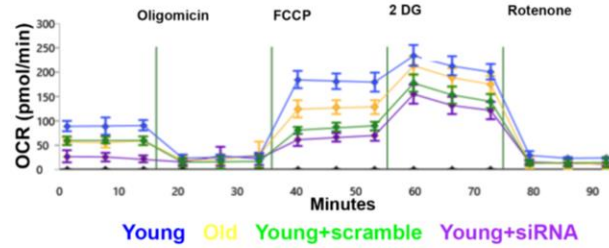
supplementation in media while inhibiting Klotho using an siRNA stimulated repair of (G) abasic lesions (n=3) and (H) 8-oxo-dG (n=3). A minimum of 150 cells were analyzed per group for A-F. (\*\*\*\*p<0.0001; \*\*\*p<0.001; \*p≤0.05, one-way ANOVA with tukey's post-hoc test). Data represented as mean ± SEM.



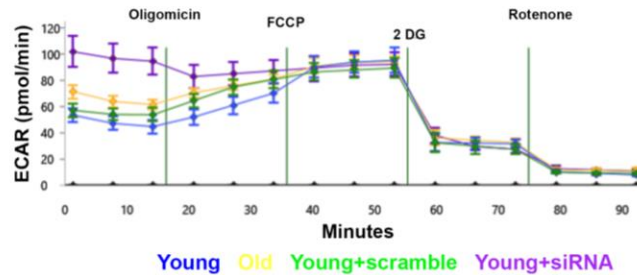
**Appendix Figure 6.  $\alpha$ -Klotho expression does not affect mitochondrial quantity or morphology.**

(A, B) Confocal and STED microscopy of young, old, young+scramble and young+siRNA MPCs revealed that there is no difference in (C) total mitochondrial volume, (D) volume of each mitochondrion within a cell, (E) the number of mitochondria per cell in any of the groups, or the (F) mitochondrial sphericity (calculated as the ratio of the surface area of the given object to the surface area of a sphere with the same volume as the given object). At least 50 cells per group were analyzed. (p>0.05, one-way ANOVA with tukey's post-hoc test). Data represented as mean ± SEM.

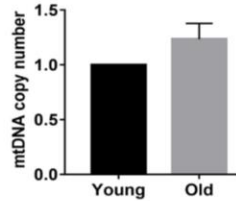
(A)



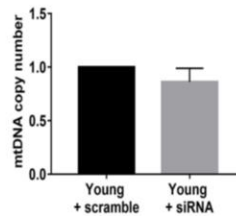
(B)



(C)

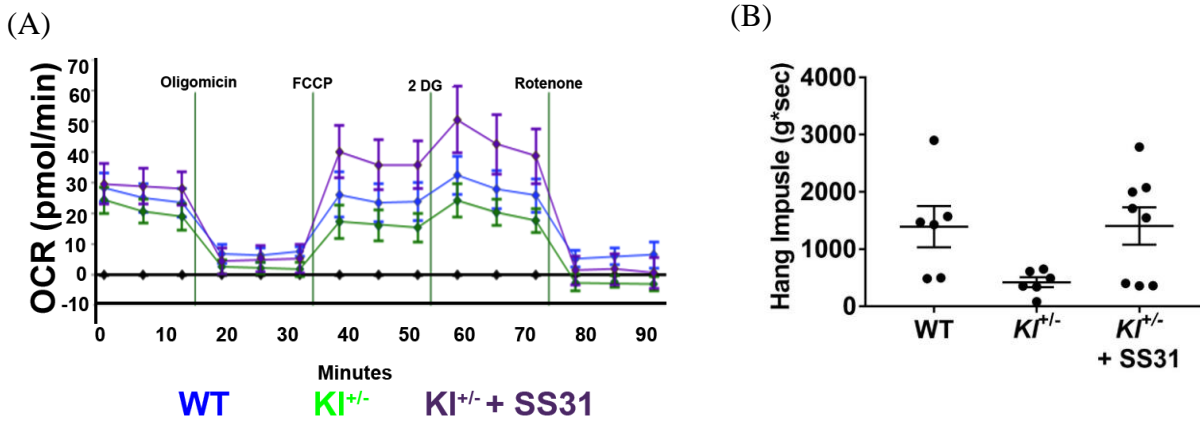


(D)



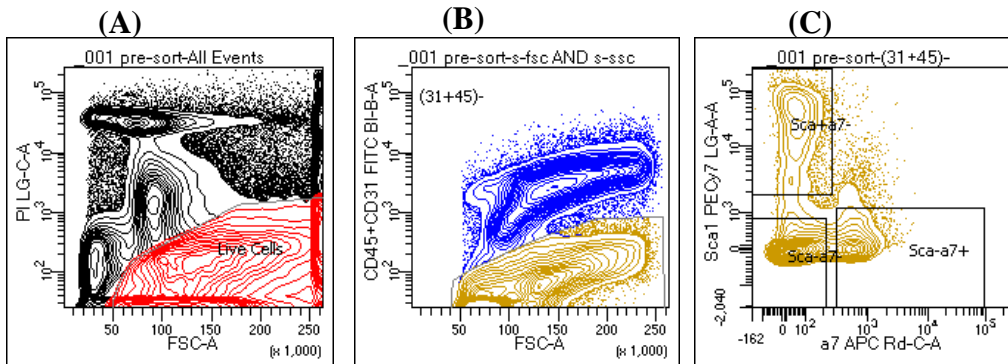
**Appendix Figure 7. Expression of  $\alpha$ -Klotho affects the bioenergetics profile of the cells but does not affect the mtDNA copy number.**

(A, B) Representative bioenergetic profiles for oxygen consumption rate (OCR) and extracellular acidification rate (ECAR) of the MPCs. OCR and ECAR were quantified using a Seahorse XF<sub>96</sub> analyzer. These profiles are representative of eight separate biological repeat experiments performed in 4-6 replicates per run. (C, D) mtDNA copy number in MPCs is not altered with aging or when  $\alpha$ -Klotho is knocked-down in young MPCs with an siRNA to  $\alpha$ -Klotho. Data represented as mean  $\pm$  SEM.



**Appendix Figure 8. SS31 rescues the bioenergetics profile of  $KI^{+/-}$  MPCs to wild-type control levels but does not significantly alter muscle strength in the absence of injury.**

(A) Representative bioenergetic profiles for oxygen consumption rate (OCR) of the muscle myoblasts isolated from  $KI^{+/-}$  mice, as determined by Seahorse XF<sub>96</sub> analyzer. These profiles are representative of four separate biological repeat experiments performed in 4-6 replicates per run. (B) No significant differences ( $p > 0.05$ , one-way ANOVA with tukey's post-hoc test) were observed in the hang impulse (weight \* number of seconds hanging on the wire) across the three experimental groups at baseline (i.e. prior to injury). Data represented as mean  $\pm$  SEM.



**Appendix Figure 9. Representative gating strategy used to flow sort MuSCs and FAPs.**

(A) Sample was gated for live cells as well as a singlet discrimination gate based on pulse processing parameters. (B) A negative population for CD31 and CD45 was gated on a forward scatter (FSC)/side-scatter (SSC) plot. (C) (CD31+CD45)- population was further gated to determine Sca1<sup>+</sup> $\alpha$ 7 integrin<sup>+</sup> and Sca1<sup>+</sup> $\alpha$ 7 integrin<sup>-</sup> populations to yield MuSCs and FAPs, respectively.

**Appendix Table 1 Skeletal muscle contractile characteristics.**

<b>Measurement</b>	<b>Saline</b>	<b>Klotho 1-3 dpi</b>	<b>Klotho 3-5 dpi</b>
Mice (n)	8	6	6
TA Weight (mg)	46 ± 1.65	46 ± 1.42	46.5 ± 1.58
Cross-sectional Area (mm <sup>2</sup> )	2.80 ± 0.12	3.26 ± 0.06*	3.30 ± 0.09*
Avg. Tetanic Torque (100 Hz, mN-m)	0.94 ± 0.09	1.01 ± 0.14	1.38 ± 0.08*
Avg. Twitch Torque (mN-m)	0.345 ± 0.012	0.422 ± 0.017*	0.472 ± 0.018*
Avg. Specific Tetanic Force (100 Hz, mN/mm <sup>2</sup> )	6.48 ± 1.37	9.21 ± 1.57	14.50 ± 1.78*#
Avg. Specific Twitch Force (mN/mm <sup>2</sup> )	11.51 ± 1.06	14.08 ± 1.46	15.74 ± 1.62
Time to Peak Twitch (s)	0.026 ± 0.002	0.025 ± 0.001	0.024 ± 0.001
1/2 Relaxation Time (s)	0.03 ± 0.004	0.036 ± 0.005	0.019 ± 0.001#
TA Length (mm)	14.41 ± 0.15	13.31 ± 0.33*	13.98 ± 0.26

Values presented are mean ± SEM. \* indicates  $p \leq 0.05$  when compared to saline control, and # indicates  $p \leq 0.05$  when compared to Klotho 1-3 dpi.

## **METHODS**

### ***Animal injury model and histological analysis of muscle regeneration***

All procedures were approved by the Institutional Animal Care and Use Committee of the University of Pittsburgh. Wild-type male C57BL/6 young (4-6 months, Jackson Laboratories), aged (22-24 months, NIA), *Kl* homozygotes ( $Kl^{+/+}$ ; B6; 129S5-Kltm1-Lex, 7-10 months, UC Davis) and *Klotho* heterozygotes ( $Kl^{+/-}$ ; B6; 129S5-Kltm1-Lex, 7-10 months, UC Davis) mice received injuries to bilateral tibialis anterior (TA) muscles via an intramuscular injection of cardiotoxin (CTX) (10  $\mu$ L of 1 mg/mL cardiotoxin). Contusion injuries were performed as previously described(221). For pain management, carprofen, an ingestible carprofen (Medigel), was provided for 3 days following injury. Fourteen days following injury, animals were euthanized, and the TAs were harvested for histological analysis. The TAs were fixed in 2% paraformaldehyde for one hour following which they were preserved in 30% sucrose overnight. Sucrose was changed 2-3 times. TAs were then frozen in liquid-nitrogen cooled 2-methylbutane and sectioned through their entirety into 10  $\mu$ m sections. Muscle samples were not included in analyses if animals displayed evidence of external injuries and/or tumor growths upon euthanasia.

### ***Muscle harvest and serum isolation***

The tibialis anterior (TA) muscles were harvested using tweezers and scissors by removing the fascia around the muscle and cutting the proximal and distal tendons. Three, seven, or fourteen days after injury in young and aged animals, TAs were snap frozen using liquid nitrogen for PCR, methylation specific PCR, and ChIP analysis. Fourteen days after injury, the TAs were either preserved for histological analyses or for SHG imaging in ScaleView solution

(Source: Olympus Microscope) for up to two weeks, after which time samples were transferred to a saline solution.

For blood extraction, animals were placed in supine position while anesthetized by inhalation of isofluorane. The skin was cut from the abdomen to the neck and separated from the abdominal wall. The abdominal wall was then cut, and the diaphragm was cut open for easy access to the apex of the heart. The chest cavity was then pulled open using a mosquito scissors. A 25 5/8 gauge, 1 mL needle was inserted into the apex of the heart, and the blood from the heart was drawn. To avoid hemolysis, the needle of the syringe was then removed, and the blood from the syringe was placed into a 1.5mL Eppendorf tube. Blood samples were kept at room temperature for 60 minutes, after which time samples were centrifuged for 20 minutes at 13,000 rpm. Using a 200  $\mu$ L micro-pipette, the serum was pipetted out of the tube. Samples were preserved as aliquots of 50  $\mu$ L for ELISA in the -20°C freezer. Any samples displaying hemolysis (as evidenced by pink/red coloration) were not included in the analysis.

### ***Real Time RT-PCR and methylation-specific PCR***

Frozen TA tissues were pulverized, and tissue powders were homogenized in Trizol reagent (Invitrogen). RNA was isolated 1 $\mu$ g of total RNA was treated with DNaseI and reverse transcribed using iScript™ gDNA Clear cDNA Synthesis Kit (BIO-RAD, Hercules, CA). The mRNA levels of the *Klotho* gene were quantified by SYBR Green-based real-time PCR (qPCR) using SsoAdvanced™ Universal SYBR® Green Supermix (BIO-RAD, Hercules, CA). *Klotho* gene expression levels were normalized to the expression level of *Rpl44*, and the fold changes of *Klotho* relative to universal mouse reference RNA was calculated using  $2^{-\Delta\Delta C_t}$  method. Each sample was measured in duplicates. Primers sequence were: *Rpl44* (Forward: 5'-

AGATGAGGCAGAGGTCCAA-3' and Reverse: 5'-GTTGTAAGAAAGGCCGGTCA-3'); Dnmt1 (Forward: 5'- GTCGGACAGTGACACCCTTT -3' and Reverse: 5'- TTTAGTGGGGCCCTTCGTG -3') and Dnmt3a (Forward: 5'- GGGCCACACGGCAGAG-3' and Reverse 5'-TGCCGTGGTCTTTGTAAGCA-3').

CpG site-specific methylation of the *Kl* promoter was quantified using previously reported sequences for muscle DNA (21). Control DNA (fully methylated and fully unmethylated) were mixed in various concentration to serve as quantification standards when determining the percentage of DNA methylation following qPCR. The frozen TA muscles were pulverized under liquid nitrogen, fixed with 1% formaldehyde for 15 minutes followed by quenching with 125mM glycine solution. Crosslinked protein/DNA complexes were pelleted and washed with PBS containing protease inhibitor cocktails. Chromatin isolation and immunoprecipitation was performed using ChIP-IT kit (Active Motif, Carlsbad, CA), following the manufacturer's instructions. ChIP-validated antibodies against DNMT3A (39206, Active Motif, Carlsbad, CA), H3K9M2 (ab1220, Abcam, Cambridge, MA), or nonspecific negative control mouse IgG (Active Motif, Carlsbad, CA) were used for immunoprecipitation of each sample. Non-immunoprecipitated chromatin was used as input. Following reverse cross-linking and elution of chromatin, DNA from each sample was purified with QIAquick PCR purification kit (Qiagen, Germantown, MD). Purified DNA sample concentrations were quantified by QubitiT DNA HS assay kit (Thermo Fisher Scientific, Waltham, MA). 10ng of purified DNA was used for PCR of the *Kl* promoter. The investigators performing the experiment were blinded to the hypotheses at the time of data analysis.

### ***DNA isolation, quantification and PCR-based assay for measuring mtDNA damage***

DNA isolation and quantification were performed using a high molecular weight genomic DNA purification kit according to the manufacturer's protocol (QIAGEN Genomic tip either 20/G or 100/G) and Quant-iT Picogreen dsDNA quantification. Following genomic DNA isolation, the purity and quality was assessed using a Nanodrop (ND-1000). A PCR-based assay was used to calculate mitochondrial DNA lesion frequency. Reaction mixtures used KAPA Long Range HotStart DNA Polymerase (KAPABiosystems) in a 96-well platform. Primers used for the mouse long amplicon are 5'-GCC AGC CTG ACC CAT AGC CAT AAT AT-3' and 5'-GAG AGA TTT TAT GGG TGT AAT GCG G-3', and the short amplicon are 5'-CCC AGC TAC TAC CAT CAT TCA AGT-3' and 5'-GAT GGT TTG GGA GAT TGG TTG ATG T-3'. Each biological DNA sample was performed in triplicate.

### ***Lentiviral in-vivo knockdown of $\alpha$ -Klotho***

*In-vivo* knockdown of  $\alpha$ -Klotho in the TAs of mice was done with a shRNA to  $\alpha$ -Klotho using a lentiviral vector. Young wild-type mice received non-targeting control shRNA (Smartvector NON-targeting hCMV-TurboGFP Control particles, GE Dharmacon) to bilateral TAs. Young mice received a dose of  $2 \times 10^5$  TU/TA  $\alpha$ -Klotho shRNA on their left TAs and a dose of  $3.82 \times 10^6$  TU/TA  $\alpha$ -Klotho shRNA on their right TAs.  $\alpha$ -Klotho shRNA used were a pool of three different clones (Smartvector Lentiviral Mouse KL mCMV-TurboGFP shRNA, Clone 11285258, Clone 11852825, Clone 17740025). Since there was no statistical significance between the  $\alpha$ -Klotho knockdown using the two shRNA doses tested, the data obtained from the two doses of shRNA were combined for analysis.

### ***Primary muscle cell isolation***

Hindlimb muscles were isolated from young, aged,  $Klf^{+/+}$  and  $Klf^{+/-}$  mice using scissors and tweezers while ensuring that minimal fat, fascia or tendons were included in the tissue harvest. The muscles removed were washed in PBS to remove hair, debris and/or blot clots. After successive digestion of the muscle with 2 mg/mL Collagenase XI (Sigma, C-7657) for 1 hour, 2.4 U/mL Dispase (Life Technologies, Cat. No. 17105-041) for 45 minutes and 0.1% Trypsin (Life Technologies, Cat. No. 15400-054) for 30 minutes, the cell suspension was filtered through a 0.70  $\mu$ m strainer and the homogenate was plated onto Collagen I (Sigma, C8919) coated flasks or 6-well plates. Muscle progenitor cells were expanded in high serum proliferation medium containing DMEM (Life Technologies, Cat. No. 11995-040), 20% FBS (Life Technologies, Cat. No. 10438026), 1% Pen/Strep (Life Technologies, Cat. No. 15140122) and 0.5% chick embryo extract (MP Biochemicals, Cat. No. 092850145). MPCs were cultured for a maximum of three passages for all experiments.

A purified population of muscle stem cells (MuSCs) were sorted by flow cytometry sorting for  $CD31^{-}$ ,  $CD45^{-}$ ,  $Sca1^{-}$  and  $VCAM^{+}$ , as previously described(123). In addition, MuSCs were sorted according to the presence of  $CD31^{-}$ ,  $CD45^{-}$ ,  $Sca1^{-}$  and  $\alpha$ -7 integrin<sup>+</sup>, whereas FAPs were sorted on the basis of  $CD31^{-}$ ,  $CD45^{-}$ ,  $Sca1^{+}$  and  $\alpha$ -7 integrin<sup>-</sup> (222).

### ***Immunofluorescence***

Cells and muscle sections were fixed with warm 2% Paraformaldehyde for 15 minutes followed by a triple wash with PBS. They were permeabilized using 0.1% Triton-X for 15 minutes followed by a triple wash with PBS. They were blocked with 3% BSA and 0.1% Triton-

X for 45 minutes. Primary antibodies such as rabbit anti-Tom20 (1:1000, SantaCruz Biotech, sc11415), rabbit anti- $\gamma$ H2AX (1:1000, ABCAM, ab11175), rabbit anti-Ki67 (1:1000, ABCAM, ab15580), rabbit anti-Laminin (1:1000, ABCAM, ab11575), rabbit anti-HMGB1 (1:1000, ABCAM, ab 18256), rabbit anti-MyoD (1:500), mouse anti-Pax7 (DSHB, 1:50) and rat anti-Klotho (1:400, R&D Systems, MAB1819, Lot# KGN0315101), were diluted in 3% BSA+5% Goat Serum+0.1% Triton-X overnight at 4°C. If antibodies produced in mouse were used (such as Pax7), 10% affinity-pure goat anti-mouse IgG Fab fragment was added during the blocking step.

After a triple wash with PBS, the samples were incubated with their respective secondary antibodies, goat-anti rat Alexa Fluor 488, goat anti-rabbit Alexa Fluor 546 and Phalloidin 647 (for F-actin) in 3% BSA+5% Goat Serum+0.1% Triton-X for 60 minutes. All secondary antibody dilutions were done at 1:500. Following a triple wash with PBS, the samples were stained with 0.02 mg/mL DAPI (Biolegend, Cat#422801) for 2 minutes and then washed with PBS again. The chamber sides and muscle sections were mounted with a glass coverslip using Gelvatol (Source: Center for Biologic Imaging (CBI), University of Pittsburgh) as a mounting media. These were dried in 4°C for at least three hours before imaging.

### ***Confocal imaging***

Imaging was performed using a Nikon Confocal Microscope at 40X magnification at the Center for Biological Imaging (CBI) of the University of Pittsburgh. Muscle sections and chamber slides were imaged at a resolution of 1024x1024 and pixel depth of 1/8. Z-stacks were taken for rendering a 3-D picture of the sample with a slice depth of 0.5  $\mu$ m.

### ***Second Harmonic Generation imaging***

Second Harmonic Generation (SHG) imaging was performed on TA muscles to visualize myofibers within the muscle. Muscle samples were first incubated at 4°C in ScaleView (CBI, Olympus) solution for at least one week to reduce opacity. Each muscle sample was rinsed with deionized water before being mounted on a custom glass plate with a v-shaped well to hold the sample in place. The well was then filled with deionized water and a cover slip was mounted. Correction for coverslip was applied and laser was set to 830 nm with 3.5-5% power. Z-stacks were taken with a thickness of roughly 180 µm from the 358 nm and 488 nm channels. Excitement wavelength for myofibers is 488nm. Investigators responsible for SHG imaging of the SS31 administration, lentiviral inhibition and the osmotic pump experiments, were blinded to the experimental groups for imaging as well as analysis.

### ***ELISA***

The levels of Klotho protein were measured by a colorimetric sandwich enzyme immunoassay (ELISA Kit SEH757Mu, Cloud-Clone Corp, Lot#L170622859), according to instructions of the kit. Briefly, for every experiment, standards and samples (Serum diluted 1:25 in PBS, 100µl/well) were added in duplicates to the 96 well microtiter plate that were pre-coated with a biotin-conjugated antibody specific for Klotho detection. The plates were incubated for one hour at 37°C. Subsequently, the samples and standard were removed. 100 µL of biotin-conjugated antibody was then added to each well and incubated for 1 hour at 37°C. The microplates were washed three times with washing buffer (2 minutes each wash), followed by the addition of 100 µL of avidin-conjugated HorseRadish-Peroxidase (HRP-avidin) to each well. The plate was

incubated for 30 minutes at 37 °C after which the plate was washed five times with washing buffer. Next, 90ul of tetramethyl benzidine (TMB) substrate was added and the plate was incubated at 37 °C for 20 minutes. A sulfuric acid stop solution was then added to terminate color development reaction and the optical density (OD) of each well was measured at wavelength of 450nm. In order to determine antigen concentration of the unknown, an OD of the sample was compared to the OD standard curve generated using known antigen concentrations. The concentration range used for standard curve was 3.25 pg/mL to 200 pg/mL.

Samples displaying evidence of hemolysis or when insufficient quantities of serum were obtained were not included in data analysis, as we have found this to affect readout of Klotho levels. Media was collected after culturing MPCs for 3 days in 3 wells of a 12-well plate. For MuSCs and FAPs, media was collected after culturing them in 3 wells of chamber slides for 3 days. The data was then normalized to the number of cells per well. No samples were subjected to freeze-thaw, as we have observed that this may dramatically affect  $\alpha$ -Klotho levels detected.

### ***In vitro inhibition of $\alpha$ -Klotho***

MPCs were plated onto collagen-coated flask and grown to 80% confluence. The cells were then treated with 25 nmol of silencing RNA (siRNA) to  $\alpha$ -Klotho or a non-targeting scramble control (GE Dharmacon, Product no. SO2462181G) in antibiotic free proliferation media for 48 hours. Following treatment, cells were passaged and prepared for Transmission Electron Microscopy (TEM), STED microscopy, immunofluorescence (IF) staining, mtDNA damage analysis or Seahorse analysis. Cells were plated at a density of 10,000 cells per well of a collagen I coated chamber slide and grown for 24 hours for IF staining. They were plated at a density of 30,000 cells per well of a 96-well plate for seahorse experiments.

### ***Structured Illumination Microscopy***

Young and Old MPCs were plated on 35 mm glass bottom dishes (Matek, P35GCOL-0-10-C) at a density of 15,000 cells per dish for 48 hours. Cells were stained for  $\alpha$ -Klotho and DAPI and preserved in PBS for imaging. The samples were illuminated with a patterned excitation light at 488 nm to detect Klotho and 405 nm to detect DAPI (nucleus). Samples were placed in a chamber on top of a 100X magnification oil lens. Type NF, Nikon immersion oil was used on the sample for imaging.

### ***Image Analysis***

ImageJ (1.49v, NIH, Bethesda) was used to quantify intensity of  $\alpha$ -Klotho in cells and muscle sections along with the mitochondrial distribution within a cell.  $\alpha$ -Klotho intensity was measured as integrated density of the pixels (i.e. intensity) in the  $\alpha$ -Klotho channel.  $\alpha$ -Klotho expression was normalized to either number of cells or to the total area of the image frame for muscle sections. For evaluation of  $\alpha$ -Klotho intensity within the muscle, one image was obtained over 3-4 muscles sections at the maximal site of injury (identified as the muscle region containing the greatest number of centrally nucleated fibers and cellular infiltrate). Fibrosis was measured as the percentage of area covered by the sirius red stain under polarized light within the frame of injury. Cardiolipin and ROS were measured as a function of intensity of NAO and MitoSox per cell, respectively. Myofiber cross-sectional area was evaluated using ImageJ by manually tracing around the Laminin rings. Impaired mitochondria were evaluated using TEM images by quantifying the ratio of damaged mitochondria to intact mitochondria. Damaged mitochondria were identified to be swollen and vacuolated.

Imaris software was used to quantify mitochondrial volume, sphericity and volume of each mitochondrion in a cell. The investigator responsible for imaging mitochondria was blinded to the hypotheses at the time of data analysis. Regeneration index was also quantified using Imaris for the SHG images and ImageJ for histological images. Stereological analysis of regeneration was done by scanning through all slices of individual SHG z-stacks (over a depth of ~180  $\mu\text{m}$ ) and calculating the ratio of centrally nucleated fibers to total number of fibers. Investigators were blinded for imaging and data analysis.

### ***Transmission Electron Microscopy***

MPCs from each of the experimental groups were plated in a well of a plastic tissue culture 6-well plate and fixed in 2.5% Glutaraldehyde for 1 hour. In addition, TA muscles from wild type and  $K1^{+/-}$  mice treated with saline or SS-31 were fixed with 2.5% Glutaraldehyde for 24 hours. Following fixation, cell monolayers or muscle tissues were washed with PBS three times. Muscle samples were cut longitudinally into small pieces. The monolayers/tissues were then subjected to post-fixation aqueous solution of 1% osmium tetroxide, 1%  $\text{Fe}_6\text{CN}_3$  for one hour. Samples were then washed in PBS three times then post-fixed in aqueous 1% osmium tetroxide, 1%  $\text{Fe}_6\text{CN}_3$  for 1 hr. Following a triple wash with PBS, samples were dehydrated with a series of 30-100% ethanol and embedded in by inverting Polybed 812 (Polysciences, Warrington, PA) embedding resin-filled BEEM capsules on top of the monolayer. Blocks were cured twice, once overnight at 37°C, followed by curing at 65°C for two days. Post-curing, monolayers or tissues were peeled from the coverslip and cross-sectioned ultrathin (60 nm) on a Riechart Ultracut E microtome. The samples were then stained in uranyl acetate for 10 min and 1% lead citrate for 7

minutes. The investigators performing imaging were blinded to the hypotheses at the time of data analysis.

### ***Analysis of MPC bioenergetics***

MPCs from each of the experimental groups were plated on a 96-well plate at a density of 30,000 cells per well. CellTak was used as a cell adhesive. The cells were then cultured in unbuffered DMEM for 1 hour at 37°C without CO<sub>2</sub>. The cells were then stressed by the successive injections of 1 μM Oligomycin, 300 nM FCCP (Carbonyl cyanide-4-(trifluoromethoxy)phenylhydrazone), 100 mM 2-DG (2-Deoxy-D-glucose) and 1 μM Rotenone. All reagents were prepared in unbuffered DMEM. The basal oxygen consumption rates (OCR, pmol/min) were plotted for each cell type by averaging the baseline levels before the first treatment with Oligomycin. The reserve capacity (pmol/min) was plotted by calculating the point-to-point difference between the maximum OCR levels (between treatment with FCCP and 2-DG) and basal OCR levels. The investigator performing the seahorse experiments was blinded to the hypotheses at the time of data analysis.

### ***MitoSox Live cell imaging***

MPCs isolated from wild type and *Kl*<sup>+/-</sup> mice were grown in collagen-coated flasks. Cells from *Kl*<sup>+/-</sup> mice were treated with SS-31. The three groups of cells (wild-type, *Kl*<sup>+/-</sup> and *Kl*<sup>+/-</sup> + SS-31) were then plated on individual 35 mm glass bottomed dishes (MatTek, P35GCOL-0-10-C) at a density of 30,000 cells per well. Cells were subsequently incubated for 24 hours, after which time cells were incubated with 5 μM MitoSox<sup>TM</sup> reagent (Invitrogen, M36008) for 10 minutes in HBSS with Calcium and Magnesium. After the incubation, the cells were imaged live with an

excitation/emission maxima of 510/580 nm on the Nikon Eclipse Ti Live Cell microscope (Nikon, CBI). The superoxide content was measured as a function of intensity per cell using Nikon's NIS Elements software. For quantification purpose, at an average 200 cells per group were analyzed.

### ***Nonyl Acridine Orange (NAO) staining***

MPCs isolated from wild type and  $Kl^{+/-}$  mice were grown in collagen-coated flasks. Cells from  $Kl^{+/-}$  mice were treated with SS-31 or a vehicle (saline) control. Next, the three groups of cells (wild-type,  $Kl^{+/-}$  and  $Kl^{+/-}$  + SS-31) were plated on chamber slides at a density of 10,000 cells per well and were incubated for 24 hours. Cells were then fixed with 2% paraformaldehyde for 10 minutes, followed by 0.1% Triton-X for 10 minutes. The cells were then stained with 5  $\mu$ M NAO for 15 minutes, which was diluted in HBSS (-Ca<sup>2+</sup>, -Mg<sup>2+</sup>) followed with triple PBS wash. The chamber slides were stained with DAPI for 2 minutes and then washed with PBS again. The chamber sides were mounted with a glass coverslip using Gelvatol. The cardiolipin content within a cell was measured as a function of intensity of NAO stain per cell.

### ***SS-31 administration***

A modified protocol was used to administer SS31 *in vivo* (Siegel et al, 2013). Isotonic saline or 3 mg/kg SS31 (SS-31 (NH<sub>2</sub>-(D)-Arg-(L)-2,6-Dimethyl Tyrosine-(L)-Lys-(L)-Phe-CONH<sub>2</sub>) was synthesized in the University of Pittsburgh Peptide Synthesis Core) dissolved in saline and was administered daily via i.p. injections to wild-type and  $Kl^{+/-}$  animals for 17 days. The animals were injured with cardiotoxin 3 days after the i.p. injections started. They were subjected to a hanging-wire test and an *in situ* contractile testing 14 dpi for functional testing.

Primary muscle progenitors were isolated from the euthanized mice using previously described method. The cells were then used for differentiation assay.

*In vitro*, SS-31 was administered to MPCs isolated from  $Kl^{+/-}$  mice at a concentration of 100 nM for 48 hours. Three groups of cells:  $Kl^{+/+}$ ,  $Kl^{+/-}$  and  $Kl^{+/-}$  + SS31 were then analyzed for ROS production (MitoSox), bioenergetics profile, cardiolipin content and mtDNA damage.

### ***RNAseq gene expression analysis***

Paired end sequences were downloaded from Gene Expression Omnibus (GEO), a public database repository (GSE97399; van Velthoven et. al., 2017). NGS tool of CLC Genomics workbench software (Qiagen) was used to perform quality control (QC) analysis for assessing quality indicators of the sequences on the basis of FastQC-project. Quality was assured by evaluating sequence-read lengths and base coverages; nucleotide contributions and base ambiguities; and quality scores that were emitted by the base caller and over-represented sequences. All samples that were analyzed, passed QC parameters and were then mapped to the annotated murine reference genome (Mus\_musculys-enembl\_v90). RNA-Seq analysis was performed using the transcriptomics analysis tool. Gene expressions were normalized by Transcripts Per kilobase Million (TPM). This method normalizes for the gene length first, following which it is normalized for sequencing depth second such that the sum of all TPMs in ever sample is the same. This allows for comparing proportion of reads that are mapped to a particular gene in each sample. Finally, a 1-Pearson correlation distance and complete linkage rule (Clus Vis package version 1.1.0) were used to provide unsupervised clustering for generating a heat-map.

RNAseq data that support the findings of this study have been queried from the publicly available NCBI database Sequence Read Archive (SRA) with the accession codes PRJNA381694; GEO: GSE97399 (<https://www.ncbi.nlm.nih.gov/gds/?term=GSE97399>)

### ***Supplementation with exogenous $\alpha$ -Klotho in vitro***

Aged MPCs were treated with 0.05  $\mu$ g/mL of recombinant Klotho (R&D Systems, Product# aa 35-982) after which time they were grown to 60% confluence. The treatment was performed in antibiotic free proliferation media for 48 hours. The cells were then passaged and prepared for TEM, immunofluorescence staining, mtDNA damage analysis or Seahorse experiments. Cells were plated at a density of 10,000 cells per well and grown for 24 hours in a collagen I coated chamber slide for IF staining. They were plated at a density of 30,000 cells per well of a 96-well plate for seahorse experiments.

### ***Systemic supplementation with $\alpha$ -Klotho via osmotic pumps***

Osmotic pumps (Alzet, mini-osmotic pump, model#2004) were used to chronically deliver saline or 324 ng/mL  $\alpha$ -Klotho (R&D Systems, Product# aa 35-982) to aged mice. Pumps were inserted subcutaneously at the back of the neck of mice, and the skin was stapled using 7 mm stainless steel wound clips (Reflex Skin Closure System, Reflex 7, Part no. 203-1000, Stoelting). For pain management, the mice were fed Carprofen as gel food (Medigel<sup>R</sup>, Clear H<sub>2</sub>O). Two days after implantation, bilateral TAs were injured using CTX. Tissues were harvested 14 days after injury for SHG imaging and histological analyses. Blood was collected to perform ELISA to test for  $\alpha$ -Klotho levels in serum.

### ***Intraperitoneal administration of $\alpha$ -Klotho***

Isotonic saline or  $\alpha$ -Klotho (10  $\mu$ g/kg body weight; R&D Systems, Product# aa 35-982) was administered to aged animals via i.p. injections on days 1-3 post-injury or 3-5 days post-injury. We confirmed the activity of the recombinant  $\alpha$ -Klotho prior to administration, as per a previously reported protocol(159).

### ***Hanging-Wire Test***

A modified four-limb wire hanging test was used to measure mouse muscular endurance non-invasively and thus characterize performance of injured mice before and after any experimental intervention(156). Mice were suspended upside down from a steel mesh grid (1 cm x 1 cm squares) above a custom-built chamber (~30 cm high) with appropriate padding to prevent harm for falling down. Four-limb strength was evaluated using a Hang Impulse (HI) score (*bodyweight in grams x time hung in sec*). Individual mice were subjected to five trials in one session with a gap of 5 minutes between trials, excluding the performance of other mice. Sessions were conducted at the same time of day and in the same order across trials. Evaluation of performance considers the average HI of three trials excluding the best trial and the worst trial for every mouse.

### ***In situ contractile testing***

*In situ* contractile testing of the TA muscles was performed as per a previously described protocol(153). Briefly, the peroneal nerve was isolated by making an incision lateral to the knee. After cutting the Achilles tendon, the foot was placed on the force transducer and stabilized with a cloth tape over the foot. The needle electrodes were then placed on the peroneal nerve beneath the

skin. Muscle peak tetanic force was evaluated with the ankle placed at 20° plantarflexion. The stimulator (Aurora Scientific, Model 701C) was used to elicit tetanic contractions at 10, 30, 50, 80, 100, 120, 150, 180 and 200 Hz, with a 2-minute rest between each contraction. From these data, the force-frequency curve was obtained. Results were collected in torque (mN-m). Force output (mN) was calculated by dividing the torque by the foot-plate length (0.03m). The specific tetanic force output at each frequency was then measured by normalizing each force output by the mean cross-sectional area (CSA, mm<sup>2</sup>). The mean CSA was calculated as the [muscle weight (mg)]/[muscle length (mm)×muscle density (1.06 mg/mm<sup>3</sup>)].

### ***Antibody validation***

We validated the  $\alpha$ -Klotho antibody (R&D systems, MAB1819, Lot# KGN0315101) used for immunofluorescence by staining the injured (7 days) muscle section from a wild type and a  $Kl^{-/-}$  mouse. We observed minimal background staining in the  $Kl^{-/-}$  muscle section as compared to the wild-type counterparts. Antibody was also validated by knocking down  $\alpha$ -Klotho using an siRNA or shRNA to  $\alpha$ -Klotho in MPCs and young TA muscle, respectively.

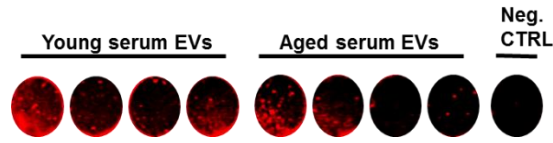
To validate the ELISA kit, serum from  $Kl^{-/-}$  mice were compared to young uninjured controls. Intra-assay precision was quantified by calculating the coefficient of variation (ratio of standard deviation to mean) within the experiment.

### ***Statistical analysis***

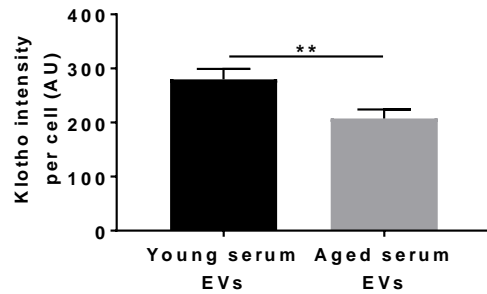
All data are shown as mean  $\pm$  SEM. Data were tested for normality by Shapiro-Wilk's test. Bartlett's-test was used to test for differences in variances. When the data were normally distributed, an independent one-way or two-way repeated measures ANOVA was used to

compare differences among different post-injury groups within the same age group or between experimental groups at different time points, followed by Tukey's post-hoc test, as appropriate. If data were not normally distributed, a Kruskal-Wallis test was performed for comparing between groups. A one-tailed unpaired student t-test was used for comparison between two groups, if data were normally distributed and the standard deviations (SD) were similar. For different SD, a welch's correction was applied to the t test. If data were not normally distributed while comparing between two groups, the statistical differences were obtained by performing a Mann-Whitney U test. Differences between groups were considered significant at  $p \leq 0.05$ . Initial sample sizes were based on preliminary data, with an estimated effect size of 0.6, which yielded a sample size of 6 mice/group after adjusting for death and unforeseen circumstances (conventionally estimated at 20%).

## Appendix B Supplementary Information to Section 3

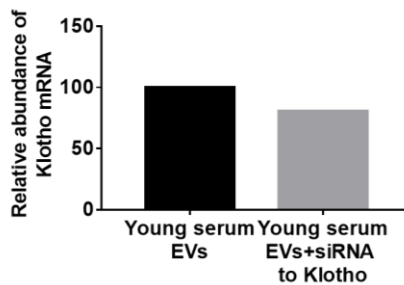


Appendix Figure 10. In-cell western blot supporting analysis in Figure 2G.



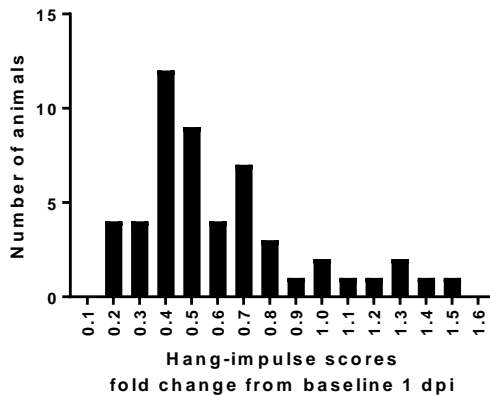
Appendix Figure 11. The impact of EV age on target cell Klotho protein expression.

Quantification of Klotho protein in aged muscle progenitor cells following culture in the presence of young or aged EVs over 24 hours.



Appendix Figure 12. Quantification of relative abundance Klotho mRNA EVs using digital PCR.

(A) Quantification of Klotho mRNA in EVs isolated from young Klotho<sup>+/-</sup> mice as compared to young Klotho<sup>+/+</sup> mice. (B) Quantification of Klotho mRNA in young EVs treated with siRNA to Klotho and compared to young serum EVs. Data is representative of 4 independent samples pooled together for digital PCR analysis.



**Appendix Figure 13. Whole body endurance of aged animals.**

The overall body endurance as determined by the hanging grid test is variable one-day post injury (1 dpi) as revealed by the hang-grid impulse scores at 1 dpi normalized to baseline scores. Only animals having a score within 25-75% percentile of the median (range:0.40-0.74) were included in the study.

## **SUPPLEMENTARY METHODS**

### ***Muscle progenitor cell isolation***

Muscle stem cell progeny were isolated as previously described(169). Briefly, hindlimb muscles were harvested and minced, after which time the tissue homogenate was weighed and treated with successive digestive enzymes. First, the homogenate was digested in 2 mg/mL of collagenase XI for one hour, followed by 2.4 U/mL dispase for 45 minutes and 0.1% trypsin for 30 minutes. The final homogenate was then centrifuged at 500 rcf for 5 minutes at 4°C, after which time the final pellet was re-suspended in high serum medium (Dulbecco's modified eagle's medium, 20% fetal bovine serum, 1% penicillin/streptomycin and 0.5% chick embryo extract). This suspension was plated in collagen I-coated plates for 24 hours after which the supernatant was transferred to another collagen coated plate. On this plate, cells grew within four-six days of plating the supernatant. Cells were not used beyond three passages.

### ***Administration of serum on aged cells***

Aged MPCs were plated at a density of 10,000 cells per well in an 8-well chamber slide. Cells were cultured for 24 hours and then treated with 10% young or aged serum in FBS-free media (optiMEM) with or without EVs for 48 hours.

***Depletion of EVs from serum***

Bulk EVs were depleted from young and aged serum using ExoQuick (Product# EXOQ5A-1) following the manufacturer’s recommended protocol. Briefly, 63 uL of Exoquick solution was added to 250 uL serum and the mixture was incubated on ice for 30 minutes. Next, samples were centrifuged at 1500 g for 30 minutes at 4°C. The EVs were pelleted at the bottom of the tube and the EV-free serum was used for *in vitro* applications.

***Immunofluorescence imaging***

Cell-seeded chamber slides were fixed with warm 2% Paraformaldehyde for 15 minutes, then washed with phosphate-buffered-saline (PBS) three times. The samples were then permeabilized with 0.1% Triton-X for 15 minutes after which the samples were blocked with 3% BSA and 0.1% Triton-X for 45 minutes. A similar process was followed for muscle cryo-sections up to the point of the blocking step. After blocking, the samples were incubated overnight at 4C with the following primary antibodies in antibody solution (3% BSA+5% Goat Serum+0.1% Triton-X), at the dilutions mentioned below:

**Appendix Table 2 Primary antibody details.**

Antibody	Host-species	Product number	Dilution
MyoD	Rabbit	SCBT, sc-760	1:500

Klotho	Rat	R&D systems, MAB1819, Lot# KGN0315101	1:400
Laminin	Rabbit	Abcam, ab11575	1:500

After incubating the samples with primary antibodies overnight, samples were washed with PBS three times, after which time they were incubated with host-specific secondary antibodies in antibody solution for one hour at room temperature at the dilutions mentioned in the table below:

**Appendix Table 3 Secondary antibody details.**

Antibody	Host-species	Product number	Dilution
AlexaFluor 594	Rabbit	Life Technologies, A11012	1:500
AlexaFluor 488	Rat	Life Technologies, A11006	1:500
Phalloidin 647	N/A	Life Technologies, A22287	1:500

After a triple wash with PBS, the cells were incubated with their respective secondary antibodies, goat-anti Rat Alexa Fluor 488, goat anti-Rabbit Alexa Fluor 546 and Phalloidin 647 in 3% BSA+5% Goat Serum+0.1% Triton-X was diluted 1:500 for 60 minutes. Following a triple wash with PBS, the chamber slides were stained with DAPI for 2 minutes and then washed with PBS again. The chamber sides were mounted with a glass coverslip using Gelvatol (Source: Center for Biologic Imaging (CBI), University of Pittsburgh) as a mounting media. These were dried in 4°C for at least three hours before imaging. Imaging was performed using 20X magnification on Zeiss-Axiovision microscope.

### ***Analysis of MPC bioenergetics***

Muscle progenitors from each of the experimental groups (young serum, aged serum, young serum-EVs and aged serum-EVs) were plated on a 96-well plate at a density of 30,000 cells per well using CellTak. The cells were then cultured in un-buffered DMEM for 1 hour at 37°C without CO<sub>2</sub>. Muscle progenitors were exposed to stressors with successive injections of 1 μM Oligomycin, 300 nM FCCP (Carbonyl cyanide-4-(trifluoromethoxy)phenylhydrazone), 100 mM 2-DG (2-Deoxy-D-glucose) and 1 μM Rotenone. The average of the first three time points prior to oligomycin treatment were averaged to get the basal oxygen consumption rate (OCR). A total of three independent experiments were analyzed with 3-8 of replicates of cell samples per experimental group within an experiment. The investigator performing the seahorse experiments was blinded to the hypotheses at the time of data analysis.

### ***Extracellular vesicle isolation***

Extracellular vesicles (EVs) were isolated from serum using single-use 35-nm or 70 nm size-exclusion chromatography columns (qEVsingle, iZON columns). EVs were isolated according to manufacturer's instructions. Briefly, columns were first washed with 2 mL of EV-free PBS (Sigma P5368). After washing, 100 μL of serum was loaded into the column and 200 μL fractions were collected as they eluted. Fractions 1-5 were collected as controls containing no microvesicles. Fractions 6-11 contained were pooled together in a microcentrifuge tube for a final volume of 1.2 mL. This pooled volume was then for subsequent EV experiments.

### ***Nanoparticle Tracking Analysis of EVs***

Nanoparticle Tracking Analysis (NTA) was performed using an NS300 NanoSight device (Malvern Panalytical). Ten microliters from each EV sample was diluted 1:100 in type 1 EV-free water and infused through the flow-cell using a syringe pump (Harvard Apparatus 98-4730). Three 45-second videos were recorded for each sample, with the camera level set to 14. These videos were batch analyzed by the software (NTA 3.3) with the detection threshold set to 3. The flow-cell was washed with 1 mL of type 1 water between each sample.

### ***Surface Plasmon Resonance Imaging (SPRi)***

Young and aged serum EVs were analyzed by SPRi to study the presence and relative amount of Klotho protein and CD63 on their membranes. First, gold SPRi chips (Horiba Scientific SAS, SPRi-Biochip, Palaiseau, France) were functionalized with antibodies against CD63 (CD63 Antibody, MAB5048, R&D Systems), Klotho (Mouse Klotho Antibody, AF1819, R&D Systems) and IgG (Purified anti-rat IgG1 Antibody, 407402, Biologend, as negative control). The surface of the chip was coated with a self-assembled monolayer of thiolated PEG molecules for the immobilization of antibodies through EDC/NHS chemistry. Following this, a microspotter (SPRi Arrayer, Horiba) was used to create spots with diameters of 0.7 mm of the selected antibodies in distinct areas of the same SPRi chip. Four spots per antibody was made at ~70% relative humidity at room temperature. The chip was then blocked with a solution of ethanolamine 1 M, pH 9, for 30 min, washed with water and used in SPRi instrument XelPleX (Horiba Scientific SAS).

HBS-ET was used as a running buffer (1.5 M NaCl, 100 mM HEPES, 30 mM EDTA, Tween 0.5%, pH 7.4). EVs were isolated from 100  $\mu$ l of serum by size-exclusion chromatography

using qEV column (IZON, qEVsingle) with PBS as running buffer, collecting fractions from 6th to 11th and adding protease inhibitors. Aliquots of 500  $\mu$ L of young and aged isolated EVs, resuspended in HBS-ET, were injected in the SPRi flow chamber with a flow rate of 10  $\mu$ L/min and the SPRi signals were collected and analyzed by using EzSuite software and OriginLab. Sensorgrams were corrected by subtracting the signal related to anti-rat IgG antibody.

### ***Characterization of EVs using in-cell western assay***

The level of EV specific marker membrane proteins, CD63, CD81, and CD9, were measured using in-cell western assay. EV samples were fixed with 3.7% formaldehyde solution in PBS for 20 minutes at room temperature followed by PBS wash, blocking with Odyssey Blocking Buffer in PBS (LI-COR Biosciences, NE) for 1 hour at room temperature, and Alexa Fluor conjugated antibody (CD63: sc-5275, CD81: sc-23962, CD9: sc-13118) incubation at 4°C overnight (1:20 dilution in the blocking buffer with 0.15% TWEEN 20). Samples were washed with PBS containing 0.15% TWEEN 20 (Sigma-Aldrich, MO) for 5 minutes and resuspended in ~160 $\mu$ L of PBS. NanoSight analysis was then performed to measure the concentration of extracellular vesicles in each sample. Concentration of all the samples were adjusted to the same level with PBS, and 150 $\mu$ L of the samples were loaded to a 96-well plate. The plate was centrifuged at 4000rcf for 30 minutes at 4°C immediately before the fluorescence measurements using LI-COR ODYSSEY CLx and LI-COR Image Studio Acquisition Software (LI-COR Biosciences, NE). All the other centrifugation for the sample preparation were conducted at 16,100rcf for 15 minutes at 4°C.

## ***Raman Spectroscopy***

Young and aged EVs that were isolated by size-exclusion chromatography were concentrated using an ultracentrifugation step (100,000 g x 70min) for 9<sup>th</sup> to 11<sup>th</sup> fractions. The concentrated EVs were analyzed by Raman spectroscopy to obtain an overall biochemical (LabRAM, Horiba Jobin Yvon S.A.S. Lille, France) following a previous published protocol(176, 223). Briefly, 5 $\mu$ l of the concentrated EV suspension was applied on calcium fluoride disks and Raman acquisitions were performed using the following characteristics: (a) 532 nm laser , (b) 50x objective, (c) grating 1800, (d) 400  $\mu$ m entrance slit and (e) in the spectral ranges 400-1800  $\text{cm}^{-1}$  and 2600-3200  $\text{cm}^{-1}$ . A reference sample (Si) at 570.7  $\text{cm}^{-1}$  was used to calibrate the instrument prior to running the experimental samples. Ten spectra per sample were collected following a line-map from the border of the drop to the edge, with an acquisition time of 30 seconds, following which the acquired data were analyzed through LabSpec6 and OriginLab software. First, a despiking (poly 5), baseline correction (fifth order polynomial curve), normalization by unit vector was performed following which multivariate statistical analysis was performed on the spectra. The Principal Component Analysis (PCA) was made for the data reduction identifying the principal components (PCs) that represent the differences in the spectra. The linear discriminant analysis (LDA) was performed by using a small number of PCs (n=15) in order to evaluate the possibility to discriminate the spectra of two groups in statistically significant way (Mann-Whitney Test). PCA was performed using OriginLab PlugIn called "Principal Component Analysis for Spectroscopy".

### ***Characterization of EVs using digital PCR***

EV RNA was isolated and purified using a plasma/serum RNA purification mini kit (Norgen Biotek Corp., product #55000 and PI55000-Exosomal RNA). For some samples, this kit was used in conjunction with an on-column RNase-Free DNase 1 kit (Norgen Biotek Corp., product #25710). All samples were eluted in 10  $\mu$ l of Elution Solution A, which was included in the plasma/serum RNA purification kit mentioned above. cDNA was generated from purified RNA using the Quantabio qScript cDNA Synthesis kit (Qiagen, product #94057-100). For some samples, 10  $\mu$ L of purified RNA was added to a full RT reaction (total volume 20  $\mu$ L) and 5  $\mu$ L of resulting cDNA was added per ddPCR reaction. Otherwise, 5  $\mu$ l of purified RNA was used in a half RT reaction (total volume 10  $\mu$ L) and 5  $\mu$ L of resulting cDNA was added per ddPCR reaction.

The ddPCR was performed following BioRad manufacturer's protocols including: Bulletin #10048730 PrimePCR ddPCR Gene Expression Probe Assays, Bulletin #10026322 QX100 Droplet Generator Instruction Manual, Bulletin #10026321 QX100 Droplet Reader and QuantaSoft Software Instruction Manual. Specifically, 25  $\mu$ L reactions were prepared in a PCR hood with 5  $\mu$ L cDNA per reaction and master mix containing final concentration 1X of 2X ddPCR Supermix for probes – no dUTP (BioRad, product #1863024), 900 nM primers (IDT), and 250 nM labeled probes (IDT). Twenty  $\mu$ L droplets were generated using a QX100 Droplet Generator (BioRad, product #186-3002).

PCR was carried out in a C1000 Touch Thermal Cycler with 96-Deep Well Reaction Module (BioRad, product #185-1197). Cycling conditions were as follows: enzyme activation 95°C for 10 minutes, 40 cycles of denaturation 94°C for 30 seconds and annealing/extension 57°C for 1 minute, followed by a 10 min hold at 98°C for enzyme deactivation and an optional

infinite 4°C hold. Following thermal cycling, a QX100 Droplet Reader (BioRad, product #186-3003) and QuantaSoft software (BioRad) were used to acquire data.

### ***Administration of EVs on aged cells and silencing Klotho mRNA in EVs***

Muscle progenitors from aged or *Klotho*<sup>-/-</sup> mice were plated at a density of 10,000 cells per well in an 8-well chamber slide for 24 hours. The cells were then exposed to e9 young and aged EVs for a duration of 48 hours.

To implicate *Klotho* mRNA as a driver for *Klotho* modulation within the recipient aged cells and *Klotho*<sup>-/-</sup> cells, young EVs were treated with non-targeting control scramble or siRNA to *Klotho* for a total of 50 minutes prior to administering them to aged cells. Every 250 µL of EVs received 10 µl of transfection reagent (Dharmacon, Dharmafect T-2001-01) and 10 µL of a smart-pool of 5µM non-targeting control (Dharmacon) or siRNA to *Klotho* (Dharmacon). First, the transfection reagent and scramble/siRNA were mixed and incubated in the incubator at 37°C for 10 minutes. Following incubation, the EVs were then placed on ice for 40 minutes prior to use for an *in vitro* application.

The cells receiving the young, aged or treated young EVs were analyzed for MyoD, cardiopilin content and *Klotho* expression 48 hours post-administration.

### ***ELISA***

Muscle progenitors were plated on a 12 well plate at a density of 20,000 cells per well prior to treatment with 2e9 EVs. Conditioned media from the samples (untreated aged cells and aged cells treated with young EVs) were collected 48 hours after treatment.

Klotho protein levels in media were measured by a colorimetric sandwich enzyme immunoassay (ELISA Kit SEH757Mu, Cloud-Clone Corp, Lot#L170622859), according to manufacturer's instructions. Briefly, 100 uL of standards and samples were added to a 96-well microtiter plate that was pre-coated with a biotin-conjugated antibody specific to Klotho. This plate was then incubated for one hour at 37°C following which the samples and standards were removed. A 100 µL of detection reagent A (Biotin-conjugated antibody) was added to each well and incubated at 37°C for one hour. The plates were washed three times with washing buffer provided by the manufacturer. After this, 100 µL of detection reagent B (Avidin conjugated Horseradish-Peroxidase (HRP-avidin)) was added to each well and incubated for 30 minutes at 37 °C. The plate was then washed with washing buffer for five times. Next, 90uL of tetramethylbenzidine substrate was added to the plate and incubated at 37 °C for 20 minutes. A sulfuric acid stop solution was then added to terminate the color development reaction. The optical density (OD) of each well was measured at 450 nm. The OD of samples was compared to OD standard curve with known antigen concentrations to determine the concentration of samples. Standard curve used had a concentration range from 3.25 pg/mL to 200 pg/mL.

The data was then normalized to the final number of cells per well. Samples were never subjected to freeze-thaw.

### ***Animal injury model***

All experiments were performed with prior approval from the Institutional Animal Care and Use Committee of the University of Pittsburgh. Male mice used in these studies were obtained from the following background: wildtype C57BL/6 (22-24 months, NIA) and *Kl* heterozygotes (*Kl*<sup>+/-</sup>; B6; 129S5-Kltm1-Lex, 4-7 months, original breeders obtained from

MMRCC at UC Davis). Mice were first anesthetized with 2% isoflurane and then received bilateral injuries to the tibialis anterior (TA) muscles via intramuscular injection of cardiotoxin (CTX, 10  $\mu$ L of 1mg/mL cardiotoxin per TA). Animals were provided with an ingestible medigel, carprofen, for pain management. Fourteen days following injury, the animals were subjected to an *in situ* contractile testing protocol to evaluate the injured muscle's force producing capacity. Following the contractile testing, blood was isolated from the mice using a cardiac puncture. The animals were then euthanized, and TAs were harvested for histological analysis. The TAs were frozen in liquid nitrogen cooled 2-methyl butane for one minute, after which time they were sectioned through their entirety in 10  $\mu$ m sections. Animals displaying evidence of external injuries and/or tumor growths were not included in the study. The animals having a score outside 25-75% percentile of the median (range: 0.40-0.74) hang-impulse scores, were excluded from the study (n=2/group).

### ***In vivo EV transplantation and functional testing***

To investigate whether young EVs have a beneficial effect on skeletal muscle regeneration of aged mice, animals were injected with  $\sim 5 \times 10^8$  EVs intramuscularly to the TA muscle three days after injury. Next, to implicate Klotho mRNA as a contributing factor for this enhanced skeletal muscle function, aged mice were injected with EVs from young *Klotho*<sup>+/+</sup> and *Klotho*<sup>+/-</sup> mice. Here, the aged mice received two injections of  $\sim 7.5 \times 10^8$  EVs at three- and five-days post-injury. EVs were pooled from isolations from at least four different mouse serum samples.

Contractile testing was performed 14 days after injury using an *in situ* testing apparatus (Model 809B, Aurora Scientific Inc, Canada), stimulator (Model 701C, Aurora Scientific Inc, Canada), and force transducer (Aurora Scientific Inc, Canada). Briefly, the peroneal nerve of

anesthetized animals was isolated through a small incision lateral to the left knee. Mice were then placed supine on a 37°C-heated platform and the foot being tested was positioned on the footplate. The left hindlimb used for testing was stabilized with cloth tape on the knee and foot. Muscles were stimulated through the peroneal nerve by an electrode inserted beneath the skin. Muscle peak twitch, time to peak twitch and half-relaxation time with the ankle positioned at 20° of plantarflexion, the position that we determined to result in the greatest force output (data not shown), were quantified. Tetanic contractions at 10, 30, 50, 80, 100, 120, 150 Hz were elicited to obtain a force- frequency curve, with a 2-minute rest between each contraction. The TA muscles that had undergone the contractile testing were then harvested and frozen in nitrogen-cooled 2-methylbutane for subsequent histological analysis by a blinded investigator.

### ***Statistical Analysis***

Analyses were performed using GraphPad Prism version 8 software. Shapiro-Wilk and Levene's tests were initially performed to assess normality of data and equality of variances, respectively. If assumptions of normality and homogeneity of variances were met, a Student's t-test was performed while comparing two groups. When conditions for normality were not met, the groups were compared using Mann-Whitney U test. A Welch's test was applied when there were differences between the standard deviations of the groups. All results were expressed as mean  $\pm$  standard error. Statistical significance was established, *a priori*, at  $p \leq 0.05$ .

## Bibliography

1. United States. Administration on Aging., American Association of Retired Persons. A profile of older Americans [HTML and PDF formats]. Washington, DC: U.S. Dept. of Health and Human Services, Administration on Aging. Available from: Pitt users please click through to access via U.S. Government Documents: 1995 to 2008 <http://purl.access.gpo.gov/GPO/LPS111610>  
Pitt users please click through to access via U.S. Government Documents: 1999 to present <http://purl.access.gpo.gov/GPO/LPS111599>.
2. Sade RM. The graying of America: challenges and controversies. *J Law Med Ethics*. 2012;40(1):6-9.
3. Wantz M, Gay JE. *The aging process : a health perspective*. Cambridge, MA: Winthrop Publishers; 1981. xiv, 322 p. p.
4. Hendrie HC, Mendelsohn LG, Readhead C. *Brain aging : molecular biology, the aging process, and neurodegenerative disease*. Toronto ; Lewiston, N.Y.: Hogrefe & Huber; 1990. xiv, 306 p. p.
5. Li Y, EBSCOhost. *Global aging issues and policies : understanding the importance of comprehending and studying the aging process*. Springfield, Illinois: Charles C Thomas, Publisher, Ltd.,; 2013. Available from: <http://pitt.idm.oclc.org/login?url=http://search.ebscohost.com/login.aspx?direct=true&scope=site&db=nlebk&db=nlabk&AN=607999> Pitt users please click through to access via EbscoHost.
6. Kirkendall DT, Garrett WE, Jr. The effects of aging and training on skeletal muscle. *Am J Sports Med*. 1998;26(4):598-602.
7. Rogers MA, Evans WJ. Changes in skeletal muscle with aging: effects of exercise training. *Exerc Sport Sci Rev*. 1993;21:65-102.
8. Blair SN, Kohl HW, 3rd, Barlow CE, Paffenbarger RS, Jr., Gibbons LW, Macera CA. Changes in physical fitness and all-cause mortality. A prospective study of healthy and unhealthy men. *JAMA*. 1995;273(14):1093-8.
9. Tinetti ME. Factors associated with serious injury during falls by ambulatory nursing home residents. *J Am Geriatr Soc*. 1987;35(7):644-8.
10. Conboy IM, Conboy MJ, Smythe GM, Rando TA. Notch-mediated restoration of regenerative potential to aged muscle. *Science*302(5650):1575-7. 2003.
11. Faulkner JA, Carlson BM, Kadhiresan VA. Review: Whole skeletal muscle transplantation: mechanisms responsible for functional deficits. *Biotechnol Bioeng*. 1994;43(8):757-63.
12. Croisier JL. Factors associated with recurrent hamstring injuries. *Sports Med*. 2004;34(10):681-95.
13. McBride TA, Gorin FA, Carlsen RC. Prolonged recovery and reduced adaptation in aged rat muscle following eccentric exercise. *Mech Ageing Dev*. 1995;83(3):185-200.
14. Brack AS, Conboy MJ, Roy S, Lee M, Kuo CJ, Keller C, et al. Increased Wnt signaling during aging alters muscle stem cell fate and increases fibrosis. *Science*. 2007;317(5839):807-10.
15. Conboy IM, Conboy MJ, Smythe GM, Rando TA. Notch-mediated restoration of regenerative potential to aged muscle. *Science*. 2003;302(5650):1575-7.

16. Conboy IM, Rando TA. Heterochronic parabiosis for the study of the effects of aging on stem cells and their niches. *Cell Cycle*. 2012;11(12):2260-7.
17. Conboy MJ, Conboy IM, Rando TA. Heterochronic parabiosis: historical perspective and methodological considerations for studies of aging and longevity. *Aging Cell*. 2013;12(3):525-30.
18. Conboy IM, Conboy MJ, Wagers AJ, Girma ER, Weissman IL, Rando TA. Rejuvenation of aged progenitor cells by exposure to a young systemic environment. *Nature*. 2005;433(7027):760-4.
19. Sinha M, Jang YC, Oh J, Khong D, Wu EY, Manohar R, et al. Restoring systemic GDF11 levels reverses age-related dysfunction in mouse skeletal muscle. *Science*. 2014;344(6184):649-52.
20. Elabd C, Cousin W, Upadhyayula P, Chen RY, Chooljian MS, Li J, et al. Oxytocin is an age-specific circulating hormone that is necessary for muscle maintenance and regeneration. *Nat Commun*. 2014;5:4082.
21. Villeda SA, Luo J, Mosher KI, Zou B, Britschgi M, Bieri G, et al. The ageing systemic milieu negatively regulates neurogenesis and cognitive function. *Nature*. 2011;477(7362):90-4.
22. Egerman MA, Cadena SM, Gilbert JA, Meyer A, Nelson HN, Swalley SE, et al. GDF11 Increases with Age and Inhibits Skeletal Muscle Regeneration. *Cell Metab*. 2015;22(1):164-74.
23. Jones JE, Cadena SM, Gong C, Wang X, Chen Z, Wang SX, et al. Supraphysiologic Administration of GDF11 Induces Cachexia in Part by Upregulating GDF15. *Cell Rep*. 2018;22(12):3375.
24. Griffin CA, Apponi LH, Long KK, Pavlath GK. Chemokine expression and control of muscle cell migration during myogenesis. *J Cell Sci*. 2010;123(Pt 18):3052-60.
25. Tieland M, Trouwborst I, Clark BC. Skeletal muscle performance and ageing. *J Cachexia Sarcopenia Muscle*. 2018;9(1):3-19.
26. Lopez-Otin C, Blasco MA, Partridge L, Serrano M, Kroemer G. The hallmarks of aging. *Cell*. 2013;153(6):1194-217.
27. Hayflick L, Moorhead PS. The serial cultivation of human diploid cell strains. *Exp Cell Res*. 1961;25:585-621.
28. Campisi J. Aging, cellular senescence, and cancer. *Annu Rev Physiol*. 2013;75:685-705.
29. McHugh D, Gil J. Senescence and aging: Causes, consequences, and therapeutic avenues. *J Cell Biol*. 2018;217(1):65-77.
30. Itahana K, Dimri G, Campisi J. Regulation of cellular senescence by p53. *Eur J Biochem*. 2001;268(10):2784-91.
31. Takahashi A, Ohtani N, Hara E. Irreversibility of cellular senescence: dual roles of p16INK4a/Rb-pathway in cell cycle control. *Cell Div*. 2007;2:10.
32. Sui X, Fang Y, Lou H, Wang K, Zheng Y, Lou F, et al. p53 suppresses stress-induced cellular senescence via regulation of autophagy under the deprivation of serum. *Mol Med Rep*. 2015;11(2):1214-20.
33. Campisi J. Cancer, aging and cellular senescence. *In Vivo*. 2000;14(1):183-8.
34. Beyfuss K, Hood DA. A systematic review of p53 regulation of oxidative stress in skeletal muscle. *Redox Rep*. 2018;23(1):100-17.
35. Saleem A, Adhietty PJ, Hood DA. Role of p53 in mitochondrial biogenesis and apoptosis in skeletal muscle. *Physiol Genomics*. 2009;37(1):58-66.

36. Zhu P, Zhang C, Gao Y, Wu F, Zhou Y, Wu WS. The transcription factor Slug represses p16(Ink4a) and regulates murine muscle stem cell aging. *Nat Commun.* 2019;10(1):2568.
37. Cosgrove BD, Gilbert PM, Porpiglia E, Mourkioti F, Lee SP, Corbel SY, et al. Rejuvenation of the muscle stem cell population restores strength to injured aged muscles. *Nat Med.* 2014;20(3):255-64.
38. Sousa-Victor P, Gutarra S, Garcia-Prat L, Rodriguez-Ubreva J, Ortet L, Ruiz-Bonilla V, et al. Geriatric muscle stem cells switch reversible quiescence into senescence. *Nature.* 2014;506(7488):316-21.
39. Chang J, Wang Y, Shao L, Laberge RM, Demaria M, Campisi J, et al. Clearance of senescent cells by ABT263 rejuvenates aged hematopoietic stem cells in mice. *Nat Med.* 2016;22(1):78-83.
40. Schafer MJ, Miller JD, LeBrasseur NK. Cellular senescence: Implications for metabolic disease. *Mol Cell Endocrinol.* 2017;455:93-102.
41. Sun N, Youle RJ, Finkel T. The Mitochondrial Basis of Aging. *Mol Cell.* 2016;61(5):654-66.
42. Choksi KB, Nuss JE, Boylston WH, Rabek JP, Papaconstantinou J. Age-related increases in oxidatively damaged proteins of mouse kidney mitochondrial electron transport chain complexes. *Free Radic Biol Med.* 2007;43(10):1423-38.
43. Petersen KF, Befroy D, Dufour S, Dziura J, Ariyan C, Rothman DL, et al. Mitochondrial dysfunction in the elderly: possible role in insulin resistance. *Science.* 2003;300(5622):1140-2.
44. Conley KE, Jubrias SA, Esselman PC. Oxidative capacity and ageing in human muscle. *J Physiol.* 2000;526 Pt 1:203-10.
45. Bua EA, McKiernan SH, Wanagat J, McKenzie D, Aiken JM. Mitochondrial abnormalities are more frequent in muscles undergoing sarcopenia. *J Appl Physiol (1985).* 2002;92(6):2617-24.
46. Tonkonogi M, Fernstrom M, Walsh B, Ji LL, Rooyackers O, Hammarqvist F, et al. Reduced oxidative power but unchanged antioxidative capacity in skeletal muscle from aged humans. *Pflugers Arch.* 2003;446(2):261-9.
47. Van Remmen H, Richardson A. Oxidative damage to mitochondria and aging. *Exp Gerontol.* 2001;36(7):957-68.
48. Paradies G, Petrosillo G, Pistolese M, Ruggiero FM. Reactive oxygen species affect mitochondrial electron transport complex I activity through oxidative cardiolipin damage. *Gene.* 2002;286(1):135-41.
49. Wei YH, Lee HC. Oxidative stress, mitochondrial DNA mutation, and impairment of antioxidant enzymes in aging. *Exp Biol Med (Maywood).* 2002;227(9):671-82.
50. Barja G. Aging in vertebrates, and the effect of caloric restriction: a mitochondrial free radical production-DNA damage mechanism? *Biol Rev Camb Philos Soc.* 2004;79(2):235-51.
51. Van Remmen H, Hamilton ML, Richardson A. Oxidative damage to DNA and aging. *Exerc Sport Sci Rev.* 2003;31(3):149-53.
52. Short KR, Bigelow ML, Kahl J, Singh R, Coenen-Schimke J, Raghavakaimal S, et al. Decline in skeletal muscle mitochondrial function with aging in humans. *Proc Natl Acad Sci U S A.* 2005;102(15):5618-23.
53. Drew B, Leeuwenburgh C. Method for measuring ATP production in isolated mitochondria: ATP production in brain and liver mitochondria of Fischer-344 rats with age and caloric restriction. *Am J Physiol Regul Integr Comp Physiol.* 2003;285(5):R1259-67.

54. Short KR, Nair KS. Mechanisms of sarcopenia of aging. *J Endocrinol Invest.* 1999;22(5 Suppl):95-105.
55. Waters DL, Mullins PG, Qualls CR, Raj DS, Gasparovic C, Baumgartner RN. Mitochondrial function in physically active elders with sarcopenia. *Mech Ageing Dev.* 2009;130(5):315-9.
56. Siegel MP, Kruse SE, Percival JM, Goh J, White CC, Hopkins HC, et al. Mitochondrial-targeted peptide rapidly improves mitochondrial energetics and skeletal muscle performance in aged mice. *Aging Cell.* 2013;12(5):763-71.
57. Grazioli E, Dimauro I, Mercatelli N, Wang G, Pitsiladis Y, Di Luigi L, et al. Physical activity in the prevention of human diseases: role of epigenetic modifications. *BMC Genomics.* 2017;18(Suppl 8):802.
58. Sharples AP, Stewart CE, Seaborne RA. Does skeletal muscle have an 'epi'-memory? The role of epigenetics in nutritional programming, metabolic disease, aging and exercise. *Aging Cell.* 2016;15(4):603-16.
59. Sebastian S, Sreenivas P, Sambasivan R, Cheedipudi S, Kandalla P, Pavlath GK, et al. MLL5, a trithorax homolog, indirectly regulates H3K4 methylation, represses cyclin A2 expression, and promotes myogenic differentiation. *Proc Natl Acad Sci U S A.* 2009;106(12):4719-24.
60. Fujimaki S, Hidaka R, Asashima M, Takemasa T, Kuwabara T. Wnt protein-mediated satellite cell conversion in adult and aged mice following voluntary wheel running. *J Biol Chem.* 2014;289(11):7399-412.
61. Bigot A, Duddy WJ, Ouandaogo ZG, Negroni E, Mariot V, Ghimbovski S, et al. Age-Associated Methylation Suppresses SPRY1, Leading to a Failure of Re-quiescence and Loss of the Reserve Stem Cell Pool in Elderly Muscle. *Cell Rep.* 2015;13(6):1172-82.
62. Blau HM, Cosgrove BD, Ho AT. The central role of muscle stem cells in regenerative failure with aging. *Nat Med.* 2015;21(8):854-62.
63. Thorley M, Malatras A, Duddy W, Le Gall L, Mouly V, Butler Browne G, et al. Changes in Communication between Muscle Stem Cells and their Environment with Aging. *J Neuromuscul Dis.* 2015;2(3):205-17.
64. Sattler FR. Growth hormone in the aging male. *Best Pract Res Clin Endocrinol Metab.* 2013;27(4):541-55.
65. Sinha I, Sinha-Hikim AP, Wagers AJ, Sinha-Hikim I. Testosterone is essential for skeletal muscle growth in aged mice in a heterochronic parabiosis model. *Cell Tissue Res.* 2014;357(3):815-21.
66. Sotiropoulos A, Ohanna M, Kedzia C, Menon RK, Kopchick JJ, Kelly PA, et al. Growth hormone promotes skeletal muscle cell fusion independent of insulin-like growth factor 1 up-regulation. *Proc Natl Acad Sci U S A.* 2006;103(19):7315-20.
67. Horsley V, Jansen KM, Mills ST, Pavlath GK. IL-4 acts as a myoblast recruitment factor during mammalian muscle growth. *Cell.* 2003;113(4):483-94.
68. Troy A, Cadwallader AB, Fedorov Y, Tyner K, Tanaka KK, Olwin BB. Coordination of satellite cell activation and self-renewal by Par-complex-dependent asymmetric activation of p38alpha/beta MAPK. *Cell Stem Cell.* 2012;11(4):541-53.
69. Fu R, Liu J, Fan J, Li R, Li D, Yin J, et al. Novel evidence that testosterone promotes cell proliferation and differentiation via G protein-coupled receptors in the rat L6 skeletal muscle myoblast cell line. *J Cell Physiol.* 2012;227(1):98-107.
70. Ahtiainen M, Pollanen E, Ronkainen PH, Alen M, Puolakka J, Kaprio J, et al. Age and estrogen-based hormone therapy affect systemic and local IL-6 and IGF-1 pathways in women. *Age (Dordr).* 2012;34(5):1249-60.

71. Baeza-Raja B, Munoz-Canoves P. p38 MAPK-induced nuclear factor-kappaB activity is required for skeletal muscle differentiation: role of interleukin-6. *Mol Biol Cell*. 2004;15(4):2013-26.
72. Salminen A, Kaarniranta K, Kauppinen A. Inflammaging: disturbed interplay between autophagy and inflammasomes. *Aging (Albany NY)*. 2012;4(3):166-75.
73. Senovilla L, Vitale I, Martins I, Tailler M, Paillet C, Michaud M, et al. An immunosurveillance mechanism controls cancer cell ploidy. *Science*. 2012;337(6102):1678-84.
74. Vasilaki A, McArdle F, Iwanejko LM, McArdle A. Adaptive responses of mouse skeletal muscle to contractile activity: The effect of age. *Mech Ageing Dev*. 2006;127(11):830-9.
75. Guttridge DC, Mayo MW, Madrid LV, Wang CY, Baldwin AS, Jr. NF-kappaB-induced loss of MyoD messenger RNA: possible role in muscle decay and cachexia. *Science*. 2000;289(5488):2363-6.
76. Pelosi M, De Rossi M, Barberi L, Musaro A. IL-6 impairs myogenic differentiation by downmodulation of p90RSK/eEF2 and mTOR/p70S6K axes, without affecting AKT activity. *Biomed Res Int*. 2014;2014:206026.
77. Oh J, Sinha I, Tan KY, Rosner B, Dreyfuss JM, Gjata O, et al. Age-associated NF-kappaB signaling in myofibers alters the satellite cell niche and re-strains muscle stem cell function. *Aging (Albany NY)*. 2016;8(11):2871-96.
78. Pont AR, Sadri N, Hsiao SJ, Smith S, Schneider RJ. mRNA decay factor AUF1 maintains normal aging, telomere maintenance, and suppression of senescence by activation of telomerase transcription. *Mol Cell*. 2012;47(1):5-15.
79. Lai RY, Ljubicic V, D'Souza D, Hood DA. Effect of chronic contractile activity on mRNA stability in skeletal muscle. *Am J Physiol Cell Physiol*. 2010;299(1):C155-63.
80. Chakkalakal JV, Jones KM, Basson MA, Brack AS. The aged niche disrupts muscle stem cell quiescence. *Nature*. 2012;490(7420):355-60.
81. Le Bihan MC, Bigot A, Jensen SS, Dennis JL, Rogowska-Wrzesinska A, Laine J, et al. In-depth analysis of the secretome identifies three major independent secretory pathways in differentiating human myoblasts. *J Proteomics*. 2012;77:344-56.
82. Forterre A, Jalabert A, Berger E, Baudet M, Chikh K, Errazuriz E, et al. Proteomic analysis of C2C12 myoblast and myotube exosome-like vesicles: a new paradigm for myoblast-myotube cross talk? *PLoS One*. 2014;9(1):e84153.
83. Takahashi K, Yan IK, Kogure T, Haga H, Patel T. Extracellular vesicle-mediated transfer of long non-coding RNA ROR modulates chemosensitivity in human hepatocellular cancer. *FEBS Open Bio*. 2014;4:458-67.
84. Valadi H, Ekstrom K, Bossios A, Sjostrand M, Lee JJ, Lotvall JO. Exosome-mediated transfer of mRNAs and microRNAs is a novel mechanism of genetic exchange between cells. *Nat Cell Biol*. 2007;9(6):654-9.
85. Desdin-Mico G, Mittelbrunn M. Role of exosomes in the protection of cellular homeostasis. *Cell Adh Migr*. 2017;11(2):127-34.
86. Forterre A, Jalabert A, Chikh K, Pesenti S, Euthine V, Granjon A, et al. Myotube-derived exosomal miRNAs downregulate Sirtuin1 in myoblasts during muscle cell differentiation. *Cell Cycle*. 2014;13(1):78-89.
87. Baraibar MA, Gueugneau M, Duguez S, Butler-Browne G, Bechet D, Friguet B. Expression and modification proteomics during skeletal muscle ageing. *Biogerontology*. 2013;14(3):339-52.

88. Kuro-o M. Klotho and aging. *Biochim Biophys Acta*. 2009;1790(10):1049-58.
89. Kuro-o M. Klotho and the aging process. *Korean J Intern Med*. 2011;26(2):113-22.
90. Kuro-o M. Klotho as a regulator of fibroblast growth factor signaling and phosphate/calcium metabolism. *Curr Opin Nephrol Hypertens*. 2006;15(4):437-41.
91. Kuro-o M. Klotho as a regulator of oxidative stress and senescence. *Biol Chem*. 2008;389(3):233-41.
92. Kuro-o M, Matsumura Y, Aizawa H, Kawaguchi H, Suga T, Utsugi T, et al. Mutation of the mouse klotho gene leads to a syndrome resembling ageing. *Nature*. 1997;390(6655):45-51.
93. Hsieh CC, Kuro-o M, Rosenblatt KP, Brobey R, Papaconstantinou J. The ASK1-Signalosome regulates p38 MAPK activity in response to levels of endogenous oxidative stress in the Klotho mouse models of aging. *Aging (Albany NY)*. 2010;2(9):597-611.
94. Brack AS, Conboy MJ, Roy S, Lee M, Kuo CJ, Keller C, et al. Increased Wnt signaling during aging alters muscle stem cell fate and increases fibrosis. *Science* 317(5839):807-10. 2007.
95. Schultz E. Satellite cell behavior during skeletal muscle growth and regeneration. [Review] [23 refs]. *Medicine & Science in Sports & Exercise* 21(5 Suppl):S181-6. 1989.
96. Schultz E, Gibson MC, Champion T. Satellite cells are mitotically quiescent in mature mouse muscle: an EM and radioautographic study. *Journal of Experimental Zoology*. (3):451-6.
97. Ryall JG, Schertzer JD, Lynch GS. Cellular and molecular mechanisms underlying age-related skeletal muscle wasting and weakness. *Biogerontology*. 2008;9(4):213-28.
98. Garcia-Prat L, Martinez-Vicente M, Perdiguero E, Ortet L, Rodriguez-Ubreva J, Rebollo E, et al. Autophagy maintains stemness by preventing senescence. *Nature*. 2016;529(7584):37-42.
99. Zerba E, Komorowski TE, Faulkner JA. Free radical injury to skeletal muscles of young, adult, and old mice. *American Journal of Physiology* 258(3 Pt1):C429-35. 1990.
100. Bernet JD, Doles JD, Hall JK, Kelly Tanaka K, Carter TA, Olwin BB. p38 MAPK signaling underlies a cell-autonomous loss of stem cell self-renewal in skeletal muscle of aged mice. *Nat Med*. 2014;20(3):265-71.
101. Price FD, von Maltzahn J, Bentzinger CF, Dumont NA, Yin H, Chang NC, et al. Inhibition of JAK-STAT signaling stimulates adult satellite cell function. *Nat Med*. 2014;20(10):1174-81.
102. Tierney MT, Aydogdu T, Sala D, Malecova B, Gatto S, Puri PL, et al. STAT3 signaling controls satellite cell expansion and skeletal muscle repair. *Nat Med*. 2014;20(10):1182-6.
103. Sacco A, Puri PL. Regulation of Muscle Satellite Cell Function in Tissue Homeostasis and Aging. *Cell stem cell*. 2015;16(6):585-7.
104. Conboy IM, Conboy MJ, Wagers AJ, Girma ER, Weissman IL, Rando TA. Rejuvenation of aged progenitor cells by exposure to a young systemic environment. *Nature* 433(7027):760-4. 2005.
105. Lukjanenko L, Jung MJ, Hegde N, Perruisseau-Carrier C, Migliavacca E, Rozo M, et al. Loss of fibronectin from the aged stem cell niche affects the regenerative capacity of skeletal muscle in mice. *Nat Med*. 2016;22(8):897-905.
106. Xiao NM, Zhang YM, Zheng Q, Gu J. Klotho is a serum factor related to human aging. *Chinese Medical Journal* 117(5):742-7. 2004.
107. Liu H, Fergusson MM, Castilho RM, Liu J, Cao L, Chen J, et al. Augmented Wnt signaling in a mammalian model of accelerated aging. *Science*. 2007;317(5839):803-6.
108. Semba RD, Cappola AR, Sun K, Bandinelli S, Dalal M, Crasto C, et al. Plasma klotho and cardiovascular disease in adults. *J Am Geriatr Soc*. 2011;59(9):1596-601.

109. Shardell M, Semba RD, Rosano C, Kalyani RR, Bandinelli S, Chia CW, et al. Plasma Klotho and Cognitive Decline in Older Adults: Findings From the InCHIANTI Study. *J Gerontol A Biol Sci Med Sci.* 2016;71(5):677-82.
110. Semba RD, Ferrucci L, Sun K, Simonsick E, Turner R, Miljkovic I, et al. Low Plasma Klotho Concentrations and Decline of Knee Strength in Older Adults. *J Gerontol A Biol Sci Med Sci.* 2016;71(1):103-8.
111. Semba RD, Cappola AR, Sun K, Bandinelli S, Dalal M, Crasto C, et al. Relationship of low plasma klotho with poor grip strength in older community-dwelling adults: the InCHIANTI study. *Eur J Appl Physiol.* 2012;112(4):1215-20.
112. Crasto CL, Semba RD, Sun K, Cappola AR, Bandinelli S, Ferrucci L. Relationship of low-circulating "anti-aging" klotho hormone with disability in activities of daily living among older community-dwelling adults. *Rejuvenation Res.* 2012;15(3):295-301.
113. Kuro-o M. Klotho in health and disease. *Curr Opin Nephrol Hypertens.* 2012;21(4):362-8.
114. Kuro-o M. Klotho as a regulator of oxidative stress and senescence. [Review] [73 refs]. *BiologicalChemistry*389(3):233-41. 2008.
115. Campbell MD, Duan J, Samuelson AT, Gaffrey MJ, Merrihew GE, Egertson JD, et al. Improving mitochondrial function with SS-31 reverses age-related redox stress and improves exercise tolerance in aged mice. *Free Radic Biol Med.* 2019;134:268-81.
116. Thomas DA, Stauffer C, Zhao K, Yang H, Sharma VK, Szeto HH, et al. Mitochondrial targeting with antioxidant peptide SS-31 prevents mitochondrial depolarization, reduces islet cell apoptosis, increases islet cell yield, and improves posttransplantation function. *J Am Soc Nephrol.* 2007;18(1):213-22.
117. Wehling-Henricks M, Li Z, Lindsey C, Wang Y, Welc SS, Ramos JN, et al. Klotho gene silencing promotes pathology in the mdx mouse model of Duchenne muscular dystrophy. *Hum Mol Genet.* 2016;25(12):2465-82.
118. Ahrens HE, Huettemeister J, Schmidt M, Kaether C, von Maltzahn J. Klotho expression is a prerequisite for proper muscle stem cell function and regeneration of skeletal muscle. *Skelet Muscle.* 2018;8(1):20.
119. van Velthoven CTJ, de Morree A, Egner IM, Brett JO, Rando TA. Transcriptional Profiling of Quiescent Muscle Stem Cells In Vivo. *Cell Rep.* 2017;21(7):1994-2004.
120. Cheung TH, Quach NL, Charville GW, Liu L, Park L, Edalati A, et al. Maintenance of muscle stem-cell quiescence by microRNA-489. *Nature.* 2012;482(7386):524-8.
121. Kurosu H, Ogawa Y, Miyoshi M, Yamamoto M, Nandi A, Rosenblatt KP, et al. Regulation of fibroblast growth factor-23 signaling by klotho. *Journal of BiologicalChemistry*281(10):6120-3. 2006.
122. Megeney LA, Kablar B, Garrett K, Anderson JE, Rudnicki MA. MyoD is required for myogenic stem cell function in adult skeletal muscle. *Genes Dev.* 1996;10(10):1173-83.
123. Liu L, Cheung TH, Charville GW, Rando TA. Isolation of skeletal muscle stem cells by fluorescence-activated cell sorting. *Nat Protoc.* 2015;10(10):1612-24.
124. Joe AW, Yi L, Natarajan A, Le Grand F, So L, Wang J, et al. Muscle injury activates resident fibro/adipogenic progenitors that facilitate myogenesis. *Nat Cell Biol.* 2010;12(2):153-63.
125. Wehling-Henricks M, Welc SS, Samengo G, Rinaldi C, Lindsey C, Wang Y, et al. Macrophages escape Klotho gene silencing in the mdx mouse model of Duchenne muscular dystrophy and promote muscle growth and increase satellite cell numbers through a Klotho-mediated pathway. *Hum Mol Genet.* 2018;27(1):14-29.

126. Nassour J, Martien S, Martin N, Deruy E, Tomellini E, Malaquin N, et al. Defective DNA single-strand break repair is responsible for senescence and neoplastic escape of epithelial cells. *Nat Commun.* 2016;7:10399.
127. Garreau-Balandier I, Lefebvre M, Jacquard S, Caillat S, Cruz-Rodriguez L, Ishak L, et al. A comprehensive approach to determining BER capacities and their change with aging in *Drosophila melanogaster* mitochondria by oligonucleotide microarray. *FEBS Lett.* 2014;588(9):1673-9.
128. Sauvaigo S, Guerniou V, Rapin D, Gasparutto D, Caillat S, Favier A. An oligonucleotide microarray for the monitoring of repair enzyme activity toward different DNA base damage. *Anal Biochem.* 2004;333(1):182-92.
129. Chen KH, Yakes FM, Srivastava DK, Singhal RK, Sobol RW, Horton JK, et al. Up-regulation of base excision repair correlates with enhanced protection against a DNA damaging agent in mouse cell lines. *Nucleic Acids Res.* 1998;26(8):2001-7.
130. Kennedy BK, Berger SL, Brunet A, Campisi J, Cuervo AM, Epel ES, et al. Geroscience: linking aging to chronic disease. *Cell.* 2014;159(4):709-13.
131. Fulco M, Cen Y, Zhao P, Hoffman EP, McBurney MW, Sauve AA, et al. Glucose restriction inhibits skeletal myoblast differentiation by activating SIRT1 through AMPK-mediated regulation of Nampt. *Dev Cell.* 2008;14(5):661-73.
132. Ryall JG, Dell'Orso S, Derfoul A, Juan A, Zare H, Feng X, et al. The NAD(+)-dependent SIRT1 deacetylase translates a metabolic switch into regulatory epigenetics in skeletal muscle stem cells. *Cell Stem Cell.* 2015;16(2):171-83.
133. Zhang H, Ryu D, Wu Y, Gariani K, Wang X, Luan P, et al. NAD(+) repletion improves mitochondrial and stem cell function and enhances life span in mice. *Science.* 2016;352(6292):1436-43.
134. de Moura MB, Van Houten B. Bioenergetic analysis of intact mammalian cells using the Seahorse XF24 Extracellular Flux analyzer and a luciferase ATP assay. *Methods Mol Biol.* 2014;1105:589-602.
135. Furda AM, Marrangoni AM, Lokshin A, Van Houten B. Oxidants and not alkylating agents induce rapid mtDNA loss and mitochondrial dysfunction. *DNA Repair (Amst).* 2012;11(8):684-92.
136. Sanders LH, Laganier J, Cooper O, Mak SK, Vu BJ, Huang YA, et al. LRRK2 mutations cause mitochondrial DNA damage in iPSC-derived neural cells from Parkinson's disease patients: reversal by gene correction. *Neurobiol Dis.* 2014;62:381-6.
137. Sanders LH, McCoy J, Hu X, Mastroberardino PG, Dickinson BC, Chang CJ, et al. Mitochondrial DNA damage: molecular marker of vulnerable nigral neurons in Parkinson's disease. *Neurobiol Dis.* 2014;70:214-23.
138. Sanders LH, Howlett EH, McCoy J, Greenamyre JT. Mitochondrial DNA damage as a peripheral biomarker for mitochondrial toxin exposure in rats. *Toxicological sciences : an official journal of the Society of Toxicology.* 2014;142(2):395-402.
139. Yakes FM, Van Houten B. Mitochondrial DNA damage is more extensive and persists longer than nuclear DNA damage in human cells following oxidative stress. *Proc Natl Acad Sci U S A.* 1997;94(2):514-9.
140. Szeto HH. First-in-class cardiolipin-protective compound as a therapeutic agent to restore mitochondrial bioenergetics. *Br J Pharmacol.* 2014;171(8):2029-50.

141. Izbeki F, Asuzu DT, Lorincz A, Bardsley MR, Popko LN, Choi KM, et al. Loss of Kitlow progenitors, reduced stem cell factor and high oxidative stress underlie gastric dysfunction in progeric mice. *J Physiol*. 2010;588(Pt 16):3101-17.
142. Yamamoto M, Clark JD, Pastor JV, Gurnani P, Nandi A, Kurosu H, et al. Regulation of oxidative stress by the anti-aging hormone klotho. *The Journal of biological chemistry*. 2005;280(45):38029-34.
143. Gonzalez-Freire M, de Cabo R, Bernier M, Sollott SJ, Fabbri E, Navas P, et al. Reconsidering the Role of Mitochondria in Aging. *J Gerontol A Biol Sci Med Sci*. 2015;70(11):1334-42.
144. Wen JW, Hwang JT, Kelly GM. Reactive oxygen species and Wnt signalling crosstalk patterns mouse extraembryonic endoderm. *Cell Signal*. 2012;24(12):2337-48.
145. Papaconstantinou J. Insulin/IGF-1 and ROS signaling pathway cross-talk in aging and longevity determination. *Mol Cell Endocrinol*. 2009;299(1):89-100.
146. Lo YY, Cruz TF. Involvement of reactive oxygen species in cytokine and growth factor induction of c-fos expression in chondrocytes. *J Biol Chem*. 1995;270(20):11727-30.
147. Rozo M, Li L, Fan CM. Targeting beta1-integrin signaling enhances regeneration in aged and dystrophic muscle in mice. *Nat Med*. 2016;22(8):889-96.
148. Kurosu H, Yamamoto M, Clark JD, Pastor JV, Nandi A, Gurnani P, et al. Suppression of aging in mice by the hormone Klotho. *Science (New York, NY)*. 2005;309(5742):1829-33.
149. Yousef H, Conboy MJ, Morgenthaler A, Schlesinger C, Bugaj L, Paliwal P, et al. Systemic attenuation of the TGF-beta pathway by a single drug simultaneously rejuvenates hippocampal neurogenesis and myogenesis in the same old mammal. *Oncotarget*. 2015;6(14):11959-78.
150. Murata M, Miwa Y, Sato I. Expression of respiratory chain enzyme mRNA and the morphological properties of mitochondria in the masseter muscles of klotho mutant mice. *Okajimas folia anatomica Japonica*. 2009;86(3):93-103.
151. de Cavanagh EA, Inserra F, Ferder L. Angiotensin ii blockade: how its molecular targets may signal to mitochondria and slow aging. Coincidences with calorie restriction and mtor inhibition. *American journal of physiology Heart and circulatory physiology*. 2015;ajpheart.00459.2014.
152. Zhou L, Li Y, Zhou D, Tan RJ, Liu YCINJASNA, Pmid. Loss of Klotho contributes to kidney injury by derepression of Wnt/beta-catenin signaling. *Journal of the American Society of Nephrology : JASN*. 2013;24(5):771-85.
153. Zhang C, Ferrari R, Beezhold K, Stearns-Reider K, D'Amore A, Haschak M, et al. Arsenic Promotes NF-Kappab-Mediated Fibroblast Dysfunction and Matrix Remodeling to Impair Muscle Stem Cell Function. *Stem Cells*. 2016;34(3):732-42.
154. Zhang C, Ferrari R, Beezhold K, Stearns-Reider K, D'Amore A, Haschak M, et al. Arsenic Promotes NF-kappaB-Mediated Fibroblast Dysfunction and Matrix Remodeling to Impair Muscle Stem Cell Function. *Stem cells*. 2015.
155. Yi L, Rossi F. Purification of progenitors from skeletal muscle. *J Vis Exp*. 2011(49).
156. Bonetto A, Andersson DC, Waning DL. Assessment of muscle mass and strength in mice. *Bonekey Rep*. 2015;4:732.
157. Lin AH, Shang Y, Mitzner W, Sham JS, Tang WY. Aberrant DNA Methylation of Phosphodiesterase [corrected] 4D Alters Airway Smooth Muscle Cell Phenotypes. *Am J Respir Cell Mol Biol*. 2016;54(2):241-9.

158. Dai DF, Chen T, Szeto H, Nieves-Cintrón M, Kuttyavin V, Santana LF, et al. Mitochondrial targeted antioxidant Peptide ameliorates hypertensive cardiomyopathy. *J Am Coll Cardiol.* 2011;58(1):73-82.
159. Shalhoub V, Ward SC, Sun B, Stevens J, Renshaw L, Hawkins N, et al. Fibroblast growth factor 23 (FGF23) and alpha-klotho stimulate osteoblastic MC3T3.E1 cell proliferation and inhibit mineralization. *Calcif Tissue Int.* 2011;89(2):140-50.
160. Pathan M, Fonseka P, Chitti SV, Kang T, Sanwlani R, Van Deun J, et al. Vesiclepedia 2019: a compendium of RNA, proteins, lipids and metabolites in extracellular vesicles. *Nucleic Acids Res.* 2019;47(D1):D516-D9.
161. Shah R, Patel T, Freedman JE. Circulating Extracellular Vesicles in Human Disease. *N Engl J Med.* 2018;379(22):2180-1.
162. Chen WW, Balaj L, Liao LM, Samuels ML, Kotsopoulos SK, Maguire CA, et al. BEAMing and Droplet Digital PCR Analysis of Mutant IDH1 mRNA in Glioma Patient Serum and Cerebrospinal Fluid Extracellular Vesicles. *Mol Ther Nucleic Acids.* 2013;2:e109.
163. Yang J, Wei F, Schafer C, Wong DT. Detection of tumor cell-specific mRNA and protein in exosome-like microvesicles from blood and saliva. *PLoS One.* 2014;9(11):e110641.
164. Salih M, Zietse R, Hoorn EJ. Urinary extracellular vesicles and the kidney: biomarkers and beyond. *Am J Physiol Renal Physiol.* 2014;306(11):F1251-9.
165. Monguio-Tortajada M, Moron-Font M, Gamez-Valero A, Carreras-Planella L, Borrás FE, Franquesa M. Extracellular-Vesicle Isolation from Different Biological Fluids by Size-Exclusion Chromatography. *Curr Protoc Stem Cell Biol.* 2019;49(1):e82.
166. Arraud N, Linares R, Tan S, Gounou C, Pasquet JM, Mornet S, et al. Extracellular vesicles from blood plasma: determination of their morphology, size, phenotype and concentration. *J Thromb Haemost.* 2014;12(5):614-27.
167. Revenfeld AL, Baek R, Nielsen MH, Stensballe A, Varming K, Jorgensen M. Diagnostic and prognostic potential of extracellular vesicles in peripheral blood. *Clin Ther.* 2014;36(6):830-46.
168. Moaddel R, Fabbri E, Khadeer MA, Carlson OD, Gonzalez-Freire M, Zhang P, et al. Plasma Biomarkers of Poor Muscle Quality in Older Men and Women from the Baltimore Longitudinal Study of Aging. *J Gerontol A Biol Sci Med Sci.* 2016;71(10):1266-72.
169. Sahu A, Mamiya H, Shinde SN, Cheikhi A, Winter LL, Vo NV, et al. Age-related declines in alpha-Klotho drive progenitor cell mitochondrial dysfunction and impaired muscle regeneration. *Nat Commun.* 2018;9(1):4859.
170. Kuro OM. The Klotho proteins in health and disease. *Nat Rev Nephrol.* 2019;15(1):27-44.
171. Tapscott SJ. The circuitry of a master switch: MyoD and the regulation of skeletal muscle gene transcription. *Development.* 2005;132(12):2685-95.
172. Pala F, Di Girolamo D, Mella S, Yennek S, Chatre L, Ricchetti M, et al. Distinct metabolic states govern skeletal muscle stem cell fates during prenatal and postnatal myogenesis. *J Cell Sci.* 2018;131(14).
173. Paradies G, Paradies V, De Benedictis V, Ruggiero FM, Petrosillo G. Functional role of cardiolipin in mitochondrial bioenergetics. *Biochim Biophys Acta.* 2014;1837(4):408-17.
174. Picca A, Guerra F, Calvani R, Bucci C, Lo Monaco MR, Bentivoglio AR, et al. Mitochondrial Dysfunction and Aging: Insights from the Analysis of Extracellular Vesicles. *Int J Mol Sci.* 2019;20(4).
175. They C, Witwer KW, Aikawa E, Alcaraz MJ, Anderson JD, Andriantsitohaina R, et al. Minimal information for studies of extracellular vesicles 2018 (MISEV2018): a position

- statement of the International Society for Extracellular Vesicles and update of the MISEV2014 guidelines. *J Extracell Vesicles*. 2018;7(1):1535750.
176. Gualerzi A, Niada S, Giannasi C, Picciolini S, Morasso C, Vanna R, et al. Raman spectroscopy uncovers biochemical tissue-related features of extracellular vesicles from mesenchymal stromal cells. *Sci Rep*. 2017;7(1):9820.
  177. Movasaghi Z, Rehman S, Rehman IU. Raman spectroscopy of biological tissues. *Applied Spectroscopy Reviews*. 2007;42(5).
  178. Gonzales PA, Pisitkun T, Hoffert JD, Tchapyjnikov D, Star RA, Kleta R, et al. Large-scale proteomics and phosphoproteomics of urinary exosomes. *J Am Soc Nephrol*. 2009;20(2):363-79.
  179. Aartsma-Rus A, van Putten M. Assessing functional performance in the mdx mouse model. *J Vis Exp*. 2014(85).
  180. Villarroya-Beltri C, Gutierrez-Vazquez C, Sanchez-Cabo F, Perez-Hernandez D, Vazquez J, Martin-Cofreces N, et al. Sumoylated hnRNPA2B1 controls the sorting of miRNAs into exosomes through binding to specific motifs. *Nat Commun*. 2013;4:2980.
  181. Eldh M, Ekstrom K, Valadi H, Sjostrand M, Olsson B, Jernas M, et al. Exosomes communicate protective messages during oxidative stress; possible role of exosomal shuttle RNA. *PLoS One*. 2010;5(12):e15353.
  182. Blake DJ, Reese CM, Garcia M, Dahlmann EA, Dean A. Soluble extracellular Klotho decreases sensitivity to cigarette smoke induced cell death in human lung epithelial cells. *Toxicol In Vitro*. 2015;29(7):1647-52.
  183. Wiley CD, Velarde MC, Lecot P, Liu S, Sarnoski EA, Freund A, et al. Mitochondrial Dysfunction Induces Senescence with a Distinct Secretory Phenotype. *Cell Metab*. 2016;23(2):303-14.
  184. Rockstein M, Brandt KF. Enzyme changes in flight muscle correlated with aging and flight ability in the male housefly. *Science*. 1963;139(3559):1049-51.
  185. Petersen KF, Shulman GI. Etiology of insulin resistance. *Am J Med*. 2006;119(5 Suppl 1):S10-6.
  186. Peterson CM, Johannsen DL, Ravussin E. Skeletal muscle mitochondria and aging: a review. *J Aging Res*. 2012;2012:194821.
  187. Kerner J, Turkaly PJ, Minkler PE, Hoppel CL. Aging skeletal muscle mitochondria in the rat: decreased uncoupling protein-3 content. *Am J Physiol Endocrinol Metab*. 2001;281(5):E1054-62.
  188. Xu X, Chen CN, Arriaga EA, Thompson LV. Asymmetric superoxide release inside and outside the mitochondria in skeletal muscle under conditions of aging and disuse. *J Appl Physiol (1985)*. 2010;109(4):1133-9.
  189. Vasilaki A, Mansouri A, Van Remmen H, van der Meulen JH, Larkin L, Richardson AG, et al. Free radical generation by skeletal muscle of adult and old mice: effect of contractile activity. *Aging Cell*. 2006;5(2):109-17.
  190. Figueiredo PA, Mota MP, Appell HJ, Duarte JA. The role of mitochondria in aging of skeletal muscle. *Biogerontology*. 2008;9(2):67-84.
  191. Lee JS, Hur MW, Lee SK, Choi WI, Kwon YG, Yun CO. A novel sLRP6E1E2 inhibits canonical Wnt signaling, epithelial-to-mesenchymal transition, and induces mitochondria-dependent apoptosis in lung cancer. *PLoS One*. 2012;7(5):e36520.

192. He Y, Mo Q, Luo B, Qiao Y, Xu R, Zuo Z, et al. Induction of apoptosis and autophagy via mitochondria- and PI3K/Akt/mTOR-mediated pathways by *E. adenophorum* in hepatocytes of saanen goat. *Oncotarget*. 2016;7(34):54537-48.
193. Park HH, Han MH, Choi H, Lee YJ, Kim JM, Cheong JH, et al. Mitochondria damaged by Oxygen Glucose Deprivation can be Restored through Activation of the PI3K/Akt Pathway and Inhibition of Calcium Influx by Amlodipine Camsylate. *Sci Rep*. 2019;9(1):15717.
194. Rohlenova K, Neuzil J, Rohlena J. The role of Her2 and other oncogenes of the PI3K/AKT pathway in mitochondria. *Biol Chem*. 2016;397(7):607-15.
195. Ma X, Dang X, Claus P, Hirst C, Fandrich RR, Jin Y, et al. Chromatin compaction and cell death by high molecular weight FGF-2 depend on its nuclear localization, intracrine ERK activation, and engagement of mitochondria. *J Cell Physiol*. 2007;213(3):690-8.
196. Srisakuldee W, Makazan Z, Nickel BE, Zhang F, Thliveris JA, Pasumarthi KB, et al. The FGF-2-triggered protection of cardiac subsarcolemmal mitochondria from calcium overload is mitochondrial connexin 43-dependent. *Cardiovasc Res*. 2014;103(1):72-80.
197. Urakawa I, Yamazaki Y, Shimada T, Iijima K, Hasegawa H, Okawa K, et al. Klotho converts canonical FGF receptor into a specific receptor for FGF23. *Nature*. 2006;444(7120):770-4.
198. Dalton GD, Xie J, An SW, Huang CL. New Insights into the Mechanism of Action of Soluble Klotho. *Front Endocrinol (Lausanne)*. 2017;8:323.
199. Kurosu H, Yamamoto M, Clark JD, Pastor JV, Nandi A, Gurnani P, et al. Suppression of aging in mice by the hormone Klotho. *Science*. 2005;309(5742):1829-33.
200. Lim SW, Jin L, Luo K, Jin J, Shin YJ, Hong SY, et al. Klotho enhances FoxO3-mediated manganese superoxide dismutase expression by negatively regulating PI3K/AKT pathway during tacrolimus-induced oxidative stress. *Cell Death Dis*. 2017;8(8):e2972.
201. Takenaka T, Kobori H, Miyazaki T, Suzuki H, Nishiyama A, Ishii N, et al. Klotho protein supplementation reduces blood pressure and renal hypertrophy in db/db mice, a model of type 2 diabetes. *Acta Physiol (Oxf)*. 2019;225(2):e13190.
202. Richter B, Haller J, Haffner D, Leifheit-Nestler M. Klotho modulates FGF23-mediated NO synthesis and oxidative stress in human coronary artery endothelial cells. *Pflugers Arch*. 2016;468(9):1621-35.
203. Hsu CG, Burkholder TJ. Independent AMP and NAD signaling regulates C2C12 differentiation and metabolic adaptation. *J Physiol Biochem*. 2016;72(4):689-97.
204. Frederick DW, Loro E, Liu L, Davila A, Jr., Chellappa K, Silverman IM, et al. Loss of NAD Homeostasis Leads to Progressive and Reversible Degeneration of Skeletal Muscle. *Cell Metab*. 2016;24(2):269-82.
205. Sansone P, Savini C, Kurelac I, Chang Q, Amato LB, Strillacci A, et al. Packaging and transfer of mitochondrial DNA via exosomes regulate escape from dormancy in hormonal therapy-resistant breast cancer. *Proc Natl Acad Sci U S A*. 2017;114(43):E9066-E75.
206. Coly PM, Boulanger CM. Extracellular Mitochondria and Vesicles. *Circ Res*. 2019;125(1):53-4.
207. Freed JK, Durand MJ, Hoffmann BR, Densmore JC, Greene AS, Gutterman DD. Mitochondria-regulated formation of endothelium-derived extracellular vesicles shifts the mediator of flow-induced vasodilation. *Am J Physiol Heart Circ Physiol*. 2017;312(5):H1096-H104.
208. Kim SJ, Cheres P, Eren M, Jablonski RP, Yeldandi A, Ridge KM, et al. Klotho, an antiaging molecule, attenuates oxidant-induced alveolar epithelial cell mtDNA damage and apoptosis. *Am J Physiol Lung Cell Mol Physiol*. 2017;313(1):L16-L26.

209. Haruna Y, Kashihara N, Satoh M, Tomita N, Namikoshi T, Sasaki T, et al. Amelioration of progressive renal injury by genetic manipulation of Klotho gene. *Proc Natl Acad Sci U S A*. 2007;104(7):2331-6.
210. Dou X, Boyd-Kirkup JD, McDermott J, Zhang X, Li F, Rong B, et al. The strand-biased mitochondrial DNA methylome and its regulation by DNMT3A. *Genome Res*. 2019;29(10):1622-34.
211. Wong M, Gertz B, Chestnut BA, Martin LJ. Mitochondrial DNMT3A and DNA methylation in skeletal muscle and CNS of transgenic mouse models of ALS. *Front Cell Neurosci*. 2013;7:279.
212. Chen CD, Sloane JA, Li H, Aytan N, Giannaris EL, Zeldich E, et al. The antiaging protein Klotho enhances oligodendrocyte maturation and myelination of the CNS. *J Neurosci*. 2013;33(5):1927-39.
213. King GD, Rosene DL, Abraham CR. Promoter methylation and age-related downregulation of Klotho in rhesus monkey. *Age (Dordr)*. 2012;34(6):1405-19.
214. Lee J, Jeong DJ, Kim J, Lee S, Park JH, Chang B, et al. The anti-aging gene KLOTHO is a novel target for epigenetic silencing in human cervical carcinoma. *Mol Cancer*. 2010;9:109.
215. Rubinek T, Shulman M, Israeli S, Bose S, Avraham A, Zundeleovich A, et al. Epigenetic silencing of the tumor suppressor klotho in human breast cancer. *Breast Cancer Res Treat*. 2012;133(2):649-57.
216. Zhang Q, Liu L, Lin W, Yin S, Duan A, Liu Z, et al. Rhein reverses Klotho repression via promoter demethylation and protects against kidney and bone injuries in mice with chronic kidney disease. *Kidney Int*. 2017;91(1):144-56.
217. Cheikhi A, Barchowsky A, Sahu A, Shinde SN, Pius A, Clemens ZJ, et al. Klotho: An Elephant in Aging Research. *J Gerontol A Biol Sci Med Sci*. 2019;74(7):1031-42.
218. Chen W, Yang M, Bai J, Li X, Kong X, Gao Y, et al. Exosome-Modified Tissue Engineered Blood Vessel for Endothelial Progenitor Cell Capture and Targeted siRNA Delivery. *Macromol Biosci*. 2018;18(2).
219. Shardell M, Semba RD, Kalyani RR, Hicks GE, Bandinelli S, Ferrucci L. Serum 25-Hydroxyvitamin D, Plasma Klotho, and Lower-Extremity Physical Performance Among Older Adults: Findings From the InCHIANTI Study. *J Gerontol A Biol Sci Med Sci*. 2015;70(9):1156-62.
220. Semba RD, Cappola AR, Sun K, Bandinelli S, Dalal M, Crasto C, et al. Plasma klotho and mortality risk in older community-dwelling adults. *J Gerontol A Biol Sci Med Sci*. 2011;66(7):794-800.
221. Ambrosio F, Ferrari RJ, Distefano G, Plassmeyer JM, Carvell GE, Deasy BM, et al. The synergistic effect of treadmill running on stem-cell transplantation to heal injured skeletal muscle. *Tissue Eng Part A*. 2010;16(3):839-49.
222. Low M, Eisner C, Rossi F. Fibro/Adipogenic Progenitors (FAPs): Isolation by FACS and Culture. *Methods Mol Biol*. 2017;1556:179-89.
223. Gualerzi A, Kooijmans SAA, Niada S, Picciolini S, Brini AT, Camussi G, et al. Raman spectroscopy as a quick tool to assess purity of extracellular vesicle preparations and predict their functionality. *J Extracell Vesicles*. 2019;8(1):1568780.